

## Chapter 5

### V. Massive black holes in galactic nuclei - Theory and Simulations

Tiziana Di Matteo <sup>\*</sup>, Daniel Anglés-Alcázar <sup>†</sup> and Francesco Shankar <sup>‡</sup>

Massive black holes are fundamental constituents of our cosmos, from the Big Bang to today. Understanding their formation from cosmic dawn, their growth, and the emergence of the first, rare quasars in the early Universe remains one of our greatest theoretical and observational challenges. Hydrodynamic cosmological simulations self-consistently combine the processes of structure formation at cosmological scales with the physics of smaller, galaxy scales. They capture our most realistic understanding of massive black holes and their connection to galaxy formation and have become the primary avenue for theoretical research in this field. The space-based gravitational wave interferometer, LISA, will open up new investigations into the dynamical processes involving massive black holes. Multi-messenger astrophysics brings new exciting prospects for tracing the origin, growth and merger history of massive black holes across cosmic ages.

#### 1. Introduction

In this chapter we will take a journey through our cosmic history to examine the role of black holes from the Big Bang to today. Black holes are fundamental components of our Universe, and they play a major role in our understanding of galaxy formation. As discussed in Chapter IX, black holes forming from the collapse of the first density peaks and associated processes at cosmic dawn (the first epoch of galaxy formation) are likely to lead to a significant population of 'seed' black holes that merge and grow. Here we will examine the emergence of the first population of supermassive black holes, the first quasars, that occurs within the first billion years of our cosmic history. As we link the formation of the first black holes to the first quasars, we also study the formation of black holes in our standard paradigm of structure formation. We will describe how we understand structure formation within the context of cosmological simulations and semi-analytic models. State-of-the-art cosmological simulations include the formation and growth of black holes

---

<sup>\*</sup>McWilliams Center For Cosmology, Carnegie Mellon University, 5000 Forbes Avenue, Pittsburgh PA, 15213.

<sup>†</sup>Department of Physics, University of Connecticut, 196 Auditorium Road, U-3046, Storrs, CT 06269-3046, USA. Center for Computational Astrophysics, Flatiron Institute, 162 Fifth Avenue, New York, NY 10010, USA.

<sup>‡</sup>School of Physics and Astronomy, University of Southampton, Highfield, Southampton SO17 1BJ, UK.

and can make direct predictions for current and future observations. We will discuss the growth of black holes in the centers of galaxies, and how mergers and gas accretion induced by large inflows and mergers connect the physics of small scales to larger cosmological scales. Cosmological simulations allow us to study directly the co-evolution of and connection between black hole growth and galaxy formation and the emergence of the fundamental relations between central black holes and their host galaxy properties.

## 2. Cosmological Simulations of galaxy formation and black holes

### 2.1. *Brief Introduction, Motivation and Challenges*

Structure formation and evolution in cosmology encompasses the description of the rich hierarchy of structures in our Universe, from individual galaxies and groups to clusters of galaxies up to the largest scale filaments along which smaller structures align. This so-called 'cosmic web' arises from the gravitational growth of the initial matter inhomogeneities, seeded at the time of inflation. The rate at which structure forms depends on the initial power spectrum of the matter fluctuations, now well measured<sup>1</sup> and on the expansion rate of the universe, which is regulated by its matter content (the largest component of which is dark matter), radiation and dark energy. The standard cosmological model has been very successful at predicting a wide range of phenomena, so that it has become worthwhile to devote the largest computer resources to studying structure formation.

To do this, we need to develop computer simulations that cover a vast dynamic range of spatial and time scales: we need to include the effect of gravitational fields generated by superclusters of galaxies on the formation of galaxies, which in turn harbor gas that cools and makes stars and is being funneled into supermassive blackholes the size of the solar system. Ultimately the study of structure formation should provide a true understanding of how galaxy formation takes place in the universe, and so allow us to use the many observations of galaxies and their clustering to gain insights into the nature of the two greatest mysteries of modern physics, dark matter and dark energy while also reproducing the formation and evolution of galaxies and their black holes across cosmic history.

There are two conflicting requirements that make the study of hierarchical structure formation extremely challenging. In order to have a statistically significant representation of all structure in the Universe, the volume studied needs to be large but the individual particle mass needs to be small to adequately resolve the scale length of the structures which form and the appropriate physics. This implies a need for an extremely large  $N$ , where  $N$  is the number of particles. Depending on the problem, a dynamic range of  $10^{10}$  or more can be necessary in principle.

The largest computer models of galaxy formation have traditionally involved the properties of dark matter only but the part of the Universe astronomers observe is made up of ordinary matter (gas, stars etc.). In order to make direct contact with

observations and predictions from our theories we must simulate the detailed hydrodynamics of the cosmic plasma. In addition, there is strong observational evidence for a close connection between the formation and evolution of galaxies and of their central supermassive black holes. Cosmic structure formation is nonlinear, involves a large variety of multi-scale physics and operates on large timescales making large scale numerical simulations the primary means for its study. Both approaches (dark matter only and full gas-dynamics, star formation and black hole physics) can be used in concert to make progress.

In hydrodynamic cosmological simulations, the complex non-linear interactions of gravity, hydrodynamics, forming stars, and black holes are treated in a large, representative volume of the universe. In this approach the physics at these much smaller galaxy scales is hence self-consistently coupled to large cosmological scales. These are therefore our most powerful predictive calculations linking the part of the universe we observe (stars, black holes etc..) to the underlying dark matter and dark energy. They capture our most realistic understanding of black holes and their connection to galaxy formation.

Over the last few years it has become possible, with newly developed and more sophisticated codes, higher fidelity physical models as well as large enough computational facilities, to simulate statistically significant volumes of the universe (down to  $z = 0$ ) with sufficient detail to resolve the internal structure of individual galaxies and follow the growth, mergers and evolution of black holes in their centers. We will review these in this Chapter. The prospect that we are in a position to use cosmology, i.e. the science of the Gigaparsec horizon, in our simulations to make predictions for the mass distribution in the inner regions of galaxies and their central black holes is extraordinary.

## **2.2. *What we simulate, codes and physics***

To simulate structure formation in the Universe we need to account for its full cosmic matter-energy content. Matter comes in two basic types: ordinary baryonic matter (e.g. atoms, stars, planets, galaxies) which accounts for 15% of the total matter content, and dark matter which accounts for the remaining 85%. In addition, there is a mysterious dark energy field which actually dominates the energy density of the universe today, with a contribution of 75%, while matter constitutes only about 25%.

The simulations which include black holes, and that are the subject of this Chapter, are carried out in our standard  $\Lambda$ CDM cosmology. They assume that the Universe has a component of its energy density driven by the cosmological constant  $\Lambda$ . Dark energy, in the form of  $\Lambda$  is then simply introduced in the initial conditions and to solve for the cosmological expansion via the Friedmann equation. It is capable of providing the acceleration in the cosmic expansion compatible with our present observational constraints.

Cosmological simulation use a number of different algorithms to self-consistently

simulate the matter fluids (dark and baryonic) components according to their appropriate physical laws.

**Dark Matter:** For dark matter, which in our standard cosmological models is thought to behave as a perfectly collisionless fluid, the N-body method is used, where a finite set of particles samples the underlying distribution function. As the only appreciable interaction of dark matter is through gravity, the evolution of the system obeys the Poisson-Vlasov equation. For the computation of the gravitational field, cosmological codes often use an FFT mesh solver on large-scales coupled to a hierarchical multipole expansion of the gravitational field based on a tree-algorithm<sup>2</sup> on small scales, leading to a uniformly high force resolution throughout the computational volume.<sup>3</sup>

For the large scales, many cosmological codes use a hierarchical multipole expansion (organized in a “tree”) to calculate gravitational forces. In this method, particles are hierarchically grouped, multipole moments are calculated for each node, and then the force on each particle is obtained by approximating the exact force with a sum over multipoles. The list of multipoles to be used is obtained with a so-called tree-walk, in which the allowed force error can be tuned in a flexible way. A great strength of the tree algorithm is the near insensitivity of its performance to clustering of matter, and its ability to adapt to arbitrary geometries of the particle distribution. While the high spatial accuracy of tree algorithms is ideal for the strongly clustered regime on small scales, there are actually faster methods to obtain the gravitational fields on large scales. In particular, the well-known particle-mesh (PM) approach based on Fourier techniques is probably the fastest method to calculate the gravitational field on a homogeneous mesh. The obvious limitation of this method is however that the force resolution cannot be better than the size of one mesh cell, and the latter cannot be made small enough to resolve all the scales of interest in cosmological simulations. Many codes offer a compromise between the two methods. The gravitational field on large scales is calculated with a particle-mesh (PM) algorithm, while the short-range forces are delivered by the tree. Thanks to an explicit force-split in Fourier space, the matching of the forces can be made very accurate. With this TreePM hybrid scheme, the advantages of PM on large-scales are combined with the advantages of the tree on small scales, such that a very accurate and fast gravitational solver results. A significant speed-up relative to a plain tree code results because the tree-walk can now be restricted to a small region around the target particle as opposed to having to be carried out for the full volume.

**Baryonic Matter:** Baryonic matter is evolved using a mass discretization of the Lagrangian equations of gas dynamics. In cosmology and galaxy formation simulations, both Eulerian and Lagrangian methods have been used to discretize the cosmic gas. Eulerian methods offer the principal advantage of high accuracy for shock capturing and low numerical viscosity.

In Lagrangian codes or Smooth Particle Hydrodynamics based codes, the bary-

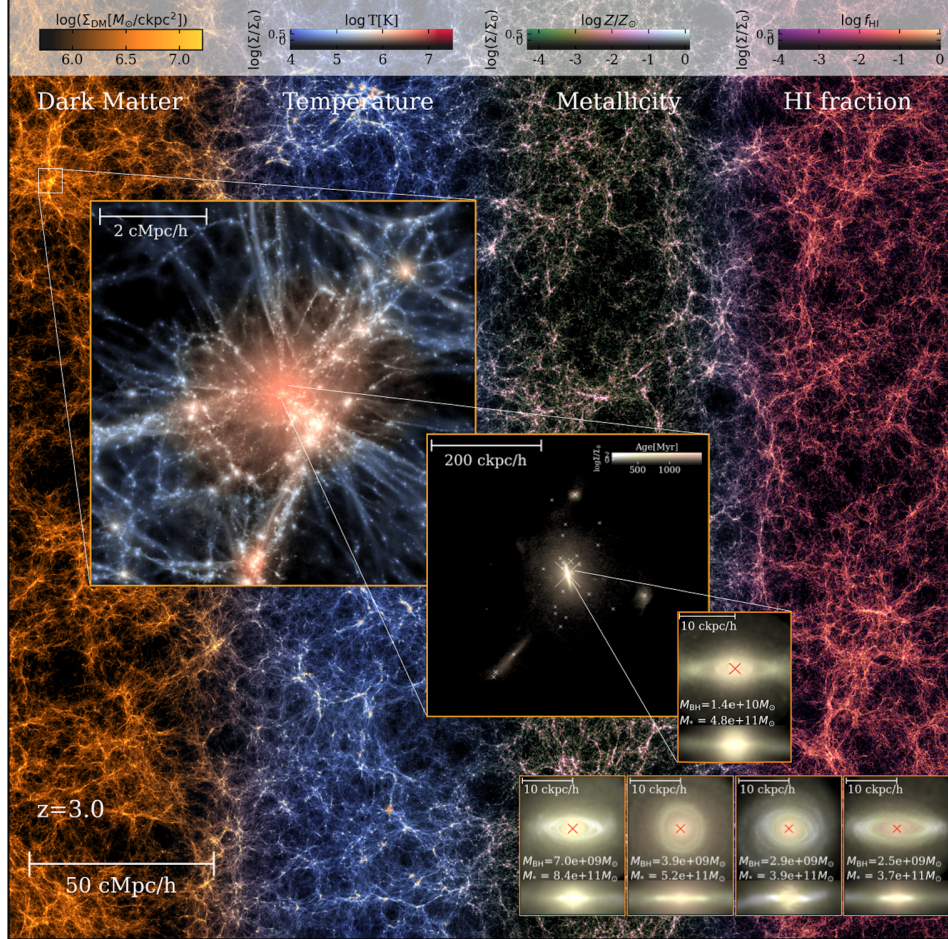


Figure 1. Illustration of state-of-the-art hydrodynamical simulation at  $z = 3$ . *Background*: A  $250 \text{ Mpc}/h \times 250 \text{ Mpc}/h$  slice of the ASTRID simulation, from left to right the colour shows dark matter density (orange), gas temperature (blue), metallicity (purple) and neutral hydrogen fraction (red) respectively. *First inset (Upper left)*: Gas density field coloured by temperature, showing a  $7 \text{ Mpc}/h$  zoomed-in region centred on a massive halo with  $M_h = 3 \times 10^{13} M_\odot$ . *Second inset*: further zoom into a  $500 \text{ kpc}/h$  region, showing the stellar density field centred on an ultra-massive  $10^{10} M_\odot$  BH. The white crosses in the panel mark the positions of SMBHs in this region with the cross size scaled by the BH mass. *Third inset*: the morphology of the host galaxy in face-on (upper panel) and edge-on (lower panel) views in a  $20 \text{ kpc}/h$  region around the central SMBH. Colours show the stellar age with older stars being redder. The bottom insets show some randomly chosen galaxies hosting  $10^9$  BHs. Credit: Yueying Ni.

onic matter is evolved using a mass discretization of the Lagrangian equations of gas dynamics. The code employs a particle-based approach to hydrodynamics, where fluid properties at a given point are estimated by local kernel-averaging over neighboring particles, and smoothed versions of the equations of hydrodynamics are solved for the evolution of the fluid (SPH).

With newer hydrodynamic algorithms such as AREPO<sup>4</sup> and GIZMO,<sup>5</sup> an unstructured Voronoi tessellation of the simulation volume allows for dynamic and adaptive spatial discretization, where a set of mesh generating points are moved along with the gas flow. This mesh is used to solve the equations of ideal hydrodynamics using a second order, finite volume, directionally un-split Godunov-type scheme, with an exact Riemann solver. The code has been thoroughly tested and validated on a number of computational problems and small scale cosmological simulations,<sup>4, 6, 7, 8, 9, 10, 11</sup> demonstrating excellent shock capturing properties, proper development of fluid instabilities, low numerical diffusivity and Galilean invariance, making it thus well posed to tackle the problem of galaxy formation. In recent years, these algorithms have enabled a computational approach to the full problem of galaxy formation.

### 2.2.1. *Physical processes, galaxy formation*

The galaxy formation model in recent simulations is based on the inclusion of:

- (i) Gas cooling and photo-ionization: the cooling function is calculated as a function of gas density, temperature, metallicity, UV radiation field, and AGN radiation field.
- (ii) Star formation and ISM model: the simulations adopt a subgrid model for the ISM, computing an effective equation of state assuming a two-phase medium of cold clouds embedded in a tenuous, hot phase. Star formation occurs stochastically and follows the Kennicutt-Schmidt law.
- (iii) Stellar evolution and feedback: stellar populations return mass to the gas phase through stellar winds and supernovae. The simulations also employ a kinetic stellar feedback scheme, which generates a wind with velocity scaled to the local DM dispersion, and mass loading inferred from the available SN energy for energy-driven winds.

In the next section we review in more detail the physical implementation of the BH physics in our cosmological simulations, which is central to this chapter.

## 3. Black Holes in Galaxy Formation Simulations

A growing number of cosmological hydrodynamic simulations incorporate subgrid models for black hole seeding (§3.1), dynamics (§3.2), growth (§3.3), and impact of feedback (§3.4), which we review in this section. Large volume cosmological simulations are a primary tool to model statistical populations of black holes and galaxies and their connection to large scale structure. Examples of large volume simulations with black hole physics include: Magneticum,<sup>12,13</sup> Horizon-AGN,<sup>14,15</sup> Eagle,<sup>16–18</sup> Illustris,<sup>19–21</sup> MassiveBlack-II,<sup>22,23</sup> BlueTides,<sup>24–27</sup> Romulus,<sup>28–30</sup> IllustrisTNG,<sup>31–34</sup> SIMBA,<sup>35–38</sup> Astrid,<sup>39–41</sup> and CAMELS.<sup>42,43</sup> Cosmological zoom-in simulations of smaller volumes are ideal to study the co-evolution of black holes and galaxies at higher resolution for individual systems (or reach the galaxy cluster regime) while maintaining a full realistic cosmological setting. Examples of

zoom-in simulations with black hole physics include: Apostle,<sup>44</sup> Auriga,<sup>45</sup> NI-HAO,<sup>46,47</sup> Cluster-EAGLE,<sup>48,49</sup> The Three Hundred,<sup>50,51</sup> Choi et al.,<sup>52–54</sup> Costa et al.,<sup>55–57</sup> MARVELous Dwarfs and the DC Justice League,<sup>58–60</sup> New-Horizon,<sup>61,62</sup> and FIRE.<sup>63–68</sup>

While we focus on simulations of black holes in a cosmological context, idealized models of galactic nuclei, isolated galaxies/halos, and galaxy mergers play a crucial role in our understanding of black hole seeding, growth, dynamics, and feedback, informing the development of improved subgrid models for cosmological simulations.

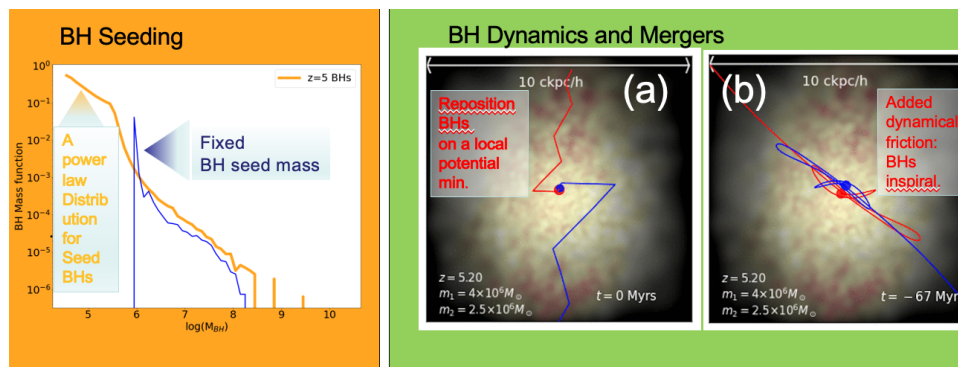


Figure 2. BH seeds and merger models in simulations: Illustration of BH mass function for BH Seeds in a power law distribution vs fixed BH mass (left). BH repositioning on the local potential minimum, BH endowed inspiraling orbits with dynamical friction added in simulations.

### 3.1. Black hole seeds

Several different scenarios exist for the formation of the initial black hole “seeds” that eventually grow to become massive black holes populating the centers of galaxies (see Chapters III and IX, and reviews by<sup>69</sup> and<sup>70</sup>). Popular models include the formation of light seeds ( $M_{\text{seed}} \sim 10^2 M_{\odot}$ ) as remnants of population III stars<sup>71,72</sup> and the formation of massive seeds ( $M_{\text{seed}} \sim 10^5 M_{\odot}$ ) by direct collapse in pregalactic haloes.<sup>73–75</sup> Despite much recent work, major uncertainties remain on the formation time, initial mass, birth place, and overall number density of black hole seeds. Regardless of seed formation scenario, the relevant physical processes occur well below the resolution of cosmological simulations, which must therefore adopt simple subgrid models to introduce the initial seed black holes.

Since the first cosmological simulations including black hole growth and feedback, a common approach to the seeding problem has been to simply assume that every halo above a given threshold dark matter (or stellar) mass hosts a central black hole,<sup>13,16,24,31,40,76–78</sup> without attempting to mimic the physics or outcome of any specific seed formation scenario. In practice, halos are selected for seeding by regularly running a “Friends-of-Friends” (FoF) halo finder on-the-fly as the

simulation proceeds, with typical linking length of  $\sim 0.2$  times the mean particle separation. Halos that satisfy the seeding criteria are then assigned a seed black hole by converting the most bound or highest density gas element into a collisionless particles, if the FOF group does not already contain a black hole particle. The mass threshold for seeding is usually resolution dependent and chosen such that halos are seeded as soon as they are resolved with a sufficient number of particles, but some simulations choose to seed black holes at later times in higher mass galaxies once they are expected to grow more efficiently.<sup>35,36</sup>

An alternative to halo-based models relying on FoF group finding is to create seed black holes based on local gas conditions.<sup>79,80</sup> When a gas element satisfies the star formation criteria in a given simulation, it can become a black hole seed (instead of a star particle) with a probability that can be adjusted to control the overall efficiency of seed formation. In some simulations, this probability is weighted such that black hole seeds form preferentially at the lowest metallicities,<sup>28,58,67,68,81–83</sup> in qualitative agreement with various theoretical models of seed formation that rely on the presence of near pristine gas. Additionally, more restrictive conditions require seeds to form preferentially in converging flows, at the highest surface densities and gravitational accelerations, and in local regions with no pre-existing black holes.<sup>67,68,82</sup>

Adopted black hole seed masses in simulations range from  $M_{\text{seed}} \sim 10^2 M_{\odot}$ <sup>67,68</sup> to  $M_{\text{seed}} \sim 10^6 M_{\odot}$ ,<sup>28,31</sup> roughly covering the full range of theoretical expectations. The seed mass is often below the resolution limit of simulations even for heavy seed formation scenarios, which requires (Lagrangian) simulations to track separately the “physical” mass of the black hole (starting at  $M_{\text{seed}}$ ) from the actual “dynamical” mass of the corresponding collisionless particle.<sup>84</sup> While constant mass is more common, some recent simulations incorporate more complex astrophysical scenarios by adopting a distribution of black hole seed masses. Examples include a power-law distribution of heavy seeds:

$$P(M_{\text{seed}}) = \begin{cases} 0 & M_{\text{seed}} < M_{\text{seed,min}} \\ \mathcal{N}(M_{\text{seed}})^{-n} & M_{\text{seed,min}} \leq M_{\text{seed}} \leq M_{\text{seed,max}} \\ 0 & M_{\text{seed}} > M_{\text{seed,max}} \end{cases} \quad (1)$$

where  $\mathcal{N}$  is the normalization factor,  $M_{\text{seed,min}} = 3 \times 10^4 M_{\odot} h^{-1}$  is the minimum seed mass,  $M_{\text{seed,max}} = 3 \times 10^5 M_{\odot} h^{-1}$  is the maximum seed mass, and  $n = -1$  defines the power-law distribution.<sup>40</sup> Other simulations attempt to represent the spectrum of light black hole seeds that could form from population III remnants,<sup>82</sup> based on theoretical expectations for the stellar initial mass function and the fate of stars of different masses.<sup>85,86</sup>

Black holes in massive galaxies grow by many orders of magnitude and therefore their final mass at  $z = 0$  should be insensitive to the initial seed mass. On the other hand, black holes in lower-mass galaxies are expected to grow significantly less and may retain memory of the initial conditions.<sup>58,63,82,87–89</sup> In either case, the choice

of seed mass may have strong implications depending on the accretion model (§3.3). If the accretion rate is strongly dependent on black hole mass, then low mass seeds may never reach the conditions for efficient growth even in massive galaxies. In contrast, if accretion is weakly-dependent on black hole mass, then black holes may converge to a similar mass regardless of the initial seed.<sup>66,78,90,91</sup> The choice of black hole seed model can also lead to widely different black hole number densities and halo occupation fractions.<sup>69,92,93</sup>

### 3.2. Black hole dynamics and mergers

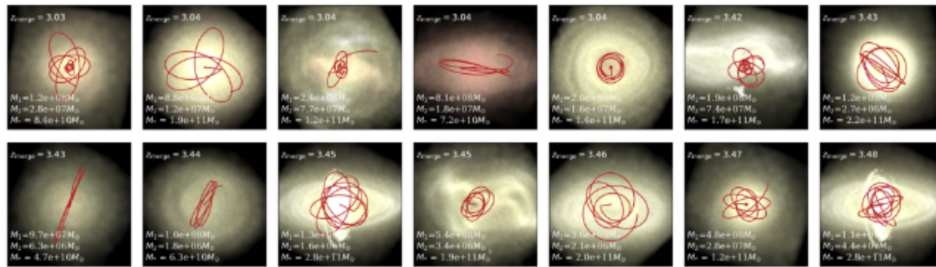


Figure 3. The last few orbits (starting from  $\sim 80$  Myrs before the merger) of a small sample binaries in the large cosmological simulation (Astrid) plotted on their host galaxies. The distance from left to right of each image is  $8 \text{ ckpc}/h$ . The brightness corresponds to the stellar density, and the colors show the stellar age with older stars being redder. The red curves are the BH pairs' position relative to their center of mass. Some BH orbits circularize over time (e.g. third row, fifth column), although the majority of the orbits still remain eccentric when merging. Credit: Nianyi Chen.<sup>39</sup>

After seed formation, the trajectory of black holes is governed by gravitational interactions with the gas, stellar, and dark matter components. Any motion of the black hole relative to a collisionless background of stars and dark matter leads to dynamical friction, effectively acting as a “drag force” owing to the integrated effect of successive gravitational two-body encounters.<sup>94</sup> This process can help the black hole sink towards the gravitational potential minimum and remain near the center of the galaxy. Similarly, the hydrodynamic disturbance generated by a black hole moving relative to the background gas distribution generates a wake slowing down the black hole,<sup>95,96</sup> though feedback in the form of winds or radiation from the black hole can significantly reduce gas dynamical friction or even result in positive net acceleration.<sup>97–101</sup>

Dynamical friction is not properly resolved in cosmological simulations owing to limited mass and gravitational force resolution. Resolving the gravitational radius of influence of a black hole with mass  $M_{\text{BH}}$ ,

$$r_{\text{inf}} \equiv \frac{G M_{\text{BH}}}{\sigma^2} \approx 1 \text{ pc} \left( \frac{M_{\text{BH}}}{10^7 M_{\odot}} \right) \left( \frac{\sigma}{200 \text{ km s}^{-1}} \right)^{-2}, \quad (2)$$

where  $\sigma$  is the velocity dispersion of the surrounding gas, stellar, or dark matter component, is only possible in idealized models<sup>102</sup> or cosmological simulations with strong hyper-refinement in the nuclear region.<sup>65</sup> However, the typical spatial scale resolved in large-volume cosmological simulations can be orders of magnitude larger ( $\sim 1$  kpc), with individual resolution elements representing the gas, stellar, and dark matter components that can be significantly more massive than the black hole particle.

In order to avoid spurious black hole trajectories owing to unresolved dynamical friction, a common approach in galaxy formation simulations is to artificially reposition the black hole to the location of the most bound particle within the neighboring gas (and/or stellar) distribution<sup>21,24,31,77,78,84</sup> or within the FoF group that contains the black hole.<sup>35</sup> Black hole repositioning operates every time step, effectively pinning the black hole location to the center of the host galaxy. In this scheme, close galaxy encounters and mergers can yield unphysical behavior with non-smooth trajectories of black hole particles, which is partially mitigated by only allowing black hole repositioning if the relative velocity of the most bound particle is lower than some fraction of the local sound speed or their mutual escape velocity. Alternatively, more gradual repositioning techniques rely on displacing the black hole continuously by small increments in the direction of the stellar mass gradient or the location of the minimum potential,<sup>67,68,103–105</sup> resulting in smoother black hole trajectories. As intended, black hole repositioning increases the density of the ambient gas and reduces the relative velocity of the black hole, increasing the accretion rate and the overall efficiency of black hole feedback in simulations.<sup>28,104,105</sup> However, artificial repositioning precludes the study of black hole dynamics in galaxies and overestimates the rate of black hole merger events, requiring post-processing calculations to account for slower orbital decays.<sup>106</sup>

Boosting the dynamical mass of the black hole until its physical mass becomes significantly larger than the dark matter particles is an alternative to allow for non-trivial gravitational dynamics while avoiding stochastic trajectories of low-mass black holes,<sup>63</sup> which can mimic the effect of black holes embedded in tightly bound stellar structures with large effective mass that can sink more efficiently to the galactic center.<sup>83,107</sup> A more physically motivated approach to modeling black hole dynamics in cosmological simulations is to include a subgrid prescription for dynamical friction.<sup>28,40,58,83,106,108,109</sup> Most current models are based on the traditional<sup>94</sup> dynamical friction formula assuming a homogeneous, infinite, idealized background medium with isotropic velocity distribution, where the deceleration experienced by a black hole of mass  $M_{\text{BH}}$  is given by:

$$\mathbf{a}_{\text{DF}} = -4\pi G^2 M_{\text{BH}} m_a \ln \Lambda \frac{\mathbf{v}_{\text{BH}}}{v_{\text{BH}}^3} \int_0^{v_{\text{BH}}} dv_a v_a^2 f(\mathbf{v}_a) \quad (3)$$

$$\approx -4\pi G^2 M_{\text{BH}} \rho(< v_{\text{BH}}) \ln \Lambda \frac{\mathbf{v}_{\text{BH}}}{v_{\text{BH}}^3}, \quad (4)$$

where  $\mathbf{v}_{\text{BH}}$  is the black hole velocity relative to the surrounding medium,  $m_a$  and  $\mathbf{v}_a$  are the masses and velocities of the background particles, and the second ex-

pression replaces the integral over the velocity distribution  $f(\mathbf{v}_a)$  by the density  $\rho(< v_{\text{BH}})$  of particles moving slower than the black hole.<sup>108</sup> The Coulomb logarithm  $\ln\Lambda \approx \ln(b_{\text{max}}/b_{\text{min}})$  depends on the maximum ( $b_{\text{max}}$ ) and minimum ( $b_{\text{min}}$ ) impact parameters. The spatial scale at which  $\rho$ ,  $v_{\text{BH}}$ , and  $\Lambda$  are measured introduces some ambiguity in the calculation of dynamical friction. In practice, the gravitational force resolution scale (or the size of the black hole “interaction” kernel) is often used to evaluate Equations 3-4, though more recent dynamical friction estimators attempt to generalize better to cases which violate these idealized conditions and remove the ambiguity in estimating ill-defined continuum quantities.<sup>83</sup>

Some simulations implement a drag force on the black hole from the surrounding gas distribution motivated by the analytical approximation of:<sup>95</sup>

$$\mathbf{F}_{\text{drag}} = -4\pi\rho \left( \frac{GM_{\text{BH}}}{c_s} \right)^2 \times \mathcal{I}(\mathcal{M}) \frac{\mathbf{v}_{\text{BH}}}{v_{\text{BH}}}, \quad (5)$$

where here  $\rho$  is the gas density,  $c_s$  is the sound speed, and  $\mathcal{I}(\mathcal{M})$  is a non-dimensional function that encapsulates the dependence on the Mach number  $\mathcal{M} = v_{\text{BH}}/c_s$ .<sup>106,110</sup> Some models simplify this expression to depend explicitly on the gas accretion rate  $\dot{M}_{\text{BH}}$ , with deceleration given by  $\mathbf{a}_{\text{drag}} \approx -\mathbf{v}_{\text{BH}} \dot{M}_{\text{BH}}/M_{\text{BH}}$ .<sup>40,107</sup> Dynamic friction from stars generally dominates over the gas drag<sup>106,109</sup> but some simulations artificially boost the gas drag to help stabilize black hole trajectories when not including dynamic friction from collisionless particles<sup>62,110</sup> or in gas-dominated systems at high redshift.<sup>111</sup> In either case, despite the addition of subgrid dynamical friction, scattering through two-body interactions can still affect the black hole trajectory if its mass is similar to that of the background particles. In practice, this implies that cosmological simulations often still need to either artificially boost the dynamical mass of the black hole or employ massive seeds ( $\gtrsim 10^6 M_{\odot}$ ) to avoid spurious dynamical heating.<sup>28,106,108,109</sup>

Despite the technical difficulties of modeling black hole dynamics in a galaxy evolution context, many independent studies indicate that efficient accretion requires black holes to remain tightly bound to the galaxy center where the highest average gas densities occur.<sup>63,66,105,111</sup> This can be achieved by dynamic friction in relatively massive galaxies with well-defined, dense, and stable central regions, but it may not be possible in turbulent, clumpy, high-redshift galaxies where frequent dynamical perturbations from mergers, bursty star formation, stellar feedback, and massive clumps can significantly increase the time-scale for orbital decay of even massive black hole seeds.<sup>28,29,61,63,83,109,112–116</sup> This black hole “sinking problem”<sup>83</sup> can explain the observed off-center location of AGN in dwarf galaxies,<sup>117,118</sup> attributed to wandering black holes,<sup>58,59,119,120</sup> but may represent a challenge for the early growth of the highest redshift QSOs and significantly affect the rate of black hole–black hole mergers.

Galaxy merger remnants will inevitably contain two or more massive black holes that may eventually merge, but cosmological simulations lack the resolution to follow this process in detail. In simulations implementing artificial repositioning, any

two black holes are allowed to merge instantaneously if they are located within their interaction kernel.<sup>21,24,31</sup> Given the  $\sim$ kpc scale resolution of large-volume simulations, black holes can merge during close fly-bys even at high relative velocity during the early stages of galaxy interactions, artificially enhancing the merger rate. In some simulations with repositioning, merging black holes are also required to have a relative velocity lower than their mutual escape velocity.<sup>16,35,78</sup> This helps prevent black holes from merging during the initial stages of galaxy mergers, though the actual black hole velocities are ill-defined owing to the repositioning approach. Simulations implementing subgrid dynamical friction, or modeling black holes massive enough that dynamical friction is resolved, can follow the evolution of merging black holes for longer time and implement a more physically meaningful gravitational binding criteria for allowing black hole mergers at the resolution scale.<sup>28,63,106</sup> Gravitational-wave recoils of merging black holes are usually neglected in cosmological simulations but may influence their dynamics, growth, and overall impact of feedback.<sup>121–123</sup>

### 3.3. Black hole accretion

Cosmological large-volume simulations cannot resolve the dominant mechanisms driving gas transport from galaxy scales down to the black hole accretion disk, requiring the implementation of sub-grid accretion models to infer the inflow of gas on unresolved scales (Fig. 4). The Bondi accretion model<sup>124,125</sup> is the most widely used prescription for black hole growth in galaxy formation simulations since its first implementation in idealized galaxy merger simulations.<sup>84,126</sup> For a black hole of mass  $M_{\text{BH}}$ , moving at velocity  $v$  relative to a uniform distribution of gas with density  $\rho$  and sound speed  $c_s$ , the Bondi rate is given by

$$\dot{M}_{\text{Bondi}} = \alpha \frac{4\pi G^2 M_{\text{BH}}^2 \rho}{(c_s^2 + v^2)^{3/2}}, \quad (6)$$

where  $G$  is the gravitational constant and  $\alpha$  is a normalization factor often included to boost the accretion rate (see below). The gas properties are measured locally around the black hole within an interaction *kernel* usually defined to contain the nearest fluid elements. Depending on the resolution of the simulation, the black hole kernel represents a physical size typically ranging from  $\sim$ 10–100pc in idealized and high-resolution cosmological zoom-in simulations to  $\sim$ 1kpc in simulations of large cosmological volumes or very massive objects such as galaxy clusters. The Bondi radius  $r_{\text{B}} \equiv GM_{\text{BH}}/c_s^2$  represents the gravitational black hole radius of influence relative to gas supported by thermal pressure and it is often not resolved in cosmological simulations.

The strong dependence  $\dot{M}_{\text{Bondi}} \propto M_{\text{BH}}^2$  implies a transition between suppressed accretion rate at low  $M_{\text{BH}}$  and very fast growth at high  $M_{\text{BH}}$ . Assuming constant

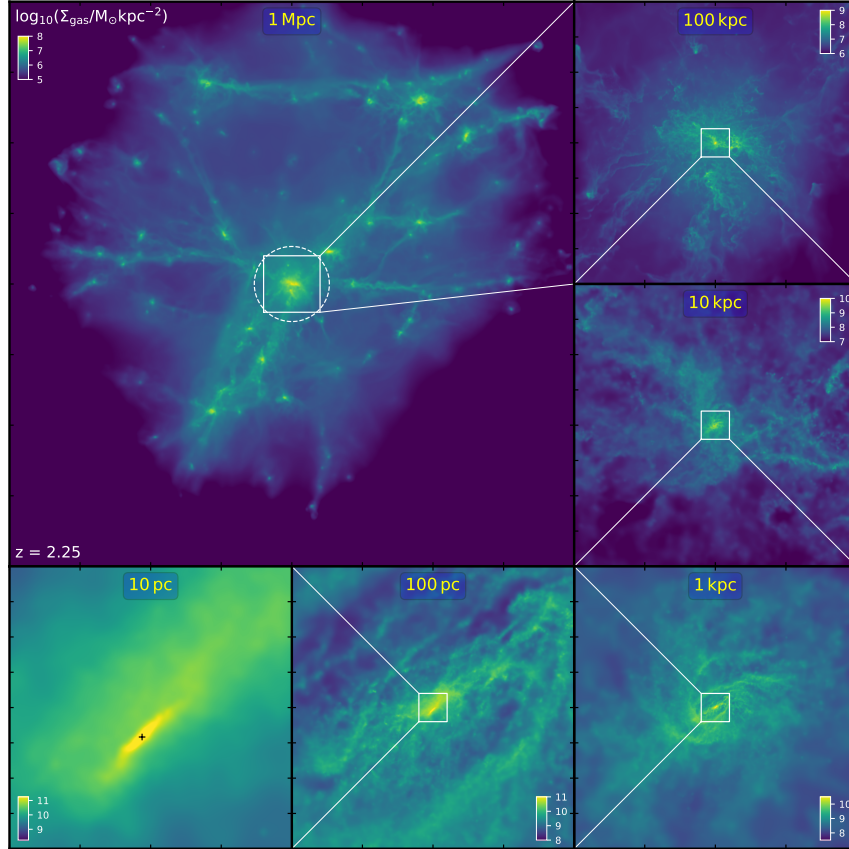


Figure 4. Distribution of gas across scales in a cosmological hyper-refinement simulation of a massive galaxy ( $M_{\text{star}} \sim 10^{10.5}$ ) at  $z \sim 2$ . The top left panel shows a Mpc-scale region containing tens of galaxies connected by cosmic filaments. Subsequent panels zoom in progressively into the nuclear region of the most massive galaxy and down to the vicinity of the central massive black hole, resolving a pc-scale, rotationally supported disk of accreting gas. Strong gravitational torques from non-axisymmetric perturbations in the stellar potential drive a sub-pc gas inflow rate of a few  $M_{\odot} \text{yr}^{-1}$ , sufficient to power a luminous quasar. Cosmological large-volume simulations cannot resolve the dominant mechanisms driving gas transport on scales  $\lesssim 100 \text{pc} - 1 \text{kpc}$ , requiring the implementation of sub-grid accretion prescriptions to parameterize the inflow of gas on unresolved scales. Figure reproduced from.<sup>65</sup>

gas density and sound speed, Equation 6 yields

$$M_{\text{BH}}(t) = \frac{M_{\text{seed}}}{1 - t/t_{\text{B}}}, \quad (7)$$

where

$$t_{\text{B}} = \frac{c_s^3}{\alpha 4\pi G^2 \rho M_{\text{seed}}} \quad (8)$$

is the timescale for divergence in  $M_{\text{BH}}$  (assuming  $v = 0$ ) and  $M_{\text{BH}}(t = 0) \equiv M_{\text{seed}}$  is the initial mass of the black hole seed. For typical kpc-scale conditions of star-forming gas in large volume simulations ( $c_s \sim 20 \text{ km s}^{-1}$  and  $\rho \sim 0.13 m_p \text{ cm}^{-3}$ , with  $m_p$  the proton mass), where the multi-phase ISM is not resolved, we obtain

$$t_{\text{B}} \approx 100 \text{ Gyr} \left( \frac{1}{\alpha} \right) \left( \frac{10^5 M_{\odot}}{M_{\text{seed}}} \right), \quad (9)$$

implying that a black hole with  $M_{\text{seed}} = 10^5 M_{\odot}$  would never reach efficient growth in standard Bondi accretion ( $\alpha = 1$ ). In order to mitigate this problem, a boost factor of order  $\alpha \sim 100$  is often adopted, which partially compensates the inability of cosmological simulations to resolve the Bondi radius and the multiphase structure of gas.<sup>84</sup> Alternative implementations include a density-dependent boost factor  $\alpha \propto \rho^2$ ,<sup>77</sup> or evaluating Bondi accretion for the inferred cold gas phase (increasing  $\rho$  and decreasing  $c_s$ ) in the context of subgrid ISM models with relatively high mean gas temperatures owing to stellar feedback.<sup>127</sup> These implementation choices together with  $M_{\text{seed}}$  can thus have significant effects on early black hole growth.

In the opposite regime, Bondi accretion reaches supra-exponential growth on very short timescales for massive black holes, with  $t_{\text{B}} \approx 100 \text{ Myr}$  for  $M_{\text{BH}} = 10^8 M_{\odot}$ . In practice, the divergence in  $M_{\text{BH}}$  at  $t = t_{\text{B}}$  (Equation 7) is avoided by limiting the accretion rate to the Eddington limit, which represents the maximum growth rate that can be achieved through spherically symmetric accretion in the presence of radiation pressure:

$$\dot{M}_{\text{Edd}} = \frac{4\pi G m_p M_{\text{BH}}}{\epsilon_r \sigma_{\text{T}} c}, \quad (10)$$

where  $\epsilon_r$  is the radiative efficiency,  $\sigma_{\text{T}}$  is the Thomson scattering cross-section, and  $c$  is the speed of light. Some models allow black holes to exceed  $\dot{M}_{\text{Edd}}$  by factors of a few, which is consistent with detailed radiation hydrodynamic simulations of non-spherical accretion flows indicating that super-Eddington feeding is indeed possible,<sup>128,129</sup> provided that the inflow rate from larger scales is sufficiently high.<sup>65,130</sup> Accretion at the Eddington rate yields exponential growth with  $e$ -folding time given by the Salpeter time,

$$t_{\text{S}} \equiv \frac{\epsilon_r \sigma_{\text{T}} c}{4\pi G m_p} \approx 45 \text{ Myr}, \quad (11)$$

where we assume  $\epsilon_r = 0.1$ .<sup>131</sup> Continuous Eddington growth would thus quickly produce over-massive black holes, implying that Eddington-limited Bondi accretion requires strong self-regulation by AGN feedback to reproduce observations such as the black hole–galaxy scaling relations.<sup>132,133</sup>

Equation 6 neglects radiative cooling, the angular momentum of inflowing gas, the gravitational influence of the gas and stellar components, and gas consumption by star formation among other key physical processes affecting gas transport in galaxy discs. High-resolution simulations of galactic nuclei show that Bondi accretion may indeed fail to reproduce gas inflow rates by orders of magnitude under a

variety of conditions,<sup>65,96,134–139</sup> demonstrating the challenge of developing accurate predictors of gas inflow rates across multiple spatial scales.

Despite these limitations, models based on Bondi accretion have been very successful at reproducing global galaxy and black hole observables when coupled with suitable AGN feedback prescriptions.<sup>13,16,18,21,24,40,76,140</sup> These include variations of the Bondi model that attempt to account for the gas angular momentum. Considering a reduction of the Bondi radius owing to a decreased effective gravitational potential due to gas rotational support yields a suppression of Bondi accretion by a factor  $\propto (c_s/v_\phi)^4$  when  $v_\phi > c_s$ , where  $v_\phi$  represents the gas rotational velocity at the resolution scale.<sup>28</sup> Considering instead the characteristic inflow time of Bondi accretion compared to the timescale of viscous accretion from the circularization radius yields a suppression of Bondi accretion by a factor  $\propto (c_s/v_\phi)^3$ .<sup>17</sup> In either case, Bondi-based accretion prescriptions retain the strong  $M_{\text{BH}}^2$  dependence.

Adaptive refinement techniques can achieve significantly higher dynamic range than standard cosmological simulations by splitting fluid elements dynamically (thereby increasing resolution) as gas approaches the central black hole,<sup>65,141</sup> albeit at the expense of significant increase in computation cost (Fig. 4). Cosmological hyper-refinement simulations of gas-rich, quasar-host galaxies show that the inflowing gas across 1pc–10kpc scales is primarily cool, with rotational support dominating over turbulence and thermal pressure.<sup>65</sup> Under a range of conditions, these simulations show that gravitational torques from multi-scale stellar non-axisymmetries dominate angular momentum transport over gas self-torquing and pressure gradients, with the gas inflow rate on sub-pc scales weakly dependent on  $M_{\text{BH}}$ . This is consistent with earlier idealized simulations of galactic nuclei<sup>134,135</sup> and points to a departure from the assumptions in Bondi-based accretion models.

Under the assumption that gravitational torques from non-axisymmetric perturbations in the stellar component (driven by galaxy interactions and instabilities in self-gravitating nuclear gas disks) induce strong gas orbit crossing and shocks that dissipate energy and angular momentum, the inflow rate is given by

$$\dot{M}_{\text{inflow}}(R) \sim \frac{|a| M_{\text{gas}}}{t_{\text{dyn}}}, \quad (12)$$

where  $M_{\text{gas}}$  is the gas mass within  $R$ ,  $t_{\text{dyn}} \equiv (R^3/GM_{\text{enc}})^{1/2}$  is the dynamical time,  $M_{\text{enc}}$  is the total enclosed mass within  $R$  (including the gas and stellar components in addition to  $M_{\text{BH}}$ ), and  $|a|$  is the fractional amplitude of the non-axisymmetric perturbation to the potential.<sup>135</sup> Equation 12 and additional considerations about the dominant perturbation modes on different scales and their amplitude, the dependence of global gravitational instability on bulge-to-disk ratio, and the local balance between inflow and star formation represent the basis of an alternative

accretion rate estimator based on gravitational torques:

$$\begin{aligned} \dot{M}_{\text{Torque}} \approx & \alpha_{\text{T}} f_{\text{d}}^{5/2} \times \left( \frac{M_{\text{BH}}}{10^8 M_{\odot}} \right)^{1/6} \left( \frac{M_{\text{enc}}(R)}{10^9 M_{\odot}} \right) \\ & \times \left( \frac{R}{100 \text{ pc}} \right)^{-3/2} \left( 1 + \frac{f_0}{f_{\text{gas}}} \right)^{-1} M_{\odot} \text{ yr}^{-1}, \end{aligned} \quad (13)$$

where  $f_{\text{d}} \equiv M_{\text{d}}/M_{\text{enc}}$  is the disk mass fraction (including both stars and gas),  $f_{\text{gas}}$  is the gas mass fraction in the disk component,  $f_0 \approx 0.31 f_{\text{d}}^2 (M_{\text{d}}/10^9 M_{\odot})^{-1/3}$ , and all quantities are evaluated within a distance  $R$  corresponding the size of the black hole kernel.<sup>135</sup> The normalization factor  $\alpha_{\text{T}} \approx 1\text{--}10$  parametrizes the dependence of sub-pc inflow rates on the assumed Schmidt-Kennicutt law of star formation on unresolved scales and the galaxy stellar density profile.

Cosmological simulations implementing gravitational torque-driven accretion show important qualitative differences compared to Bondi-based accretion models.<sup>63,68,78,90,91,142</sup> The inflow rate driven by gravitational instabilities and resulting torques is nearly independent of  $M_{\text{BH}}$ . This implies that black holes do not show the characteristic behavior seen in Equation 7 for Bondi-based models, where a marked transition occurs from suppressed black hole growth at low  $M_{\text{BH}}$  to supra-exponential growth at high  $M_{\text{BH}}$ . Instead, gravitational torque-driven inflow predicts efficient growth of under-massive black holes (without the need for an  $\alpha$  accretion boost factor) and does not require strong self-regulation of massive black holes by galaxy-scale AGN feedback. Explicitly including the physics of gravitational torques between the stellar and gas components therefore yields qualitatively different results to that of modifications of Bondi accretion that attempt to incorporate angular momentum transport.

The gravitational torque model assumes conditions relevant for black hole fueling in self-gravitating gas disks with a dominant stellar component. These conditions are less likely to apply in the gas dominated regime at early times, where other processes such as scattering of dense gas clouds or turbulent transport may be required,<sup>143–145</sup> or the gas poor regime at late times in massive elliptical galaxies where Bondi accretion of hot, pressure supported gas with low angular momentum may be a better representation. Ideally, cosmological simulations should implement black hole accretion prescriptions able to incorporate the dominant gas transport mechanisms operating on different regimes as the host galaxy evolves. A first attempt at implementing a hybrid accretion model considered separately the cold ( $T < 10^5 \text{ K}$ ) and hot ( $T > 10^5 \text{ K}$ ) gas components within the black hole kernel, modeling the accretion of cold, rotationally supported gas following the gravitational torque model and the accretion of hot, pressure supported gas following the Bondi parameterization.<sup>35–37</sup>

In addition to modeling the inflow of gas across galaxy scales, simulations should also consider the transport of gas within the black hole accretion disk itself. Some models incorporate an intermediate accretion disk reservoir from which the black hole grows at a rate motivated by accretion disk theory.<sup>67,68,146–148</sup> In some cases,

simulations track the evolution of black hole spin, which can modify the radiative efficiency of the accretion disk and the efficiency of accretion-driven winds and jets.<sup>148–150</sup>

### 3.4. Black hole feedback

Radiatively efficient accretion disks convert a significant fraction of the rest mass energy of accreted material into radiation, with the total bolometric luminosity given by

$$L_{\text{bol}} = \epsilon_r \dot{M}_{\text{BH}} c^2, \quad (14)$$

where the radiative efficiency depends on the spin of the black hole and can range from  $\epsilon_r \sim 0.05$ – $0.35$ .<sup>151</sup> The total integrated power radiated by the central massive black hole is thus expected to be orders of magnitude larger than the binding energy of the host galaxy,

$$\frac{\epsilon_r M_{\text{BH}} c^2}{M_{\text{star}} \sigma^2} \sim 100 \times \left( \frac{\epsilon_r}{0.1} \right) \left( \frac{300 \text{ km s}^{-1}}{\sigma} \right)^2, \quad (15)$$

where  $\sigma$  is the galaxy stellar velocity dispersion and we have assumed a typical black hole mass to galaxy stellar mass ratio  $M_{\text{BH}}/M_{\text{star}} \sim 10^{-3}$ . Radiation can affect the thermodynamic state of gas through Compton, photoionization, and photo-electric heating and driving winds through radiation pressure on free electrons and dust or via coupling to spectral lines. Accretion disks can also drive mechanical winds and jets that can extract a larger fraction of the accreted rest mass energy  $\dot{M}_{\text{BH}} c^2$  compared to radiation.<sup>152</sup> Even if only a small fraction of  $L_{\text{bol}}$  couples to the surrounding gas through some of these processes, Equation 15 implies that AGN feedback can have a significant impact in galaxy evolution.<sup>126,153,154</sup>

Observations of AGN feedback in action include fast nuclear outflows,<sup>155,156</sup> galaxy-scale winds,<sup>157–160</sup> radio-emitting jets,<sup>152,161</sup> and ionized QSO proximity zones.<sup>162,163</sup> Regardless of the specific form of feedback, the energy is originated in the central engine on scales comparable to the Schwarzschild radius,

$$R_s \equiv \frac{2GM_{\text{BH}}}{c^2} \approx 10^{-6} \text{ pc} \times \left( \frac{M_{\text{BH}}}{10^7 M_{\odot}} \right), \quad (16)$$

but can affect the properties of gas out to Mpc scales. Modeling the generation and impact of feedback across more than ten orders of magnitude in spatial scales is computationally unfeasible. The implementation of AGN feedback in galaxy formation simulations is thus schematic by necessity, owing to limited resolution but also to uncertainties in observational constraints and the lack of a full theoretical understanding of the different feedback channels.

A popular AGN feedback model since its first implementation in idealized galaxy merger simulations assumes that a fraction  $\epsilon_f$  of the bolometric luminosity couples to the surrounding gas in the form of thermal energy.<sup>84,126</sup> The input energy

$\dot{E} = \epsilon_f L_{\text{bol}}$  is deposited isotropically into the nearest gas resolution elements, typically within the black hole kernel used to evaluate the accretion prescription (§3.3). This thermal feedback model represents the basis for many AGN feedback implementations in large-volume cosmological simulations.<sup>12,14,16,24,28,31,40,76</sup> The feedback efficiency  $\epsilon_f$  is a free parameter that represents the expected impact of AGN feedback, without necessarily corresponding to a specific physical mechanism, and it is usually calibrated to reproduce the observed black hole–galaxy scaling relations. The overall effect of thermal feedback depends on the resolution of the simulation, the accretion prescription, and other implementation details, but typical values in the range  $\epsilon_f \sim 0.05\text{--}0.15$  have been shown to yield efficient self-regulation of black hole growth while generating strong outflows that help reduce the star formation rate in galaxies.

Reproducing the observed decline in the abundance of galaxies at the high mass end<sup>164,165</sup> and the bimodality in galaxy colors with a growing population of red galaxies at low redshift<sup>166,167</sup> requires efficient quenching of star formation. Rapid cooling in metal-rich gas can decrease the efficiency of thermal feedback by radiating away a fraction of the injected energy, which may represent a challenge to fully quenching massive galaxies. Some simulations artificially accumulate the feedback energy produced by each black hole until it is enough to heat the neighboring gas elements to a minimum temperature  $T \sim 10^9\text{K}$  where cooling is inefficient, reducing cooling losses.<sup>16</sup> Other approaches resort to temporarily inhibiting cooling of gas that has received a thermal feedback injection.<sup>28</sup> Alternatively, simulations incorporating mechanical energy deposition instead of thermal feedback benefit from the fact that the injected momentum cannot be radiated away, reducing cooling losses and potentially increasing the impact of feedback.<sup>52</sup>

The momentum injection rate owing to radiation pressure on dust can be approximated as

$$\dot{P}_{\text{rad}} = \tau \frac{L_{\text{bol}}}{c}, \quad (17)$$

where  $\tau > 1$  corresponds to the total FIR optical depth in the nuclear region assuming absorption of UV radiation by dust and multi-scattering re-radiation in the infrared. Idealized galaxy merger simulations suggest that radiation pressure on dust assuming  $\tau = 10$  can efficiently self-regulate black hole growth,<sup>168,169</sup> and more detailed radiation hydrodynamic simulations show that radiation pressure-driven feedback may be an important ingredient in regulating star formation in compact starbursts in the initial obscured QSO phase, producing galactic winds qualitatively different to that of thermal feedback models.<sup>57,170</sup> The increased computational cost of radiation hydrodynamics has limited its use in galaxy formation simulations, but approximate radiative transport methods allow more efficient implementation of radiative feedback in cosmological simulations.<sup>67,138</sup>

The momentum and kinetic energy imparted by mechanical winds can be modeled in simulations by prescribing the mass loading factor  $\eta_m \equiv \dot{M}_{\text{out}}/\dot{M}_{\text{BH}}$  (parameterizing the mass outflow rate relative to the black hole accretion rate) and the

corresponding outflow velocity  $v_{\text{out}}$ . With these choices, the “momentum loading” and the kinetic energy efficiency relative to the bolometric luminosity are given by

$$\eta_{\text{p}} \equiv \frac{\dot{P}_{\text{wind}}}{L_{\text{bol}}/c} = \frac{\eta_{\text{m}}}{\epsilon_{\text{r}}} \left( \frac{v_{\text{out}}}{c} \right), \quad (18)$$

$$\epsilon_{\text{k}} \equiv \frac{\dot{E}_{\text{wind}}}{L_{\text{bol}}} = \frac{\eta_{\text{m}}}{2 \epsilon_{\text{m}}} \left( \frac{v_{\text{out}}}{c} \right)^2. \quad (19)$$

In some implementations of mechanical winds in Lagrangian hydrodynamics, gas resolution elements within the black hole kernel receive a velocity kick corresponding to  $v_{\text{out}}$  with a probability set to reproduce the prescribed mass outflow rate on average.<sup>52,78,171</sup> Alternatively, new gas elements can be introduced into the simulation to represent the wind at higher mass resolution.<sup>67,68,172–174</sup> In the case of grid-based simulations, mass and momentum are injected into neighbouring gas cells according to the prescribed values of  $\eta_{\text{m}}$  and  $v_{\text{out}}$ .<sup>175</sup> Isotropic winds are generally implemented by assigning velocity kicks directed radially outward from the black hole, but equatorial winds<sup>138</sup> and collimated winds<sup>35</sup> have also been implemented in simulations.

The appropriate mass loading and wind velocity depend on the resolution of the simulation, which sets the physical scale at injection and therefore the type of winds that are represented. High resolution simulations (usually idealized) can attempt to model nuclear winds similar to those observed in broad absorption line QSOs<sup>176</sup> and in absorption against X-ray emission from AGN,<sup>155,156,177</sup> with mildly relativistic velocity ( $v_{\text{out}} \sim 30,000 \text{ km s}^{-1}$ ) and mass outflow rate comparable to the black hole accretion rate ( $\eta_{\text{m}} \sim 1$ ).<sup>138,172–174,178</sup> These winds appear to generate on accretion-disk scales ( $< 100 R_{\text{s}}$ ) and are broadly consistent with predictions from accretion disk simulations, corresponding to a kinetic energy efficiency  $\epsilon_{\text{k}} \sim 0.05$  similar to the feedback coupling efficiency used in simulations implementing thermal feedback. Analytic models suggest that inefficient cooling of high-velocity shocked winds entraining ISM gas results in energy-conserving outflows where the momentum flux can be boosted by  $\eta_{\text{p}} \sim 20$ ,<sup>179,180</sup> which may explain the highly mass-loaded ( $\eta_{\text{m}} \sim 1,000$ ) and slower ( $v_{\text{out}} \sim 1,000 \text{ km s}^{-1}$ ) outflows observed on kpc scales.<sup>157–159</sup> Cosmological large-volume simulations cannot resolve this process but can instead implement mechanical AGN winds with the boosted momentum flux and velocity expected on kpc scales.<sup>35,78</sup>

Some simulations implement two different modes of AGN feedback motivated by observations of two distinct populations of AGN, with (1) “quasar-mode” (or “radiative-mode”) AGN associated with radiatively efficient accretion at high Eddington ratio ( $\lambda_{\text{Edd}} \equiv \dot{M}_{\text{BH}}/\dot{M}_{\text{Edd}} \gtrsim 0.01$ ) in less massive black holes growing in star-forming galaxies, and (2) “jet-mode” (or “radio-mode”) AGN associated with radiatively inefficient accretion at low Eddington ratio ( $\lambda_{\text{Edd}} \lesssim 0.01$ ) in more massive black holes in early type-galaxies.<sup>181</sup> Quasar-mode feedback is associated with intense radiation and galaxy-scale outflows with high momentum flux in luminous AGN while jet-mode feedback is primarily driven by highly collimated jets

of relativistic particles which inflate hot, X-ray emitting bubbles in galaxy groups and clusters. The role and impact of each AGN feedback mode is still not fully understood and their outcome in simulations depends on their specific implementation, but quasar-mode feedback is believed to be important in regulating black hole growth and central densities in massive galaxies while jet-mode feedback is believed to be most relevant to prevent cooling of hot gas in massive halos and maintain massive galaxies quenched. In practice, the distinction of feedback modes in simulations allows for different forms of energy injection and efficiencies operating in different regimes, which provides more flexibility to accomplish quenching in massive galaxies, groups, and clusters, while not significantly affecting lower mass galaxies.

The first two-mode AGN feedback model in cosmological hydrodynamic simulations was implemented as thermal feedback injection either in the vicinity of the black hole for the quasar mode or at two locations outside of the galaxy and in opposite sides to represent the expansion of hot bubbles driven by jet-mode feedback.<sup>182</sup> A similar model was implemented into the Illustris large volume simulation,<sup>19,20</sup> with the thermal coupling efficiency increasing from  $\epsilon_f = 0.05 \rightarrow 0.35$  when black holes transition from quasar to radio mode feedback, successfully quenching galaxies but over-evacuating gas from high mass halos.<sup>19</sup> A more recent implementation of radio-mode feedback in IllustrisTNG replaced thermal coupling by the injection of mechanical winds with spherical symmetry and higher coupling efficiency ( $\epsilon_k \sim 1$ ), producing a red galaxy sequence and simultaneously more realistic thermodynamic profiles in large haloes.<sup>31</sup> Other implementations of radio-mode feedback in large-volume simulations attempt to represent relativistic jets, though resolving their propagation and structure remains a challenge even in idealized simulations.<sup>183–185</sup> The Horizon-AGN simulation<sup>14</sup> implements quasar-mode feedback as “standard” thermal coupling and a transition to mechanical bipolar outflows with velocity  $\sim 10,000 \text{ km s}^{-1}$ , corresponding to an increase in feedback efficiency  $\epsilon_f = 0.15 \rightarrow 1$ . In contrast, the SIMBA simulation<sup>35</sup> implements collimated outflows with constant momentum flux ( $\eta_p = 20$ ) in both feedback modes,<sup>78</sup> with a mass-dependent outflow velocity increasing from  $v_{\text{out}} \sim 1,000 \rightarrow 8,000 \text{ km s}^{-1}$  when transitioning from quasar mode to full-speed jets. Implementations of two-mode AGN feedback in cosmological hydrodynamic simulations usually rely on a threshold in Eddington ratio ( $\lambda_{\text{Edd}} \sim 0.01$ ) above and below which black holes operate in the quasar and jet feedback mode, motivated by observations and accretion disk theory. However, the success of some models requires additional criteria such as a minimum black hole mass required to transition to radio-mode feedback<sup>35</sup> or a mass-dependent threshold in Eddington ratio such that higher mass systems can more easily transition into the powerful radio mode while low-mass galaxies remain unaffected.<sup>31</sup>

The strong degeneracy between model parameters controlling black hole seeding, dynamics, accretion, and feedback remains a challenge for building fully-predictive

black hole prescriptions in cosmological simulations. This has been emphasized in a large suite of hundreds of cosmological zoom-in simulations from the FIRE project<sup>64,67</sup> varying independently the numerical schemes and efficiency parameters for black hole accretion and mechanical, radiative, and cosmic ray feedback.<sup>68</sup> Several plausible combinations of models satisfy observational constraints (e.g., stellar mass–halo mass relation and black hole–galaxy scaling relations) but it is non-trivial to reproduce scaling relations across the full mass range (from dwarfs to massive galaxies) without relying on artificial numerical implementations. Many model variations produce qualitatively incorrect results regardless of parameter choices, which may help discriminate models.<sup>68</sup> Interestingly, cosmic rays accelerated by massive black holes are emerging as a plausible important feedback channel,<sup>68,185</sup> currently ignored in most large-volume cosmological simulations.

## 4. Analytic evolutionary models of Supermassive Black Holes in a cosmological context

### 4.1. *Semi-analytic models*

Semi-analytic models (SAMs) have been conceived as an alternative methodology to numerical simulations to model galaxies in a cosmological context from first principles.<sup>186–206</sup> SAMs start from dark matter N-body simulations or analytic merger trees. A number of physically and/or observationally motivated analytic recipes are then set up in SAMs to control the cooling, star formation and ejection of baryons in/from the potential wells of the host dark matter haloes through cosmic time. Each of these recipes is characterized by one or more adjustable parameters, which are then fitted to best fit a variety of independent data sets on the galaxy population at different epochs and environments. SAMs represent a valuable and flexible tool to more rapidly test against observational data the effectiveness of some theoretical models and/or to bracket the values of some relevant physical parameters.

Although SAMs had been originally designed to mostly focus on galaxy evolution, a lot of attention has been devoted in the last decades to also include in SAMs the formation and evolution of SMBHs.<sup>188,190,192,195,199,200,206–210</sup> Similarly to hydrodynamic simulations, SAMs start by seeding galaxies with black holes of varying mass, from light seeds of a few tens to hundred solar masses (Pop III remnants), to massive seeds of a few thousands solar masses (direct collapse from supermassive stars). In more recent times, a third avenue has been proposed to form SMBH seeds, which lies somewhat in between the previous two models, and it is based on the accretion of stellar mass black holes that fall onto the centre via dynamical friction in the dense environments of starforming galaxies. Given the initial high star formation rates of the host galaxies, calculations have shown that central black holes could grow rapidly and efficiently towards the formation of seed black holes

comparable to those from direct collapse.

Seed black holes are then allowed to grow, similarly to galaxies, via gas accretion and mergers with other (intermediate and supermassive) wandering black holes brought in by past mergers with other galaxies. Gas accretion onto SMBHs has been often associated to galaxy mergers, during which the gas accretion rate onto the SMBH has been approximated by the relation<sup>188,206</sup>

$$\dot{M}_{\text{BH,Q}} = f_K f(V_{\text{vir}}) m_{\text{ratio}} M_{\text{cold}}, \quad (20)$$

where  $M_{\text{cold}}$  is the mass of available cold gas,  $f_K$  is an efficiency parameter, usually chosen in a way to match the local scaling relations between SMBH mass and host galaxy stellar/bulge mass,  $m_{\text{ratio}}$  is the mass ratio of the merging galaxies, and  $f(V_{\text{vir}})$  is a function of the virial velocity of the host halo, usually parameterised as<sup>211</sup>

$$f(V_{\text{vir}}) = \frac{1}{1 + \left(\frac{V_{\text{vir}}}{280 \text{ km/s}}\right)^{-2}} \quad (21)$$

to take into account the possibility that in lower-mass galaxies/haloes, with shallower potential wells, gas is more easily expelled and thus less available for accretion onto the SMBH. The accretion formula in Equation 20 is usually referred to as “quasar-mode”, as it easily generates large accretion rates onto the SMBH and thus high luminosities.

The quasar-mode accretion has not always been strictly associated to galaxy mergers in SAMs, but also to a more general formation epoch of the host halo. In this approach, each virialization/formation of a host dark matter halo, identified by its early phase of fast collapse, promotes infall and cooling of baryons. Baryonic cooling is then rapidly followed by bursts of star formation which can induce, via different physical processes such as photon radiation drag, the formation of a central gas reservoir of low angular momentum, which can in turn feed the central SMBH<sup>188,195,212</sup>

$$\dot{M}_{\text{lowJ}} = f_{\text{lowJ}} \Psi, \quad (22)$$

where  $\Psi$  is the galactic star formation rate and  $f_{\text{lowJ}}$  a free parameter, again usually tuned to reproduce the scaling relations between SMBHs and galaxies or the AGN luminosity functions. Equation 22 has been often adopted as an intermediate step to better mimic the gradual loss of angular momentum in the gas component from the larger to the smaller scales around the SMBH. Equation 22 has been used in merger models.

The actual accretion onto the central SMBH from the reservoir of low angular momentum gas has then been modelled on the viscous accretion timescale<sup>188,213</sup>

$$\dot{M}_{\text{BH}} = f_{\text{BH}} \frac{\sigma_B^3}{G} \left(\frac{M_{\text{res}}}{M_{\text{BH}}}\right)^{3/2} \left(1 + \frac{M_{\text{BH}}}{M_{\text{res}}}\right)^{1/2}, \quad (23)$$

where  $M_{\text{BH}}$ ,  $M_{\text{res}}$ , and  $\sigma_B$  are, respectively, the mass of the central SMBH, the mass of the gas reservoir, and the stellar velocity dispersion of bulge. We note that

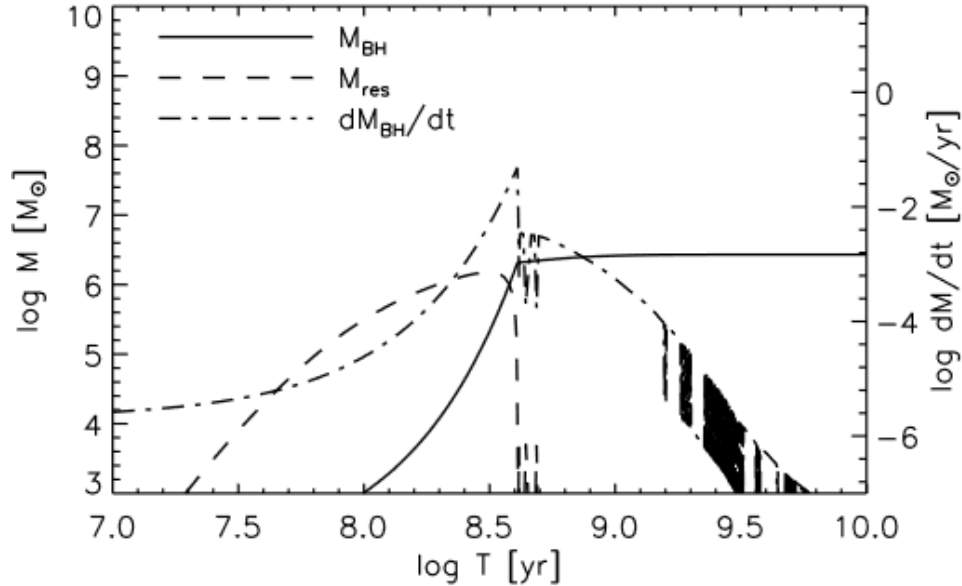


Figure 5. Dependence on galactic age of the SMBH mass, reservoir mass, and SMBH accretion rate<sup>213</sup>).

in Equation 23, and in fact in all analytic recipes of SMBH accretion, the rate of gas accretion onto the central SMBHs is usually capped at a chosen multiple of the SMBH Eddington accretion rate.

The accretion onto the central SMBH has also been sometimes modelled in SAMs following a “light-curve”, i.e., the varying accretion rate suggested by hydrodynamic simulations and analytic models. Such light-curve models are typically characterized by a fast (super-)Eddington accretion phase, which lasts until the SMBH reaches a peak mass marking the self-regulation limit between accretion and feedback, followed by a power-law decline as a function of time of the type<sup>188,206,207,209,213–215</sup>

$$\dot{M}_{\text{BH}} = \frac{\dot{M}_{\text{Edd}}}{1 + \left(\frac{t}{t_{\text{Edd}}}\right)^2}. \quad (24)$$

It has been shown several times in the literature that replacing instantaneous accretion with a gradual redistribution of gas accretion modulated by a physically motivated light curve, provides a closer match to different AGN observables, most notably the shape and evolution of the AGN bolometric luminosity function, and the large-scale AGN clustering.<sup>216</sup>

We show in Figure 5 a light curve that is not parameterized but it is generated by the balance between accretion and feedback in a self-regulated mode. It is straightforward to distinguish the initial, Eddington-limited growth of the SMBH from an initial seed, followed by a descending phase regulated by the availability of gas in the reservoir and the surrounding interstellar medium. The transition

between the self-regulated mode to the starvation mode is what sets the scaling relation between SMBH mass and host galaxy stellar velocity dispersion.<sup>188</sup>

While in SAMs the accretion of cold gas controls the growth rate of SMBHs in the quasar-mode regime, as given in Equation 20, the accretion of hot gas onto a central SMBH occurs from a static hot halo around the SMBH host galaxy, and it is expressed as<sup>206</sup>

$$\dot{M}_{\text{BH,R}} = k_{\text{R}} \left( \frac{M_{\text{BH}}}{10^8 M_{\odot}} \right) \left( \frac{f_{\text{hot}}}{0.1} \right) \left( \frac{V_{\text{vir}}}{200 \text{ km s}^{-1}} \right)^3, \quad (25)$$

where  $f_{\text{hot}}$  is the fraction of the total halo mass in the form of hot gas,  $V_{\text{vir}}$  is the virial velocity of the host halo, which is proportional to the total mass of hot gas in the halo, and  $k_{\text{R}}$  is an adjustable parameter, tuned to reproduce the local scaling relations between SMBHs and their host galaxies. The radio-mode AGN feedback mostly acts at stalling or heating up the late re-accretion of cold gas in the host galaxy (the so-called “cooling flow”), along with limiting the growth of the central SMBH, which always occurs at very sub-Eddington regimes.

As in hydrodynamic simulations, explicit inclusion of AGN feedback in the quasar-mode regime have been included in some SAMs. Inspired by analytic arguments,<sup>217</sup> the first examples of quasar-mode feedback in SAMs assumed that at any given time of episodic accretion, the central SMBH back reacts by heating the interstellar medium and removing a fraction of gas from the cold phase  $\frac{M_{\text{cold}}}{M_{\text{gas}}}$  at a rate<sup>188</sup>

$$\dot{M}_{\text{cold}}^{\text{QSO}} \propto \frac{L_K}{\sigma^2} \frac{M_{\text{cold}}}{M_{\text{gas}}}, \quad (26)$$

where  $L_K$  is the kinetic luminosity of the quasar and  $\sigma$  the stellar velocity dispersion of the host galaxy. It is interesting to note that SAMs inclusive of only quasar-mode feedback are still capable of reproducing the same local galaxy stellar mass function as in models inclusive of explicit radio-mode feedback, as long as the quasar-mode feedback is powerful enough to ejecting cold and infalling gas beyond the virial radius.<sup>188</sup>

#### 4.2. Semi-empirical models

Along the past decades, several groups have attempted to probe the growth SMBHs, or at least to set some general constraints on their evolutionary patterns and average properties, by adopting a number of “data-driven” approaches, without necessarily adopting ab-initio cosmological models. One of the very first of these attempts is the so-called Sołtan “argument”.<sup>218</sup> The aim of this seminal work was to yield an average estimate of the radiative efficiency  $\epsilon_r$  of SMBHs (and thus of their spin) via the relation

$$\rho_{\text{BH}} = \frac{1 - \epsilon_r}{\epsilon_r c^2} \Psi, \quad (27)$$

which is the equivalent of Equation 14 but at “population” level. In Equation 27,  $\rho_{\text{BH}}$  is the relic local mass density of SMBHs, estimated from galaxy number densities converted to SMBH number counts via any of the local scaling relations between SMBH mass and host galaxy property, such as stellar/bulge mass,<sup>219</sup> stellar velocity dispersion,<sup>220</sup> or even light profile<sup>221</sup> or host dark matter haloes.<sup>222</sup> The  $\Psi$  term in Equation 27 represents instead the integrated AGN emissivity across redshifts and (bolometric) luminosities. Along the years, the application of Equation 27 has yielded a wide range of values  $\epsilon_r \sim 0.06 - 0.30$ ,<sup>223-227</sup> mainly due to the still noticeable systematics in bolometric corrections,<sup>228</sup> SMBH scaling relations,<sup>226,229</sup> and AGN obscured fractions.<sup>225,227</sup>

Continuity equation models<sup>223,230-233</sup> can be considered as a “differential” generalization of Soltan’s argument. Given values of the radiative efficiency and the Eddington ratio distribution, the bolometric AGN emissivity at any time can be linked to the average growth rate of SMBHs of the corresponding mass, via a continuity equation describing the average mass “flow” of SMBHs of any given mass, and thus capable of predicting the time evolution of the global SMBH mass function  $n(M_{\text{BH}}, t)$ . This continuity equation is usually written as

$$\frac{\partial n(M_{\text{BH}}, t)}{\partial t} = - \frac{\partial [\langle \dot{M}_{\text{BH}} \rangle n(M_{\text{BH}}, t)]}{\partial M_{\text{BH}}}, \quad (28)$$

where  $\langle \dot{M}_{\text{BH}} \rangle$  is the average accretion rate averaged over the full population of black holes of mass  $M_{\text{BH}}$  at time  $t$ . Figure 6 shows an example of the SMBH mass function at different redshifts, as labelled, as predicted from Equation 28, giving in input the bolometric AGN luminosity function derived from X-rays,<sup>225</sup> and adopting an average value of the radiative efficiency  $\epsilon_r = 0.06$ . It is interesting to show that, without any specific fine-tuning, the continuity equation model is able to naturally generate a SMBH mass function that well aligns with the number density of local SMBHs at all masses. Allowing for a significant fraction of (dry) SMBH mergers in Equation 28 tends to overproduce the high-mass end of the SMBH mass function with respect to local data.<sup>224,232</sup> However, given the still unclear systematics in the SMBH scaling relations adopted to infer the local SMBH mass function,<sup>229,234</sup> and the uncertainties on the radiative efficiency and its dependence on SMBH mass,<sup>235</sup> no firm conclusions can be drawn yet on the importance of SMBH mergers in shaping the SMBH mass function along cosmic time. Continuity equation models have been further utilised to impose constraints on the mean Eddington ratio distribution characterizing SMBH growth in time. Several studies have suggested that mean Eddington ratio should be below unity<sup>236</sup> and progressively decreasing towards low redshifts<sup>224,232</sup> to accommodate the decreasing emissivity in the AGN luminosity function<sup>225</sup> and the local values of the observed fractions of AGN in galaxies.<sup>224</sup>

In a more general attempt to probe the coevolution of SMBHs and their host galaxies in a transparent, data-driven approach, several groups have included SMBHs in either semi-empirical models of galaxy evolution,<sup>226,237-240</sup> or by assigning galaxies and SMBHs at fixed redshift (ignoring evolutionary links) to de-

rive some basic properties on their number densities, clustering, and scaling relations.<sup>234,241–245</sup> Let’s start by reviewing the latter type of approach, which are particularly relevant to the creation of active and normal galaxy mock catalogs,<sup>246</sup> a vital component of the planning of imminent extragalactic surveys such as Euclid<sup>247</sup> and the Vera C. Rubin Observatory Legacy Survey of Space and Time (LSST).<sup>248</sup> In these more basic models, galaxies are first assigned via “abundance matching techniques”, based on the number equivalence between galaxy and dark matter number density counts, on top of N-body dark matter simulations.<sup>249–255</sup> SMBHs are then assigned to host galaxy/haloes by either assuming a direct scaling with the host dark matter haloes,<sup>237</sup> or via a relation with their host galaxies.<sup>234,240,243</sup> An example of this procedure is shown in Figure 7, in which an underlying scaling is assumed between SMBH mass and halo virial velocity of the type  $M_{\text{BH}} \propto V_{\text{vir}}^\alpha$ , through which the halo mass function is converted into a SMBH mass function and then into an AGN luminosity function via a mean Eddington ratio.<sup>237</sup> The plot reports the constraints on the radiative efficiency  $\epsilon_r$  and slope  $\alpha$  of the SMBH-halo relation derived from the matching with high-redshift AGN number counts. In other instances, the SMBH mass is bypassed and instead galaxies are directly assigned an X-ray AGN luminosity as extracted from a  $P(\lambda)$  Eddington ratio distribution as determined from X-ray and optical AGN surveys, which usually well approximated by a Schechter function.<sup>241,242</sup>

Full-fledged semi-empirical models (SEMs) are based on a cutting-edge “data-driven” methodology that avoids the modelling of galaxy and SMBH growth and assembly within dark matter haloes from first principles, as in the more traditional modelling approaches discussed in the previous Section. The main input parameter in SEMs is a monotonic relation between host galaxy stellar mass and its host halo mass (SMHM relation hereafter), which is derived from the equivalence between the cumulative number densities of galaxies and dark matter haloes. Applying these “abundance matching” techniques, one can assign galaxies to dark matter haloes in an N-body simulation at any specified redshift. Central galaxies along the main progenitor branches of their dark matter merger trees can be reinitialised via a time-dependent SMHM relation, and can also gradually transform their morphologies from discs to bulges via “in-situ” processes such as disc instabilities, or “ex-situ” processes such as mergers with other galaxies. Satellite galaxies are those associated via the SMHM relation to each dark matter branch merging to the main progenitor.<sup>257–259</sup> The SMHM relation is thus capable to convert a dark matter halo assembly history into a galaxy merger history. By using an epoch-dependent SMHM relation, it can be shown that one can predict the mean assembly and merger histories of galaxies,<sup>238,260–262</sup> along with their star formation histories, which are ultimately computed from the difference between the total growth and the contribution from mergers.<sup>263</sup> It is clear that the predicted merger and star formation histories will strongly depend on the input SMHM relation.<sup>264,265</sup> Alternatively, star formation histories can be fitted as a function of halo properties and integrated

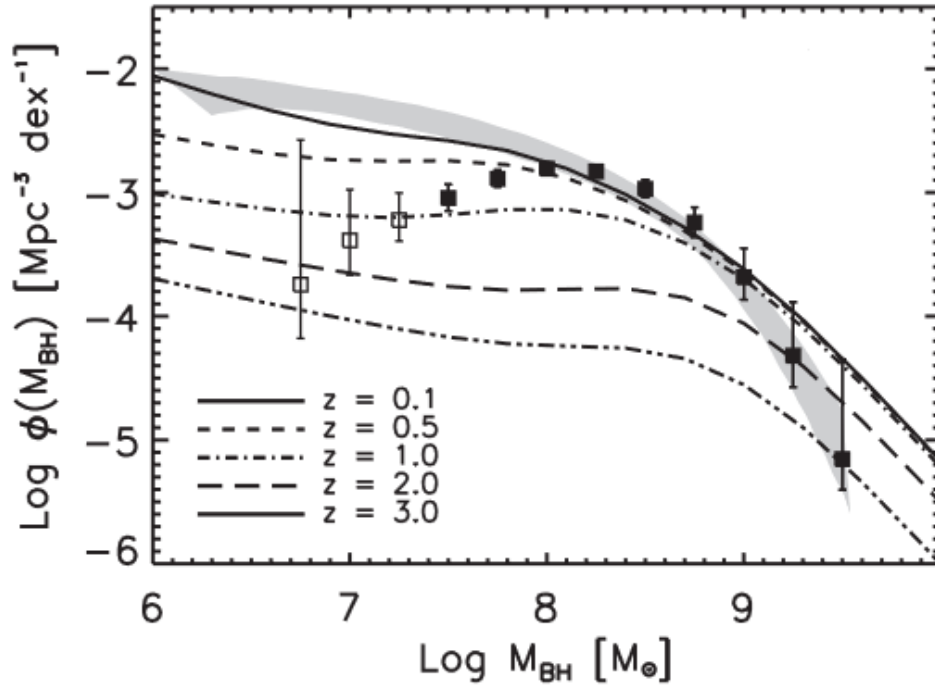


Figure 6. The SMBH mass function at different redshifts, as labelled, as predicted from the continuity equation models presented in Equation 28, assuming a mean radiative efficiency of  $\epsilon_r = 0.06$ , and compared to local measurements of the SMBH mass function (grey area<sup>231</sup> and data points<sup>256</sup>).

forward in time to derive, when coupled to the contribution from mergers, the full assembly histories of galaxies.<sup>266,267</sup>

In the context of a SEM, the growth and assembly histories of black holes can be derived in multiple ways. One of the most straightforward one is to adopt a monotonic mapping between galaxy properties and the mass of their central black hole, as informed by direct observations at different redshifts. For example, one could assume a constant or slowly-varying scaling between the black hole mass and the host galaxy stellar mass or stellar velocity dispersion,<sup>240</sup> and predict the rate at which black holes would grow in mass and merge following the assembly histories of their host galaxies and dark matter haloes.<sup>226,239</sup> Other groups have instead included some physically-motivated light curves of SMBHs into the merger histories of their host dark matter haloes/galaxies, to infer properties on, e.g., AGN luminosity functions,<sup>214,268–271</sup> AGN clustering,<sup>216,270,272,273</sup> SMBH merger rates and implied gravitational waves,<sup>274</sup> or more general galaxy properties.<sup>275</sup>

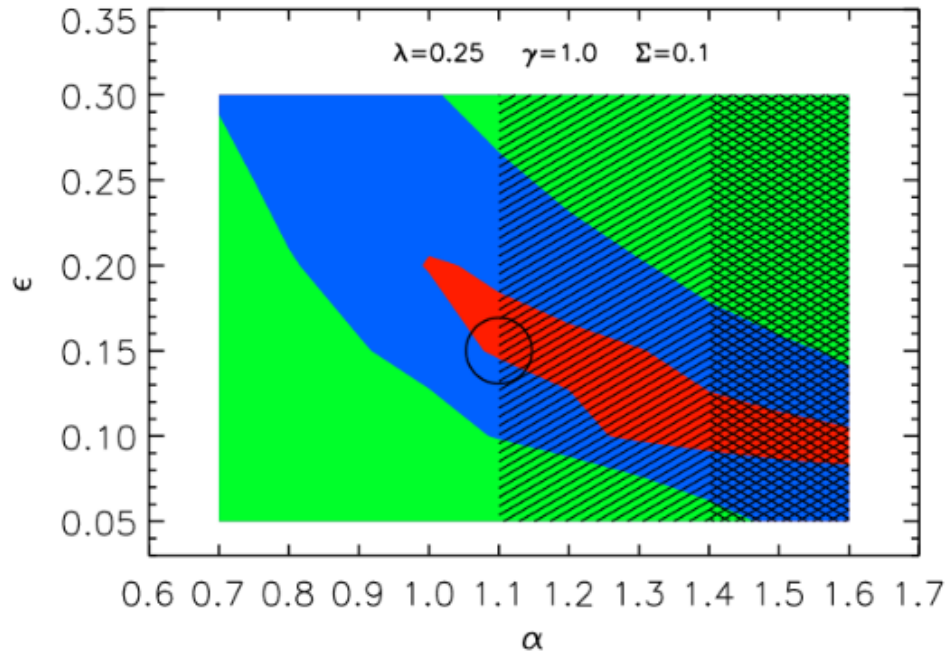


Figure 7. The  $\chi^2$  per degree of freedom as a function of the radiative efficiency and slope  $\alpha$ , the normalization of the  $M_{\text{BH}} \propto V_{\text{vir}}^\alpha$  relation, with other parameters fixed at the values listed on top of the panel. The blue and red areas define the regions where the  $\chi^2$  for the luminosity is below 3 and 1.5, respectively.

## 5. Model predictions across cosmic time

### 5.1. Large Volume Simulations: The first, rare quasars at $z > 6$

How the first supermassive black holes formed in the early Universe and evolved into the bright quasars, among the most luminous sources in the cosmos, is still an open question hotly debated by the community. In order to address it, one must simulate a large volume of the Universe, sufficient to include a statistical sample of bright quasars and their associated large scale structures, as well as having enough mass resolution to successfully model the physics and gas inflows close to black holes (the scales of an actual black hole accretion disk are still impossible to resolve in a fully cosmological simulations).

In Chap III, the authors focus more on the formation of the black hole seed populations and the physics of pristine gas on very small scales, which are typically not captured in large cosmological volume we discuss here. We are therefore focusing our discussion on what we can learn about the infall of gas on larger scales and subsequent growth of the central black hole seed.

In the current and coming decade, a new generation of astronomical instruments, all in the billion dollar class will start making observations of the Universe during the

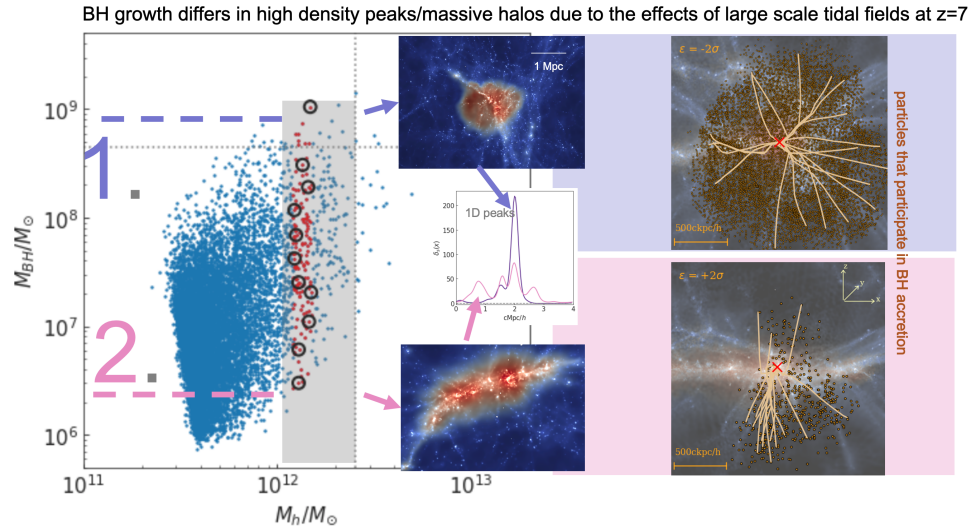


Figure 8. The BH masses as a function of halo mass in the BT simulation and examples of low and high tidal field environments for 5-sigma peaks at  $z = 7$ . The gray shaded area highlight the BH masses in 5-sigma@ peaks ( $10^{12} M_{\odot}$ ) halos. The BH mass in galaxies within these halos can range from  $10^6 M_{\odot}$  (example 2) to  $10^9 M_{\odot}$  (example 1). In the center the large scale environments of 1 and 2. On the left panel we show all the particles that end up contributing to BH accretion by  $z = 7$ . In region 1, a region of low tidal field, particles have accreted quasi-radially in region 2, of large tidal fields the only particles that accrete flow perpendicular to the main large scale density.

period of the first stars and quasars, and opening up the last frontier in astronomy and cosmology. Those that are specifically targeting this epoch as their highest priority include the Square Kilometer Array radio telescope, the NASA James Webb Space Telescope, and several huge ground-based telescopes, such as the Thirty Meter Telescope, the European Extremely Large Telescope, and the Giant Segmented Meter Telescope, each of which have collecting areas an order of magnitude larger than the current largest telescopes. The scientific community has obviously decided that research targeting the epoch of the first quasars and black hole formation and growth matters enormously. These observation and experiments will gain a lot of value if we have theories to test our models.

To decide which physical problem is best suited to which scale of computation one should consider both the space density of the relevant objects, which governs the size of the computational volume, and the mass resolution needed to follow the relevant small scale physical processes. In the case of the first quasars a volume of 1 Gpc/h is needed in order to have a statistical sample of at least 10 objects of the type seen at high redshifts by the Sloan Digital Sky Survey. The minimum mass resolution can be gauged using some smaller volume simulations that can be used to study convergence, i.e. carrying out cosmological simulations of black hole

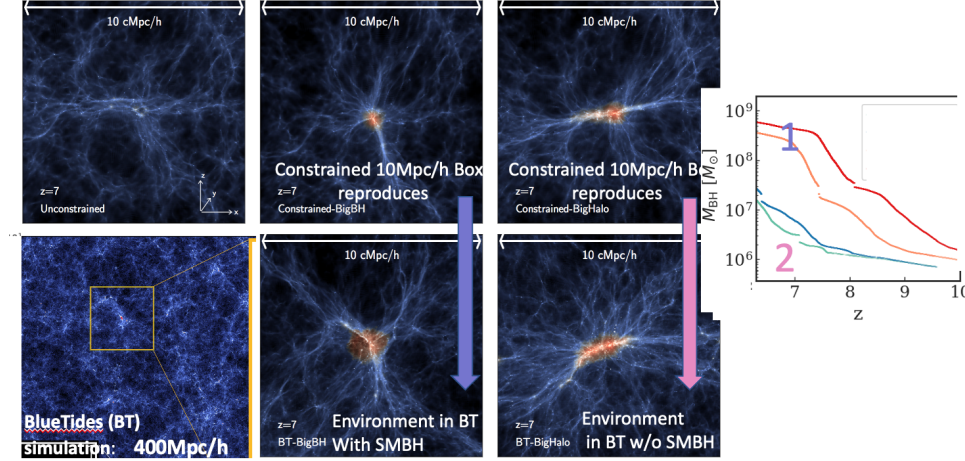


Figure 9. Illustration of the gas density field around the SMBH at  $z = 7$ . The top middle and top right panels are the simulations with constrained IC of 1 and 2 and using the peak parameter sets extracted from IC of BLUE TIDES 400Mpc/h simulation (in the corresponding bottom panels). The right panel shows the actual BH history in these two highly biased regions in constrained runs which match the exact results in BT.

formation with different particle masses.

At high redshifts the requirements are quite stringent, as galaxies are extremely compact, with sizes close to a few kpc in scale at best, and the structure and inflow within each galaxy needs to be resolved. This pushes the resolution requirements to only a few hundred parsec. With Peta and upcoming Exascale computational facilities this has just become possible: a qualitative advance, running, arguably, the first complete simulation (at least in terms of the hydrodynamics and gravitational physics) of the creation of the first galaxies and quasars in simulations at Gpc scales. This is one of the primary aims of the BlueTides simulation, which we use to discuss the emergence of the first quasars. BlueTides is the largest simulation yet run with full physics (hydrodynamics, star formation, black holes), and is targeted at the early Universe of galaxies and quasars. The simulation can be compared to cutting edge observations from the Hubble Space telescope, finding good agreement with the properties of observed galaxies when the Universe was only 10 percent of its current age ( $z \sim 6$ ).

#### The first quasars: high overdensity and low tidal field environment

With the recent high-resolution, large volume simulations we have been able to investigate directly the property of the environments/density field that causes the growth of the most massive black holes in the early Universe, and found that tidal fields in the large-scale (megaparsec and more) environments of black hole hosting galaxies play a critical role. The necessary growth (black hole mass in simulations at  $z = 6 - 7$  is consistent with the detection of highly luminous quasars at  $z > 6$ ) im-

plies sustained, critical accretion of material to grow and power them. Given a black hole seed scenario, it is important to understand which conditions/environments in the early Universe allow the fastest black hole growth. Large scale hydrodynamical cosmological simulations of structure formation allow us to explore the conditions conducive to the growth of the earliest supermassive black holes. We use the cosmological hydrodynamic simulation BlueTides, which incorporates a variety of baryon physics in a  $(400Mpc/h)^3$  volume with 0.7 trillion particles to follow the earliest phases of black hole critical growth.

At  $z > 6$  the most massive black holes (a handful) approach masses of  $10^9$  Msun with the most massive being found in an extremely compact spheroid-dominated host galaxy. Examining the large-scale environment of hosts, we find that the initial tidal field is more important than overdensity in setting the conditions for early BH growth (Figure 9). However necessary it is not sufficient. It is only in those high-density ( $4-5\sigma$  peaks of the density field) regions, in which large scale tidal fields are very suppressed that the BHs are able to accrete copious amount of 'cold' gas at a sufficiently fast rate. Only in low tidal field regions the gas falls along thin, radial filaments straight into the center forming the most compact galaxies and most massive black holes at earliest times. Equally high density region (massive halos) in high tidal field regions instead easily acquire large coherent angular momentum, providing most of the accretion perpendicular to the main large scale filament which significantly suppressed the early BH and galaxy growth (while influencing the formation of the first population of massive compact disks). This can be seen clearly in Figure 8 where the environment of the most massive black hole is visualized alongside a massive disk galaxy<sup>276,277</sup>

Recently effective techniques of constrained Gaussian realisations have been used and validated it in detail by comparing halo assembly histories (halo, stars, gas, and black hole growth) against large volume cosmological hydrodynamic simulations environments (Bluetides and ASTRID, see Figure 8 and Figure 9.<sup>278,279</sup>

The CR technique provides an efficient and powerful tool for generating the desired large-scale structures in cosmological simulations. It can be used to effectively simulate a particular region of interest, using a small volume, with a given large scale feature and learn about the impact of large scale structure on the smaller galaxy scales which regulate star and BH formation history. The technique works by generating ICs with imposed and precise constraints on the large-scale features of the primordial density field such as the height and shape of the density peaks, as well as the peculiar velocity and tidal field at the site of the peak, which fully represent the environments in that region of a large volume, statistically representative simulation. The theory of constrained random fields was first set forth by<sup>280,281</sup> and extended by<sup>282</sup> which is what our implementation is based on.

This technique is similar to, another common method of 'zoom-in' simulation, which is designed to completely reproduce a "user-selected" region (for example, a specific halo) from a low-resolution large volume simulation by tracing it back to the

IC. The CR simulation technique reproduces a statistical representation of that halo at the prescribed resolution (this will not be the same exact, extracted-halo as in a 'zoom-in') and it has far higher computational efficiency than zoom-in simulations. The demand in computational resources is very modest (factors on 1000 less than traditional zooms). One is able to carry out a systematic exploration to construct a sizeable suite of halo environments (with minimal computational effort) and run at high-resolution and with full physics. This method is already fully validated, and working and we have performed sets of 20-30 constrained simulations using the environments from BT in.<sup>278</sup> More work is upcoming using this technique to investigate different seed BH models and other different accretion prescriptions.

From the analytic side of cosmological models, several possibilities have been put forward to explain the growth of the first SMBHs,<sup>283</sup> which all require either super-Eddington accretion onto relatively small, stellar-like BHs,<sup>284–287</sup> and/or accretion onto relatively massive seed BHs of the order of  $10^3 - 10^5 M_\odot$ .<sup>25,288,289</sup> In more recent times, it has been highlighted that the migration and merging of stellar compact remnants (neutron stars and stellar-mass BHs) via gaseous dynamical friction toward the central high density regions of highly starforming (proto)galaxies, could potentially build up central BH masses of the order of  $10^4 - 10^6 M_\odot$ , within a few  $10^7$  yr, effectively providing heavy seeds before standard disk (Eddington-like) accretion takes over.<sup>290</sup> (Proto)stars can also migrate and merge quickly to yield a massive black hole seed via a supermassive star.<sup>291</sup> It has been shown via semi-analytic models simultaneously incorporating both light and heavy seeds BHs, that a gap can be generated in both the low end of the predicted BH mass and luminosity functions at  $4 \leq z \leq 6$ , mainly induced by the light BH seeds, which cannot “catch up” with the more massive counterparts unless super-Eddington accretion and/or enhanced accretion during mergers are invoked.<sup>292</sup>

## 5.2. Black Hole–Galaxy Scaling Relations

In the local universe, the discovery of close relationships between the masses of SMBHs and several properties of their bulges such as the stellar mass ( $M_{\text{BH}} - M_\star$  relation) and the velocity dispersion ( $M_{\text{BH}} - \sigma$  relation) have revolutionized our view of massive black holes, linking their growth to that of their host galaxy.<sup>132,133,293,294</sup> To understand the evolution of these relations at higher redshifts (mostly up to  $z \sim 2 - 4$ ), observational studies rely on galaxies with active galactic nuclei for which SMBH mass estimates use the virial method (see Chapter VI). Some of these studies find an evolution in which black hole growth precedes galaxy growth while other studies imply little or no evolution.<sup>295–300</sup> Systematic uncertainties in high redshift measurements are still large and come from both the method for black hole mass estimation and from measuring host galaxy properties.

A popular way to interpret these relationships is by assuming that SMBHs regulate their own growth and that of their hosts by coupling some (small) fraction of their energy output to their surrounding gas.<sup>126,153,154,301,302</sup> In this scenario,

black holes grow until AGN feedback is able to unbind a significant fraction of gas from the host galaxy, shutting down their own growth, inhibiting star formation, and driving the black hole–galaxy correlations. Other scenarios interpret the scaling relations as a consequence of mass averaging by hierarchical merging<sup>303–305</sup> or the result of a common gas supply for star formation and BH growth, regulated by gravitational torques.<sup>78,90,91,306,307</sup> The scaling relations of black hole mass and global properties of the host galaxies form a way to understand the importance and the effects of AGN fueling and feedback.

Many cosmological hydrodynamic simulations of structure formation (e.g. Horizon-AGN,<sup>14,15</sup> MassiveBlack-II,<sup>22,23</sup> Illustris,<sup>20,21</sup> IllustrisTNG,<sup>31,34,308</sup> EAGLE,<sup>18,309</sup> and SIMBA<sup>35,36</sup>) have been used to predict the black hole–galaxy scaling relations for representative populations of black holes and compare them to observational constraints at different redshifts. We show in Fig. 10 examples of the black hole mass–stellar mass relation derived from a sub-set of recent simulations, as presented in.<sup>140</sup> The detailed shape, normalization, and scatter depends on the specific subgrid black hole model but most simulations agree with the observed  $M_{\text{BH}}-M_{\star}$  relation at  $z = 0$ , partially reflecting the careful tuning of free parameters to match observations. The scatter in black hole mass at fixed stellar mass generally correlates with the specific star formation rate (sSFR) of their host galaxy, in agreement with observations.<sup>310</sup> The origin of the scatter is still not well understood, but a generic prediction of simulations is that overmassive black holes preferentially live in galaxies with lower sSFR due to the negative impact of AGN feedback. Some simulations show a systematic trend with redshift where the normalization of the  $M_{\text{BH}}-M_{\star}$  relation increases at higher redshift while other simulations show the opposite trend, but current models are generally consistent with no strong evolution in the scaling relations.

Despite the overall agreement of cosmological simulations, the main physical driver of the scaling relations is still not fully understood. Simulations implementing Bondi-like subgrid accretion<sup>15,21,76</sup> support the scenario of AGN feedback self-regulation, where the AGN feedback efficiency controls the normalization of the scaling relations. However, simulations implementing subgrid accretion driven by gravitational torques support a scenario where the scaling relations are the result of a common gas supply for star formation and black hole growth, where the black hole accretion efficiency (rather than feedback) controls the normalization of the scaling relations.<sup>35,36,63,78,90,91</sup> Cosmological simulations also often differ in their predictions at the low mass end of the scaling relations, where black hole growth is very sensitive to the specific numerical implementations of black hole seeding and dynamics. Recent simulations indicate that stellar feedback can also significantly suppress early black hole growth by efficiently evacuating gas from galactic nuclei,<sup>63,66,82,110,311–317</sup> which may explain observed undermassive black holes in low mass galaxies,<sup>318,319</sup> but the details depend on resolution and interstellar medium physics in the simulations.

Interestingly, simulations now have enough sophistication that we can mock up observations to the point that we can test the simulated population for possible selection biases in all types of observed relations<sup>23, 320</sup>. Indeed, we typically find that for samples selected on the basis of  $M_{\text{BH}}$  or  $M_*$  (and of size similar to those observed) the slopes can be steeper than for randomly selected samples. Such sample selection also biases toward finding stronger evolution with redshift than for a random sample as they tend to pick objects at the high-end of the relation (consistent with stronger evolution). This is relevant for some of the claims of evolution in the measurements.<sup>295, 296</sup> It is an interesting direction that simulations can indeed be used to pin down possible observational biases from actual physical evolution.

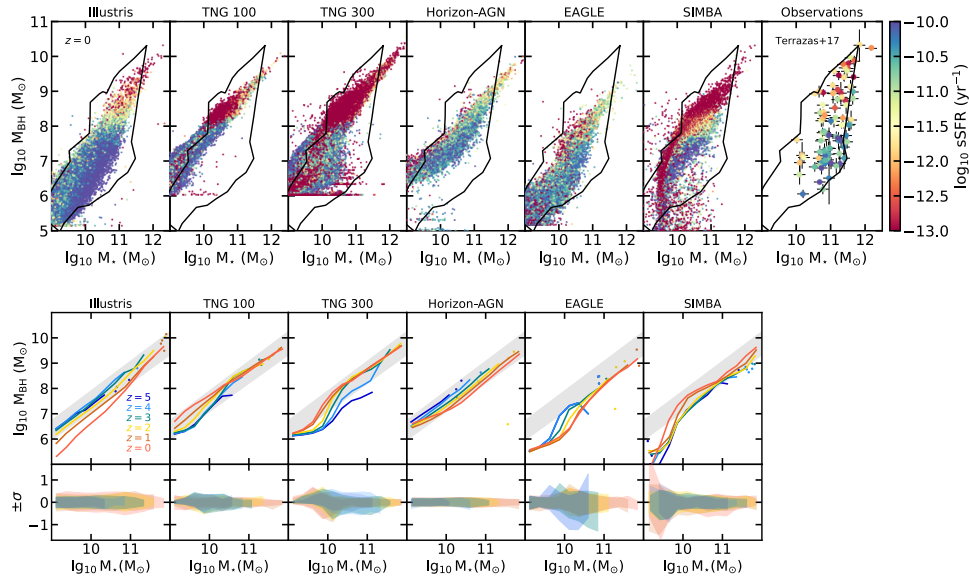


Figure 10. Correlations between black hole mass and host galaxy stellar mass predicted by several large-volume cosmological simulations (figures reproduced from<sup>140</sup>). The top panels show individual black holes color-coded by the specific star formation rate (sSFR) of their host galaxy. The black line indicates the region of the diagram occupied by the observational sample of<sup>294</sup> and the rightmost panel shows the observed star-forming and quiescent galaxies of.<sup>310</sup> Simulations generally agree with the observed  $M_{\text{BH}}-M_*$  relation at  $z = 0$  and the observed anti-correlation of black hole mass and sSFR at fixed stellar mass (indicative of the negative impact of black hole feedback). However, the detailed shape, normalization, and sSFR connection in the predicted scaling relation depends on the specific subgrid black hole model. The bottom panels show the redshift evolution of the median  $M_{\text{BH}}-M_*$  relation for the same simulations (and the 15-85th percentile of the distributions). The grey shaded area indicates the range of variation between several best-fit observed relations.<sup>132, 293, 321</sup> Some simulations show a systematic trend for higher black hole to galaxy mass ratio at higher redshift while others show the opposite trend, but current models are generally consistent with no strong evolution in the  $M_{\text{BH}}-M_*$  relation.

### 5.2.1. *Semi-empirical models*

In a semi-empirical approach, SMBHs are often included using a SMBH-galaxy scaling relation,<sup>240</sup> thus the latter cannot be defined as a true prediction of the model, though it is possible to still test, for example, how much SMBH mergers can influence the shape and or scatter of a given input SMBH mass-galaxy mass relation.<sup>322</sup> In many instances, SMBHs have been included by adopting empirical or theoretically motivated relations between the SMBH accretion rate and the host galaxy stellar mass or star formation rate,<sup>226,239,245</sup> or by directly including the SMBH light curve during, e.g., galaxy mergers.<sup>270,271,275</sup> In most cases, when integrating forward in time the cumulative accretion rates, the relic SMBH masses appear to be linearly correlated with their host galaxy stellar mass, where the normalization of the relation is mostly controlled, as expected, by the chosen input radiative efficiency  $\epsilon_r$ . Recent work<sup>239,323</sup> showed that the ratio between SMBH accretion rate, as traced by the X-ray AGN luminosity, and the SFR in the host galaxy, does not evolve with redshift, although it depends on stellar mass. When combining the mean black hole accretion rate as a function of stellar mass and redshift with empirical models of galaxy stellar mass growth<sup>266</sup> and integrating over time, the resulting  $M_{\text{BH}} - M_*$  relation appears to be nearly independent of redshift,<sup>226,239,245,323</sup> indicating that stellar and black hole masses grow, on average, at similar rates, a conclusion supported by several independent studies on the scaling relations of AGN at different redshifts and luminosities.<sup>324-326</sup> An example of this procedure is shown in Figure 11, where the resulting  $M_{\text{BH}} - M_*$  relation, obtained from direct integration of the SMBH accretion rate along each stellar mass accretion track, is plotted for two different values of the mean radiative efficiency, as labelled, and compared with different determinations of the  $M_{\text{BH}} - M_*$  from local SMBHs. Similar approaches have also been applied to the  $M_{\text{BH}} - \sigma$  relation, showing evidence<sup>327,328</sup> for a negligible evolution of the latter up to, at least,  $z \sim 2$ .

### 5.3. *The Black Hole mass function and AGN luminosity functions*

Even though the QLF has been studied for over 30 years, we still do not understand the fundamental physical parameters that regulate its shape and evolution. Ultimately the evolution of the quasar luminosity function (QLF) is one of the basic cosmological measures providing insight into structure formation and its relation to black hole growth. The QLF is typically described by two power-law components: flatter and steeper at the faint and bright end respectively, and with a break luminosity that evolves with redshift (luminosity density evolution). The bright-end slope also appears to evolve becoming flatter at the highest redshifts ( $z = 5 - 6$ ), although the most recent measurements are hinting that this may not be the case<sup>331, 332</sup>.

Theoretical investigation of the QLF has been done using semi-analytical models or halo models. Since, by construction, these models do not self-consistently follow

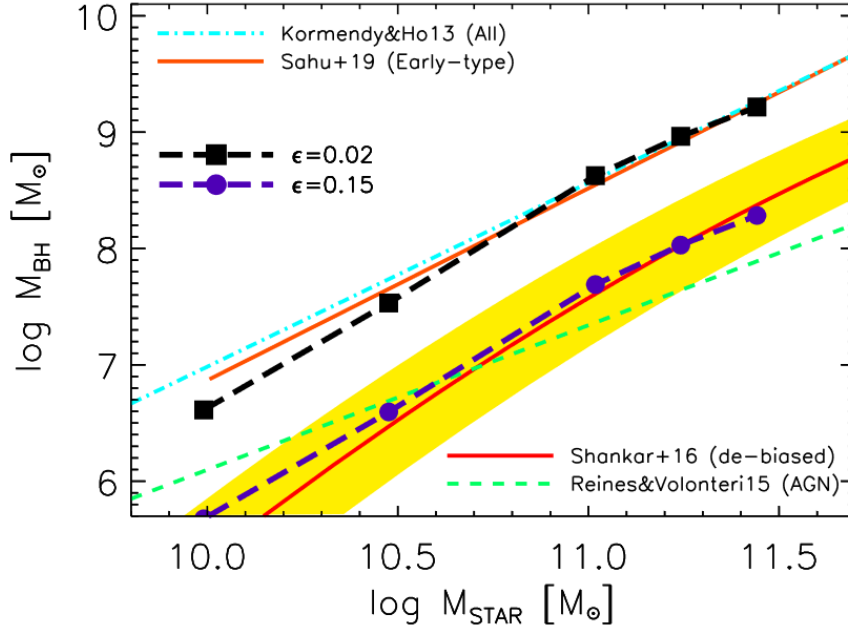


Figure 11. Correlations between central black hole mass and host galaxy total stellar mass in the local Universe.<sup>132,229,329,330</sup> The solid red line with its scatter (yellow region) is the de-biased  $M_{\text{BH}} - M_{\star}$  relation.<sup>229</sup> The green dashed line is the fit to the local AGN.<sup>330</sup> Also included are the predicted average black hole mass as a function of host stellar mass at  $z = 0.1$  for two different values of the radiative efficiency, as labelled. Values of  $\epsilon \sim 0.02$  are required (black long-dashed with filled squares) to match the normalization of the raw black hole  $M_{\text{BH}} - M_{\star}$  relation for local dynamically measured quiescent black holes.

black hole growth, the quasar lightcurves (and luminosities) have to be calculated via imposed prescriptions and a number of parameters are introduced for quasar triggering, quasar lifetimes etc. So while these models offer more flexibility for testing a variety of reasonable prescriptions and have produced promising results it is still ideal to complement these approaches with detailed hydrodynamic simulations. For example, in Figure 12 we showed a particular a view of two regions that contain two massive BHs but with very different accretion histories, black hole masses and luminosities. In particular, these frames show the underlying distribution of gas (color coded by temperature, red is hot and blue cold) with stars (in white) and black holes indicated by the diffraction spikes whose size is scaled by the QSO luminosity. Many things are evident from this picture. For example there is a clear distribution of quasar luminosities related to large scale properties, and effects of BH feedback (clearly seen as hot gas around the BHs). The same mass halos, can be found in different large scale environments hosting dramatically different AGNs. (see also Fig. 12). We see clearly that the effects modeled in the simulations also directly provide for each BH a detailed prediction of its full lightcurve across cosmic

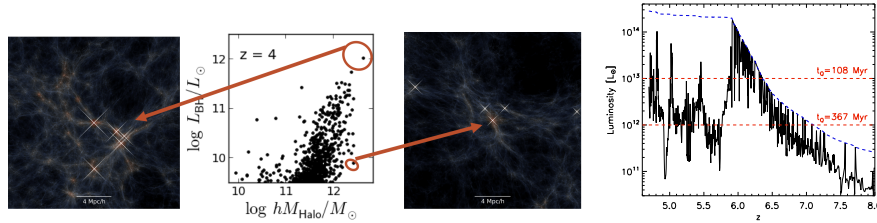


Figure 12. Left: An example environment of quasars in simulations. Two galaxies are shown, along with their location in the scatter plot of BH mass vs halo mass. Both halos have a mass  $\sim 10^{12} M_{\odot}$ , but have experienced very different gas inflow and hence black hole growth. Right: An example of a bolometric lightcurve (over a selected redshift range to show details) from the bright quasar in the left panels. The dashed blue line shows the Eddington luminosity and the red quasar lifetimes at corresponding luminosities.

history with high time resolution. This is directly predicted by the interaction of the cosmological gas supply and resulting BH feedback. An example of a lightcurve and the predictions of the associated luminosity functions derived from such a population is shown in Fig 12 (in black).

If we relate this to the QLFs, while the bright end QLF may inform us about feedback, the faint-end where BHs are already mostly self-regulated, should inform us about gas supply. In our simulations we typically find that although the low (high) luminosity ranges of the faint-end QLF are dominated by low (high) mass black holes, a wide range of black hole masses still contributes to any given luminosity range. The faint-end of the QLF can indeed be formed by quasars radiating well below their peak luminosities, rather than by quasars with low peak luminosities. This is consistent with the complex lightcurves of black holes, which show that any given black hole can undergo significant changes in its luminosity and hence (while its mass always grows) it can occupy different parts of the LF. The complex light curve, and the resulting effects on the LFs are a result of the detailed hydrodynamics followed in the simulations.

Fig. 13 shows examples of the black hole mass function, the typical Eddington ratio of AGN as a function of redshift, and the evolution in the comoving number density of AGN derived from a sub-set of recent simulations and presented in.<sup>140,333</sup> As in Fig. 10, here we compare predictions from Horizon-AGN,<sup>14,15</sup> Illustris,<sup>20,21</sup> IllustrisTNG,<sup>31,34,308</sup> EAGLE,<sup>16,18</sup> and SIMBA.<sup>35,36</sup> Cosmological hydrodynamic simulations generally agree in the overall build up of the black hole mass function over time and are in good agreement with constraints from population synthesis models. This reflects the overall agreement in the predicted black hole–galaxy scaling relations and the evolution of the stellar mass function, which are primary observational targets to match in simulations and often used to constrain the subgrid parameters that control the efficiency of stellar and black hole feedback.

While detailed black hole accretion histories depend on each specific model, most simulations agree between them and with observations on the overall redshift

dependence of the median Eddington ratio of AGN. Active black holes typically accrete gas at high Eddington ratios at early times ( $z \sim 4$ ) and decrease their specific growth rates at lower redshift, mimicking the overall decline in the specific star formation rate of galaxies.<sup>91,306,334–337</sup> Cosmological simulations are also used to predict the evolution in the number density of AGN at different luminosities, as illustrated in the bottom panels of Fig. 13. Most simulations agree in the overall shape of the number density evolution (roughly in agreement with observational constraints), with increasing number density of AGN (of any luminosity) at early times and decreasing number density at lower redshifts. However, the amplitude and the redshift at which the maximum number density is reached can vary significantly from simulation to simulation.<sup>333</sup> Some models reproduce the observed “downsizing” effect, with brighter AGN reaching their peak number density at earlier times and fainter AGN becoming more abundant at later times.<sup>338,339</sup>

Continuity equation models have provided significant contribution in unveiling the evolution of the SMBH mass function, its duty cycle, and overall Eddington ratio distribution.<sup>223,232,343–348</sup> The main results from these studies can be summarised as follows. The overall SMBH mass function growth via gas accretion is sufficient to fully reproduce the local SMBH mass function extracted from SMBH-host galaxy scaling relations. The impact of SMBH-SMBH mergers has the natural effect of increasing the the high-mass end of the SMBH mass function, which can then be reconciled with the high-mass end of the local SMBH mass function via an increased radiative efficiency at high SMBH mass. The observed AGN fractions at low redshift requires a characteristic Eddington ratio  $\lambda_c$  that declines at late times, and matching observed Eddington ratio distributions requires a  $P(\lambda)$  that broadens at low redshift. To reproduce the observed increase of AGN fraction with black hole or galaxy mass, the  $\lambda_c$  that decreases with increasing SMBH mass, reducing the AGN luminosity associated with the most massive SMBHs.

#### 5.4. Quasar Clustering

Clustering measurements provide the means to better understand the relation between quasars, their hosts and the underlying dark matter distribution, as well as to allow estimates of quasar lifetimes once coupled with QLF constraints, e.g.,<sup>352, 353</sup> With clustering we learn about the co-evolution of quasars, mergers. For example, strong clustering would suggest that quasars should reside in massive halos. If so, they should be rare and in order to reproduce the quasar luminosity density, they must have long lifetimes. Conversely, low spatial correlations would suggest more common quasars, and thus shorter quasar lifetimes.

##### Large Scale Clustering

The large scale quasar clustering properties are quantified with the quasar bias, which is defined as the square root of the ratio of the two-point correlation function of the quasars to that of the dark matter. Comparing it with the bias of DM halos predicted by, for example, Sheth et al. (2001), the typical DM halo mass

Massive black holes in galactic nuclei - theory/simulations

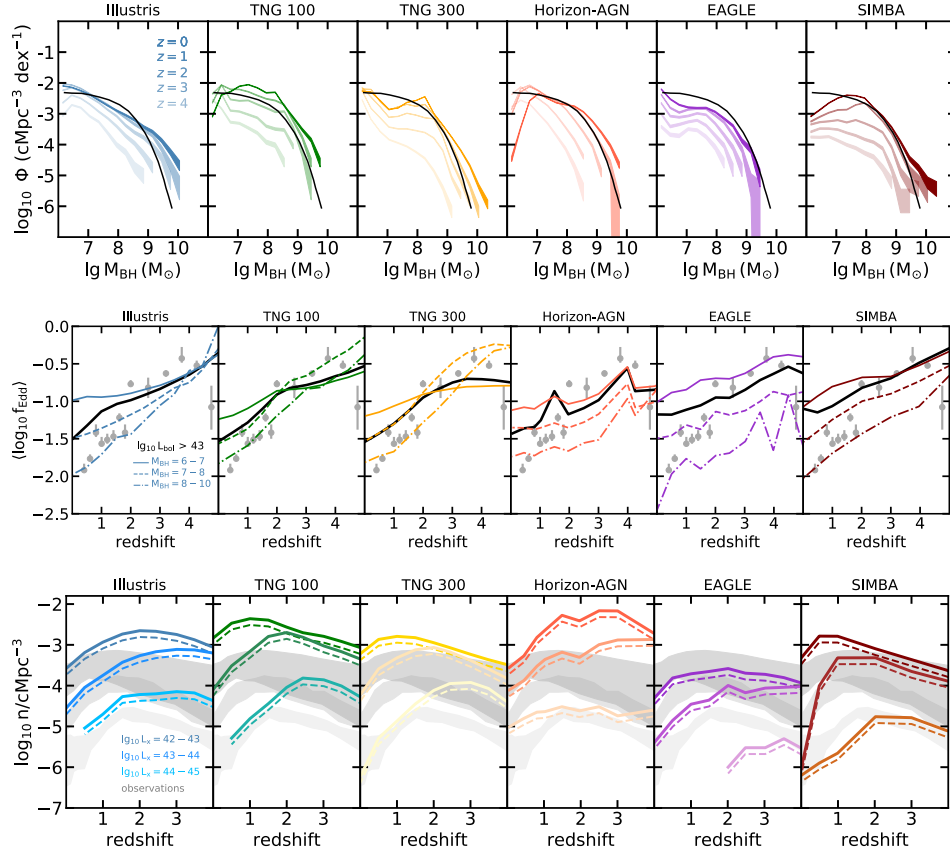


Figure 13. Redshift evolution of the black hole mass function (top), the median Eddington ratio (middle), and the comoving number density of AGN of different hard X-ray luminosities (bottom) as predicted by several large-volume cosmological simulations (figures reproduced from<sup>140,333</sup>). Simulations are compared against the black hole mass function at  $z = 0.1$  from the population synthesis model of<sup>340</sup> (black line; top panel), the observational constraints on Eddington ratios from<sup>341</sup> (grey points; middle panel), and the observed hard X-ray luminosity functions of<sup>338,339,342</sup> (dark-to-light grey bands corresponding to increasing luminosity ranges; bottom panel). Simulations qualitatively agree on the overall shape and build up of the black hole mass function, the decreasing median Eddington ratios at lower redshifts, and the early increase of AGN number density followed by a decline at low redshift, roughly following observational constraints.

of the quasars is derived (see Figure 7 for one recent example). The clustering properties have been reported using some large-scale surveys. Simulations have been used to compare to constraints on clustering showing that quasar hosts at high- $z$  are consistent with the level of the observed quasar clustering bias for  $10^{12} - 10^{13} M_{\odot}$  halos. This is an important starting point which gives us some confidence to further pursue lower redshifts—towards the peak epoch of quasar activity and overlap with the and other upcoming quasar surveys

Because of the detailed information and lightcurves and QLF we have from the

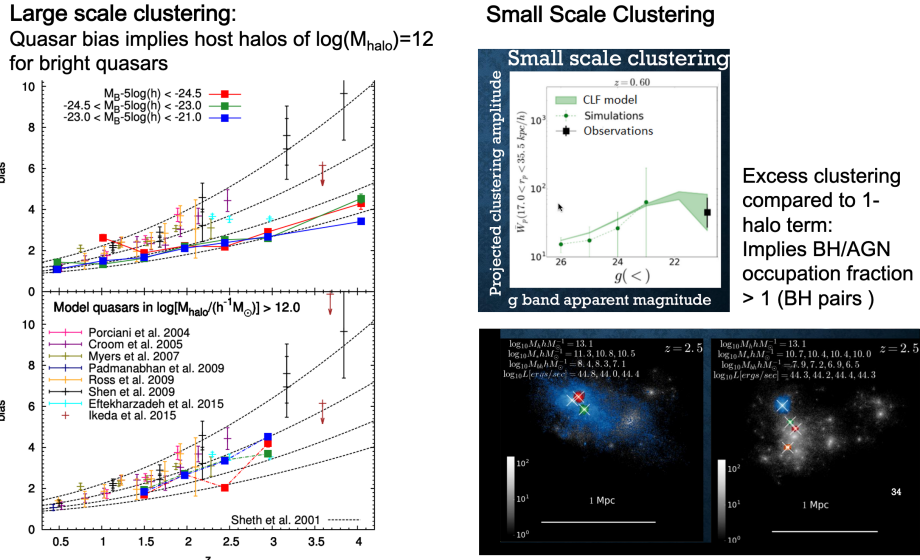


Figure 14. Left: From<sup>349</sup> Redshift evolution of the bias of bright intermediate and faint quasars (from<sup>350</sup>). The dashed lines are halo bias factor evolution for fixed halo mass of  $\log[M_{\text{halo}}/(h^{-1} M_{\odot})] = 11.5, 12.0, 12.5$  and  $13.0$  from bottom to top, respectively, using the Sheth et al. (2001) fitting formula with the Planck cosmology. Observational results are also plotted (plus signs and error bars). Bottom: the same as the top panel, but for only model quasars which are hosted DM haloes ( $M_{\text{halo}} \gtrsim 10^{12} h^{-1} M_{\odot}$ ). Credit Oogi et al. 2016. Right: From<sup>351</sup> Small scale clustering measurements and predictions from simulations.  $W_p$  is the volume-averaged projected correlation function averaged over  $17.0 < r_p < 36.6$  kpc/h for quasars brighter than a given magnitude threshold, which we denote by ‘g(i)’. The dashed lines correspond to predictions from the simulations. The black squares correspond to the observational constraints at  $g = 20.85$ . Below, examples of systems of quasar pairs and triplets that give rise to the enhanced clustering.

simulations we can directly derive host halo masses for a given luminosity range and translate that into predicted quasar clustering as a function of  $z$  or luminosity. from the ongoing BOSS and upcoming eBOSS analyses and pushing large volume simulations all the way to  $z = 2$ , clustering as a function of luminosity should be able to discriminate between different models, and directly constrain duty cycles and the effects of gas inflows and feedback in regulating quasar active phases.

**Small Scale Clustering**

In addition to large scale behavior, the possibility of excess quasar clustering on small scales has arisen in several recent studies. While some observed quasar pairs are believed to be the result physically distinct quasar binaries (double nuclei), which would suggest quasars cluster much more strongly on small scales than extrapolation of large scale clustering would imply, indication perhaps direct evidence for connection between galaxy mergers and quasar activity Several recent studies have managed to probe even smaller scales, where they do indeed find (some level) of excess.

Small scale clustering measurements for AGNs/quasars have been also been significant interest over the last two decades as they may constrain signatures of the physical processes that trigger AGN activity, such as galaxy mergers and the related efficiency of BH mergers resulting from presence AGN pairs, triplets etc in the center of galaxies. Over the last 20 years the small-scale clustering of quasars, mainly from the SDSS and 2dF-QSO surveys, at scales ranging from  $\sim 10$  kpc to  $\sim 1$  Mpc. Cosmological hydrodynamic simulations are valuable tools to study AGN clustering (see Figure 14<sup>351</sup>). Large volume hydrodynamic simulations are invaluable tools to study properties of AGN and quasar populations. Simulations currently indicate that the excess small scale clustering is due to quasars pairs likely correspond to extremely luminous quasars in satellite galaxies which are triggered by galaxy mergers.<sup>351,354</sup> Multiple sequence of such galaxy mergers can also lead to formation quasar triples and quadruples. Several detections of such exotic systems have been made in the recent past.<sup>355,356</sup>

#### 5.4.1. *Semi-empirical models*

From the semi-empirical approach, significant insights have become available in the last years in relating the clustering of AGN and their hosts, to the physical properties of their central SMBHs.<sup>234,242,243</sup> It has been shown that model validation is often affected by degeneracies when comparing theoretical predictions and observational data, with the same AGN number densities and spatial distributions being reproduced by radically different models.<sup>243</sup> However, recent work has also shown that, although multiple parameters are responsible for shaping SMBH demography through time, they all play different roles in generating different observables. For example, the stellar mass-halo mass relation can be constrained by the large-scale clustering as a function of stellar mass, because the spatial distribution of AGN in relatively narrow bins of stellar mass is largely independent of, e.g., the level and frequency of AGN activity in the host galaxies, at least in the limit in which AGN hosts are a random subsample of all galaxies of similar stellar mass. On the other hand, the AGN large-scale bias as a function of SMBH mass can be used to constrain the normalization and shape of the scaling relation between SMBH mass and host galaxy stellar mass.<sup>234</sup> Observational constraints on the AGN duty cycle can then be derived from the comparison of the model predictions with the measured AGN large-scale bias as a function of AGN luminosity. Finally, the combination of the AGN luminosity function and of the specific accretion rate distribution<sup>241</sup> allow to constrain the input Eddington ratio distribution and duty cycle. Additional observables can be considered, such as the average correlation between X-ray luminosity and host galaxy stellar mass/star formation rate in sample of active galaxies to constrain the mean Eddington ratios in AGN.<sup>245</sup> Figure 15 provides the different steps that one needs to follow to create a robust and realistic mock catalog of AGNs avoiding the risk of strong degeneracies, showing that the starting point is the large-scale clustering (bias  $b$ ) as a function of galaxy stellar mass, SMBH

mass, and AGN luminosity, with additional, complementary constraints offered by the AGN luminosity function, the relative fraction  $f_{\text{SAT}}^{\text{AGN}}$  of satellite AGN in groups and clusters, and the specific accretion rate distribution  $P_{\text{AGN}}$ .

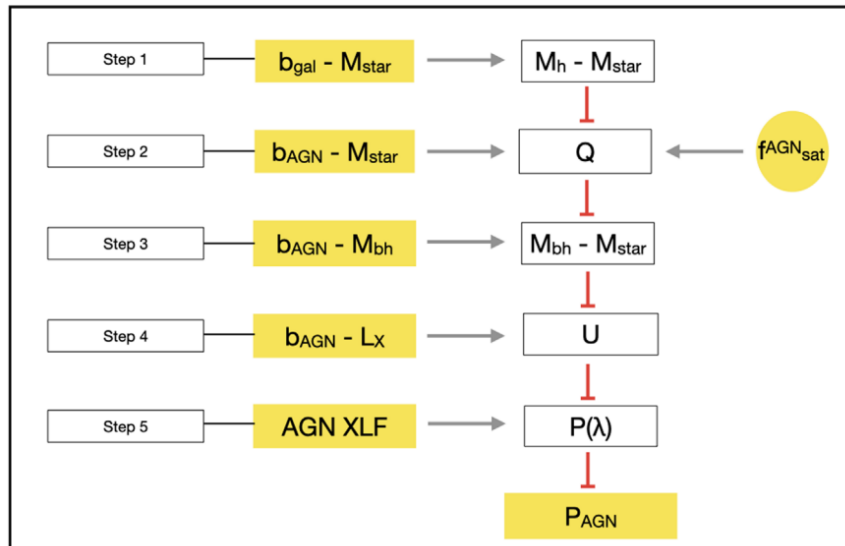


Figure 15. Sketch of how to build realistic AGN mocks. The dependence of each observable on one or a few input model parameters (open black boxes) is shown as red lines. From the comparison of observationally derived relations and the AGN mock catalog predictions, we can constrain (gray arrows) the input parameters. Additional observables, such as the fraction of satellite AGNs (filled yellow circle), can help in breaking the degeneracies among the input model parameters.

### 5.5. AGN feedback and cosmology

AGN feedback is key for reproducing the global evolution of the stellar mass function and galaxy luminosity functions.<sup>357</sup> Simulations are also able to firmly predict the quasar bias across scales. The newest surveys coupled with these predictions will allow us to determine how quasars probe large scale structure from very small scales to Cosmic Microwave Background scales, which will be important for planning future surveys.

Current and forthcoming cosmological experiments such as Dark Energy Spectroscopic Instrument,<sup>358</sup> Dark Energy Survey,<sup>359</sup> Rubin Observatory’s Legacy Survey of Space and Time (LSST),<sup>360</sup> the Roman Space Telescope,<sup>361</sup> and Euclid<sup>362</sup> rely on observed galaxy properties to constrain the properties of dark matter and dark energy with increasing accuracy. The fundamental challenge is that galaxy formation involves a complicated blend of different physical processes that is non-linearly coupled on a wide range of scales, leading to extremely complex dynamics. The required percent level accuracy to extract cosmological information from future

surveys can only be reached through a much better understanding of galaxy formation in direct cosmological hydrodynamic simulations. Massive black holes are one of the most important pieces of baryonic physics that we need to understand for constraining dark energy with upcoming weak lensing surveys. AGN feedback can potentially spread baryons over multi-Mpc scales,<sup>38</sup> but the effects of AGN feedback on cosmological observables depend heavily on calibration from simulations.

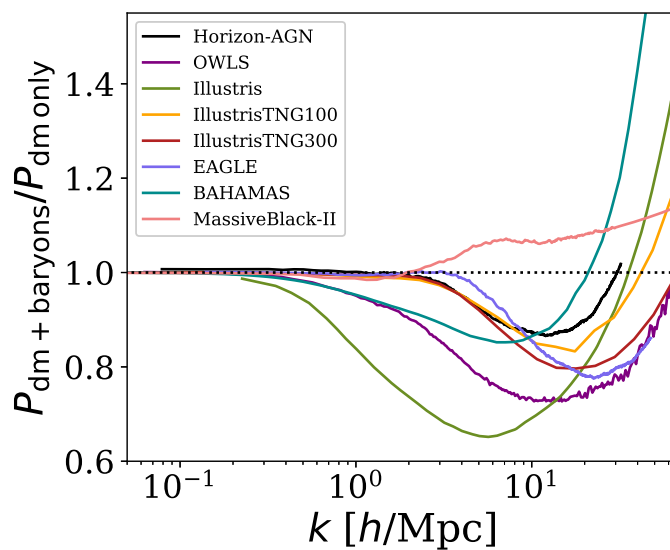


Figure 16. Ratio of total matter power spectrum at  $z = 0$  in different cosmological hydrodynamic simulations to that of the corresponding dark matter-only simulations (figure reproduced from<sup>363</sup>). The inclusion of baryonic physics increases the power on small scales relative to dark matter-only simulations owing to gas cooling and star formation, while generally suppressing power on large scales owing to the redistribution of gas and dark matter due to feedback processes.

As an example, Fig. 16 illustrates the importance of galaxy formation modeling in cosmology by comparing the impact of baryonic physics in the total matter power spectrum at  $z = 0$  as predicted by different cosmological hydrodynamic simulations.<sup>363</sup> Predicted power spectra differ substantially from expectations based on dark matter-only simulations on a range of scales probed by cosmological surveys ( $k \gtrsim 0.1 h \text{ Mpc}^{-1}$ ). Most simulations agree qualitatively on the overall impact of baryonic physics. Gas cooling and star formation increase the power on small scales relative to dark matter-only simulations while feedback processes suppress power on larger scales by ejecting gas out of halos, with the overall redistribution of baryons affecting also the dark matter component via back-reaction effects.<sup>42,363–369</sup> However, there is significant uncertainty in theoretical predictions, as indicated

by the large quantitative differences between simulations.<sup>42,363,369</sup> Some models predict a suppression of power of  $\gtrsim 30\%$  at wave numbers  $k \sim 10 h \text{Mpc}^{-1}$  while others predict  $<10\%$  suppression (or even enhancement of power) on similar scales. Effects on the power spectrum of this size must be accurately taken into account in order to achieve precise constraints on dark energy through missions such as Euclid or Rubin-LSST. As Fig 16 shows, the changes in the dark matter power spectrum induced by AGN feedback are of the same order of magnitude as those due to a different cosmological models.<sup>368</sup>

Comprehensive studies of the impact of quasar-mode and radio-mode feedback in full cosmological semi-analytic models<sup>188,192,194,195,200,202,206,210</sup> have been performed using a variety of recipes for both accretion and feedback inspired by both hydrodynamic simulations<sup>370</sup> and analytic models.<sup>179,371</sup> First off, the inclusion of a light curve in SAMs to modulate accretion onto the central SMBH,<sup>207,209,213,214</sup> provides a more extended, delayed triggering of the SMBH, and an improved match to the AGN luminosity function, especially at the faint end, and possibly to the large-scale clustering as a function of AGN luminosity. In the latest renditions of SAMs, the accretion onto the central SMBH is not only related to galaxy mergers, but to any event, e.g., disc instabilities or galaxy interactions<sup>206,372</sup> that can generate loss of angular momentum in the gas and contribute to the reservoir of low angular momentum feeding the central SMBH. The main prominent consequence of the inclusion of quasar-mode or radio-mode AGN feedback in SAMs has been to reduce the number densities of massive galaxies.<sup>188,192</sup> However, the inclusion of more refined AGN feedback recipes in SAMs in more recent times has revealed a plethora of additional interesting features that could be observationally testable.<sup>373</sup> In some instances, the star formation rates tend to decrease at fixed stellar mass, and the amount of ejected material instead increases, whilst maintaining a low level of star formation in the most massive galaxies at all times, although in tandem with the effect of stellar feedback.

### **5.6. Massive Black hole Binaries, Mergers and Gravitational Waves**

While black holes grow predominantly via accretion, a second mode of black hole growth is through mergers which occur when dark matter halos merge into a single halo, such that their black holes fall toward the center of the new halo, eventually merging with one another. Mergers of massive black holes are then a natural consequence of our current hierarchical structure formation paradigm. In much of what has been discussed in this chapter and in our current understanding, massive black holes form and reside at the centers of galaxies and hence they grow and merge closely intertwined with their host galaxies. The presence of luminous quasars observed within the first billion years of the Universe highlights that the black hole seeds for the massive black hole population were assembled at the cosmic dawn, concurrently with the time of the formation of the first galaxies. In our standard

$\Lambda$ CDM cosmology cosmic structure formation occurs hierarchically by the continuous merging of smaller structures and accretion of surrounding matter. SMBHs growth and evolution is expected to follow a similar process in which black hole seeds grow both through accretion and mergers with other BHs.

The upcoming Laser Interferometer Space Antenna (LISA)<sup>374</sup> mission will be sensitive to low-frequency ( $10^{-4} - 10^{-1}$  Hz) gravitational waves from the coalescence of MBHs with masses  $10^4 - 10^7 M_{\odot}$  up to  $z \sim 20$ . At lower frequencies, Pulsar Timing Arrays (PTAs) are already collecting data and the Square Kilometer Array (SKA) in the next decade will be a major leap forward in sensitivity. While MBH binaries are the primary sources for PTAs and LISA, these two experiments probe different stages of MBH evolution. PTAs are most sensitive to the early inspiral (orbital periods of years or longer) of nearby ( $z < 1$ ) massive ( $M_{\text{BH}} \gtrsim 10^8 M_{\odot}$ ) sources.<sup>375</sup> In contrast, LISA is sensitive to the inspiral, merger, and ringdown of MBH binaries at a wide range of redshifts<sup>376</sup> and from smaller sources ( $M_{\text{BH}} \in [10^4 M_{\odot}, 10^7 M_{\odot}]$ ).

In the last decade major efforts have been made to predict the event rate of GWs in the frequency band of LISA,<sup>377, 378</sup> These predictions range from a few to a few hundred events per year, depending on the assumptions underpinning the calculation of the SMBHs coalescence rate. Early works derived the SMBH coalescence rate from observational constraints such as the observed quasar luminosity function, whilst more recent studies have utilised semi-analytical galaxy formation models and/or hybrid models that combine cosmological N-body simulations with semi-analytical recipes for the SMBH dynamics.<sup>379-384</sup>

In contrast to semi-analytic models, hydrodynamical simulations follow the dynamics of the cosmic gas by direct numerical integration of the equations of hydrodynamics, capturing non-linear processes that cannot be described by simple mathematical approximations. Hence a more complete and consistent picture of the evolution of SMBHs and their host galaxies can be obtained.

Predicting SMBH mergers inevitably involves following a variety of complex physical processes that cover many orders of magnitude in physical scale. Black hole mergers occur at sub-parsec scales when two galaxies within large dark matter halos are driven together by large scale gravitational forces that drive the formation of the cosmic web at  $> \text{Mpc}$  cosmological scales. After the galaxy merger, the central SMBHs are brought near the center of the main halo due to dynamical friction against the dark matter, background stars, and gas. Eventually the final SMBH merger occurs via the emission of GWs. For reviews of SMBH dynamics in galaxy mergers we refer to<sup>385, 386, 387</sup> The dynamical evolution of the SMBH binary is expected to happen fast (coalescence timescale 10-100 Myrs) in gas rich environments, thanks to the efficient dissipation of angular momentum and energy from the binary. Conversely, three-body interactions slow things down in gas poor systems (leading to coalescence timescales  $\sim \text{Gyrs}$ ).

Newly developed, large volume hydrodynamic cosmological simulations self-

consistently combine the processes of structure formation at cosmological scales with the physics of smaller, galaxy scales and thus capture our understanding of black holes and their connection to galaxy formation on many relevant scales. They thus provide a good tool for predicting for MBHB merger rates. These simulations directly associate MBH binaries with their host galaxies, and they are carried out in large enough cosmological volumes to provide the statistical power to make merger rate predictions across cosmic time which are crucial for the upcoming observations.

In order to accurately predict when MBH mergers occur in these simulations, one must account for the orbital decay and binary hardening timescales in a wide dynamical range. During galaxy mergers, the central MBHs start at large separation in the remnant galaxy (as much as a few tens of kpc). These MBHs then gradually lose their orbital energy and sink to the center of the remnant galaxy due to the dynamical friction exerted by the gas, stars, and dark matter around them<sup>94,95</sup>. When their separation is  $\lesssim 1$  parsec, a MBH binary forms and other energy-loss channels begin to dominate, such as scattering with stars,<sup>388–394</sup> gas drag from the circumbinary disk,<sup>395</sup> or, if relevant, three-body scattering with a third black hole.<sup>396</sup>

Among these processes, only the dynamical friction decay affects the dynamics at orbital separation above the resolution of large-volume cosmological simulations. However, so far there is limited attempt to directly model dynamical friction (at small scales, close to the resolution) in the large-volume cosmological simulations mentioned above. In most cosmological simulations, once MBHs are within a given halo, they are simply repositioned to the minimum potential position of the host galaxy at each time step. For these simulations, (although sometimes the effects of subgrid dynamical friction are treated in post-processing), many spurious mergers occur during fly-by encounters. Among simulations that do include subgrid modeling of DF on-the-fly,<sup>14</sup> only includes the friction from gas but not stars, while<sup>397</sup> and<sup>12</sup> model the dynamical friction from stars and dark matter particles. Most recently,<sup>398</sup> uses a hybrid model to track the MBH dynamics during galaxy mergers on small scales, while including on-the-fly dynamical friction and stellar scattering computations.

Recent simulations directly incorporates additional dynamical friction modeling,<sup>399</sup> for the MBH dynamics down to the resolution limit,<sup>12,400</sup> With more physical modeling of the MBH dynamics, we can follow the in-simulation mergers for a more extended period of time over hundreds of Myrs, and almost completely prevent mergers during fly-by encounters. Moreover, for the first time we can aim to measure the orbital evolution and eccentricities of MBH pairs on sub-kpc scales. Such information should be important both for estimating the binary hardening timescales and for predicting the GW signals from the MBH mergers.

The launch of LISA will extend the GW window to low frequencies, opening new investigations into dynamical processes involving these massive black hole binaries. MBHB are also the primary multimessenger astrophysics sources. The GW events

will be accompanied by electromagnetic (EM) counterparts and, since information carried electromagnetically is complementary to that carried gravitationally, a great deal can be learnt about an event and its environment (binary AGN and its host galaxy and beyond) across cosmic history as it becomes possible to measure both forms of radiation in concert.

Devising observing strategies for the new multimessenger astrophysics LISA opens up will significantly benefit from predictions of EM counterparts of binary AGN and SMBH host galaxies. It will require 'full-physics' hydrodynamical cosmological simulations with sufficient resolution and volume. One of the major goal objectives of LISA is to trace the origin, growth and merger history of massive black holes across cosmic ages.

The state-of-the art multi-scale hydrodynamical simulations that we have been describing include different implementations for BH growth and associated feedback. They can be used to predict SMBH merger rates, and perform accurate studies of the predictions for SMBH merger rates (Figure 20). Excitingly they can also provide corresponding EM counterparts and host galaxies for the MBHBs that can be observed in future and upcoming facilities. Host galaxy identification of MBHB provides unique information on galaxy-BH coevolution (and precise determination of the distance-redshift relation). The first LISA detections of massive black hole mergers will mobilize global astronomical resources and be an astronomical event of enormous excitement. The mock catalogs and synthetic observations that one can obtain should be able bring traditional astronomers into the LISA community and begin LISA science with MBHM even before LISA is launched.

To illustrate some of the data products that we have available in the simulations we show some preliminary analyses. For each SMBH merger that takes place in the simulations we store the mass of both SMBHs,  $M_1$  and  $M_2$ , and the redshift  $z$  at which the merger event takes place. Figure 18 we show the 2D histogram of the mass of each BH member for all the mergers the Illustris simulations considered here. The total number of BH mergers in each simulation model is indicated in the figure.

After compiling a database of massive binary BH candidates from the large cosmological simulations, we can construct and organize predictions for their host galaxy morphologies and AGN signatures. The goal is to enable multi-messenger astronomy with LISA sources via detailed comparisons between putative LISA events and telescope data that would illuminate properties of the EM counterparts and histories of their host galaxies.

Following the dynamics of galaxy mergers with their black holes we can estimate the incidence of *dual AGN* (at least down to typical separation of a few kpc, at which we still can resolve dynamical friction directly) and the detectability of these binary systems. Correspondingly we have detailed properties of the stellar distribution of the host galaxies, with age, metallicities, star formation rates and associated morphologies. As illustrated in Fig. 17 we are able to statistically characterize the

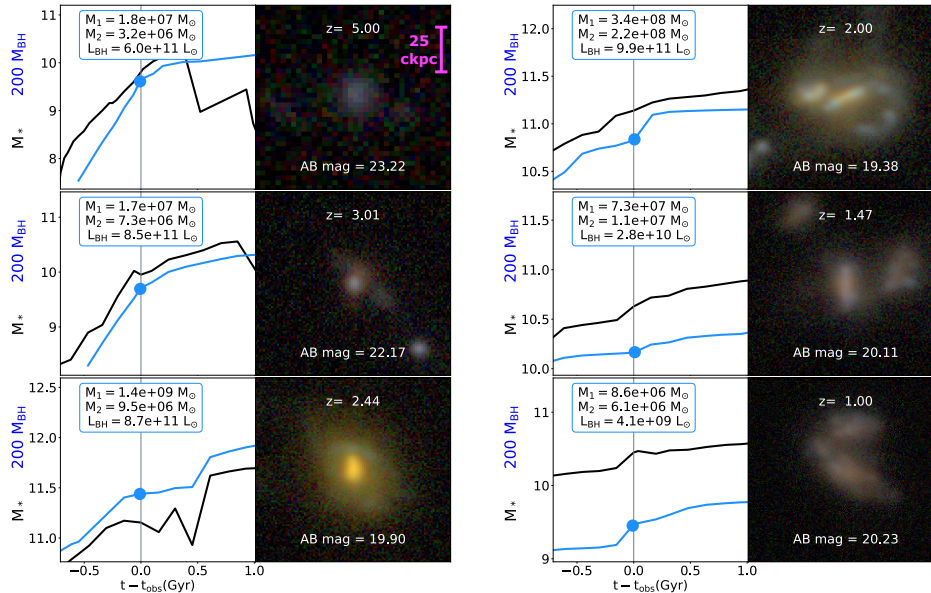


Figure 17. Six example potential LISA sources from a catalog of MBHB mergers in Illustris, spanning mass, mass ratio, and redshift. These plots represent a small window on the  $M_*$  and  $M_{\text{BH}}$  history of the main progenitor host in the left panel. The right panel shows simulated JWST-Nircam images of the hosts.<sup>401</sup> Many of these sources are associated with obvious galaxy mergers, and there is substantial diversity in the host morphology, luminosity, and color.

type of galaxy for given minor/major BH merger events across redshift. Even with LISA more than a decade away, our aim would be to predict which future facilities (Webb, Luvoir, OST) will be needed to observe the type of galaxy which will be MBHB hosts out to high redshifts. For example, the  $z = 5$  example shown in Fig. 17 is the highest redshift host galaxy of a MBHB event in Illustris that will be detectable by JWST (as at these redshifts a MBHB typically involves lower masses).<sup>402</sup>

In Figure 17, we show mock JWST images and mass assembly histories of several galaxies hosting MBHB sources in Illustris. We selected these sources to span a range of redshifts, masses, and mass ratios. Such products can be used to characterize galaxy morphology and AGN activity which may indicate recent (bulges) or ongoing (companions, tails, etc) merging activity and therefore link (in simulations) the population of LISA sources to the story of how galaxy populations assembled. Figure 19 shows the time evolution of a single such source over  $\sim 500 Myr$ . In this evolution, a minor galaxy merger delivers a MBH with  $M_2/M_1 \sim 100$  to the primary host ( $M_1 \sim 10^9$ ), and these BHs merge near the time shown in the 3rd panel. We can see that this MBHB merger occurs during a period of rapid galaxy assembly in the host.

Currently a few teams have been able to carry out impressive MHD simulations

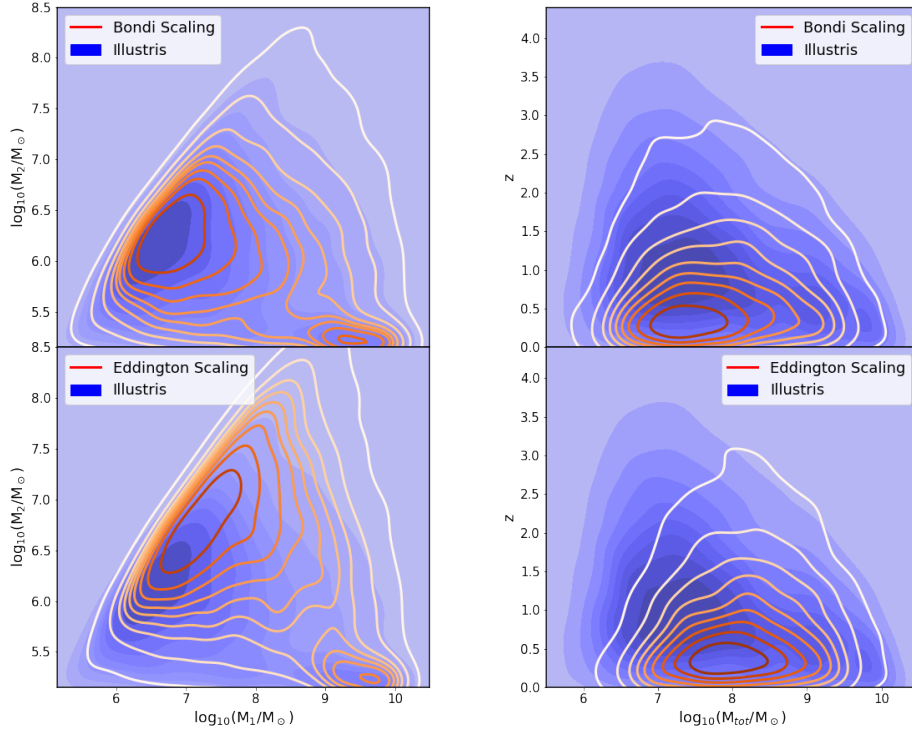


Figure 18. *Top:* Distribution of merger masses ( $M_1$  and  $M_2$ ), from the original Illustris simulation (blue) and after mass growth during the merger delay time, assuming growth follows a Bondi scaling (orange contours). *Bottom:* Same as top, but assuming growth follows an Eddington scaling. Distribution of mergers across redshift and total merger mass ( $M_{tot} = M_1 + M_2$ ) from the original Illustris simulation (blue), and after imposing a dynamical friction time delay, assuming growth follows a Bondi scaling. *Bottom:* Same as top, but assuming black hole growth follows an Eddington scaling.

of circumbinary disks,<sup>404, 405, 406</sup> around relativistic binary BHs which are now starting to produce detailed EM counterpart signatures for these events. In the near future it will be possible to use large scale simulations to provide reasonable 'initial conditions' of the gas environments for these smaller scales around the BHs at the time of mergers that the detailed simulations could use to derive realistic EM signatures for a given mass ratio event in a given environment/galaxy host.

From an analytic modelling point of view, SMBH merger rates have been investigated by incorporating SMBHs in merging galaxies in a full cosmological context by assigning SMBHs to galaxies via different scaling relations.<sup>274, 407, 408</sup> An ex-

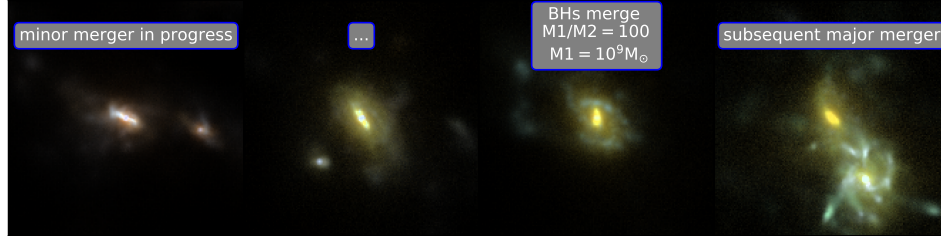


Figure 19. Roughly  $500\text{Myr}$  of evolution of the host galaxy for the  $z = 2.44$  source in Figure 17 (3rd panel). Labels describe the visible assembly processes acting on the galaxy and MBHB. The primary MBH has AGN emission visible as a bright blue point source in the first 3 panels. Each panel has a fixed  $50$  physical kpc field of view.<sup>402</sup>

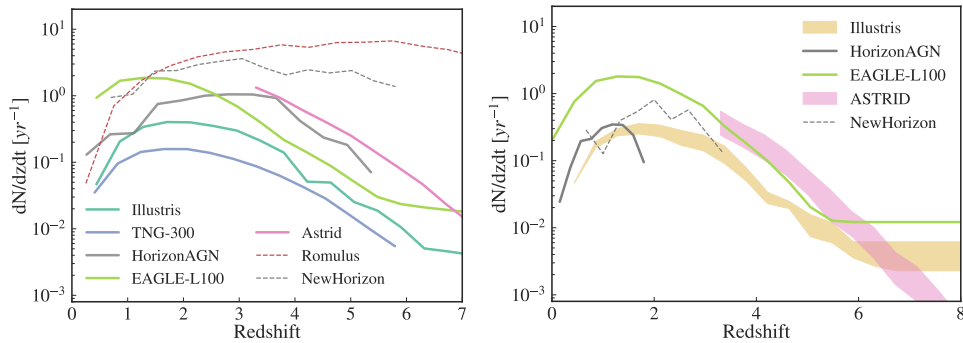


Figure 20. The merger rates for all binaries in a suite of recent hydrodynamical simulations with different levels of delays. Without considering any post-processing delays we expect a total of  $\sim 2$  mergers per year. The rate when considering only DF and hardening decreases the merger rates significantly at high redshifts. Credit for these figure: Nianyi Chen.

ample<sup>274</sup> of this procedure is shown in Figure 22, in which two scaling relations have been adopted, one characterizing the sample of local, dynamically measured SMBHs<sup>132</sup> (green lines), and one that includes a possible correction for observational biases induced by the sphere of influence of the central SMBH<sup>229</sup> (purple lines). It is found that the latter SMBH–host galaxy relations imply a drop of a factor of  $\sim 3$  in the signal amplitude  $A$ . This result by itself could help resolving any potential tension between recent PTA upper limits and theoretical predictions, without invoking any additional physics related to the dynamics of SMBH binaries, such as stalling, high eccentricity or strong coupling with the surrounding stellar and gaseous environment.

## 6. Concluding remarks

In this extensive review we have analysed in some detail several aspects of the modelling of SMBHs in a cosmological context, from full hydrodynamic simulations,

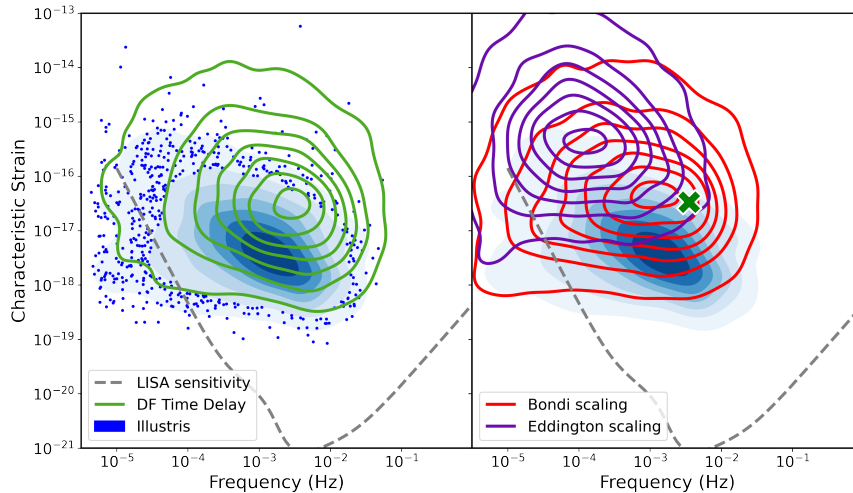


Figure 21. *Left panel:* Illustration of the distribution of GW signals in frequency-strain space for BH binaries in Illustris simulation (blue), and after incorporating a dynamical friction time delay (green). In black the LISA sensitivity curve. *Right panel:* Distribution of GW signals after incorporating black hole mass growth according to Bondi scaling (red) or Eddington scaling (purple). The green cross shows the peak of the distribution without any mass growth (i.e. peak of the green contours from left panel). Incorporating a time delay primarily increases the strain, with a minor increase in frequency. Incorporating mass growth decreases the frequency and further increases the strain, especially for more efficient growth (i.e. assuming Eddington scaling).<sup>403</sup>

to semi-analytic and semi-empirical models. A number of interesting conclusions can be drawn from this varied discussion:

- Cosmological semi-analytic and hydrodynamic simulations grow SMBHs from seed BHs that range from  $10^2$  to  $10^6 M_{\odot}$ , roughly covering the full range of theoretical expectations. All recent both numerical and analytic models, predict a steep rise in the SMBH mass function at low masses.<sup>292,409</sup> Recent hydrodynamic simulations have revealed that such seed SMBHs can effectively grow into the giants rare quasars observed at  $z > 6$  thanks to the large-scale tidal fields destabilizing significant amounts of gas funnelling onto the seed BHs (see Figure 8).
- SMBHs grow primarily by (gas) accretion. Although other possibilities have been put forward in the literature,<sup>410,411</sup> as it stands, all current models have shown that, by making use of standard values of the radiative and kinetic efficiencies, gas accretion by itself could be a sufficient condition to reproduce the SMBH demography (in terms of both mass density and scaling relations) as calibrated in the local Universe (see, for example, Figures 6 and 13).
- Relatively frequent SMBH mergers are nevertheless predicted to occur in almost all hydrodynamic simulations, with a frequency that could be as

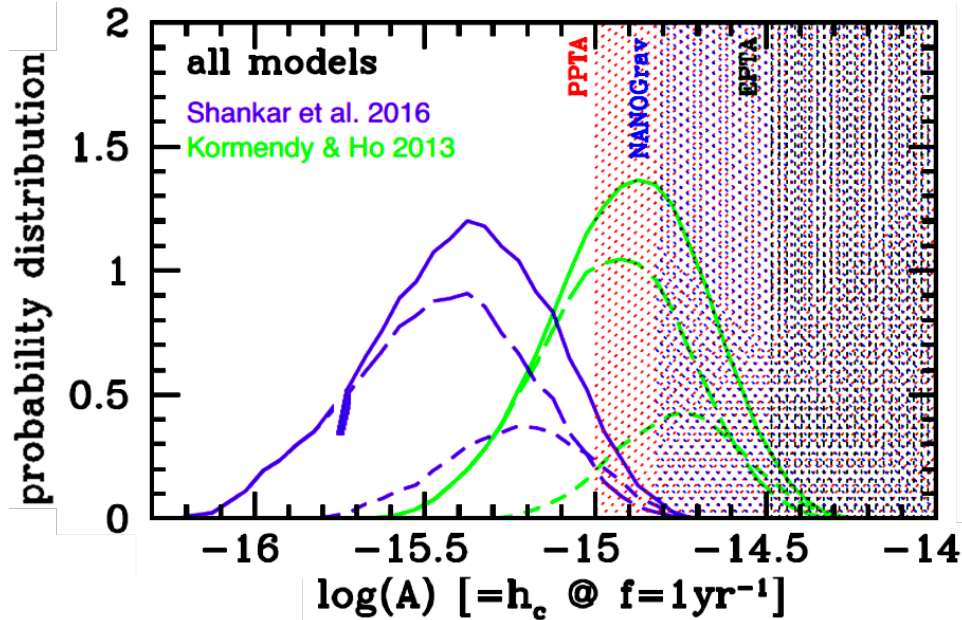


Figure 22. Probability distribution<sup>274</sup> of the signal amplitude  $A$  assuming different scaling relations, as labelled. The two sets of lines for each scaling relation corresponds to two evolution patterns in the input stellar mass functions.

high as a couple of mergers per year, but most probably much lower when including any sources of stalling (see Figure 20). LISA will be key to discern among the viable models of SMBH mergers (Figure 17).

- SMBHs can feed back to the ISM significant amounts of energy and momentum via radiation pressure on free electrons and dust, as well as via large-scale mechanical winds and jets. Several cosmological models implement both a quasar-mode and radio-mode SMBH feedback, with the former regulating the initial growth of the SMBH and inner mass density, and the latter shown to be effective in producing a red galaxy sequence, in preventing overgrowth in massive galaxies, and in generating more realistic galactic and thermodynamic profiles.
- Strong degeneracies in the input parameters within a single model (among seeding, dynamics, accretion, and feedback), as well as degeneracies among the different implementations of SMBH feedback (e.g., Figure 1), still prevent to underpin the true underlying processes at play shaping SMBH and host galaxy growth. We note, however, that cosmological models implementing gravitational torque-based accretion predict the latter to be nearly independent of SMBH mass and with less need of self-regulation.
- Present cosmological models, both numerical and analytic ones, have been

able not only to reproduce the number densities of SMBHs, both active and inactive ones, but also their spatial distribution as traced in the small and large-scale clustering properties of active SMBHs (see, e.g., Figure 14). Quasars hosts are predicted to be always related to host dark matter haloes of the order of  $10^{12} - 10^{13} M_{\odot}$ , at all relevant redshifts, while the same models also suggest that excess small scale clustering is possibly due to quasar pairs in satellite galaxies.

## References

1. D. N. Spergel, R. Bean, O. Dore' et al., Wilkinson Microwave Anisotropy Probe (WMAP) Three Year Results: Implications for Cosmology, *ArXiv Astrophysics e-prints* (Mar., 2006).
2. J. Barnes and P. Hut, A hierarchical  $O(N \log N)$  force-calculation algorithm, *Nature* . **324**, 446–449 (Dec., 1986). doi: 10.1038/324446a0.
3. V. Springel, The cosmological simulation code GADGET-2, *Mon. Not. R. Astron. Soc.* . **364**(4), 1105–1134 (Dec., 2005). doi: 10.1111/j.1365-2966.2005.09655.x.
4. V. Springel, E pur si muove: Galilean-invariant cosmological hydrodynamical simulations on a moving mesh, *Mon. Not. R. Astron. Soc.* . **401**, 791–851 (Jan., 2010). doi: 10.1111/j.1365-2966.2009.15715.x.
5. P. F. Hopkins, A new class of accurate, mesh-free hydrodynamic simulation methods, *Mon. Not. R. Astron. Soc.* . **450**, 53–110 (June, 2015). doi: 10.1093/mnras/stv195.
6. A. Bauer and V. Springel, Subsonic turbulence in smoothed particle hydrodynamics and moving-mesh simulations, *Mon. Not. R. Astron. Soc.* . p. 3102 (May, 2012). doi: 10.1111/j.1365-2966.2012.21058.x.
7. D. Sijacki, M. Vogelsberger, D. Kereš et al., Moving mesh cosmology: the hydrodynamics of galaxy formation, *Mon. Not. R. Astron. Soc.* . **424**, 2999–3027 (Aug., 2012). doi: 10.1111/j.1365-2966.2012.21466.x.
8. M. Vogelsberger, D. Sijacki, D. Kereš et al., Moving mesh cosmology: numerical techniques and global statistics, *Mon. Not. R. Astron. Soc.* . **425**, 3024–3057 (Oct., 2012). doi: 10.1111/j.1365-2966.2012.21590.x.
9. P. Torrey, M. Vogelsberger, D. Sijacki et al., Moving-mesh cosmology: properties of gas discs, *Mon. Not. R. Astron. Soc.* . **427**, 2224–2238 (Dec., 2012). doi: 10.1111/j.1365-2966.2012.22082.x.
10. S. Genel, M. Vogelsberger, D. Nelson et al., Following the flow: tracer particles in astrophysical fluid simulations, *Mon. Not. R. Astron. Soc.* . **435**, 1426–1442 (Oct., 2013). doi: 10.1093/mnras/stt1383.
11. D. Nelson, M. Vogelsberger, S. Genel et al., Moving mesh cosmology: tracing cosmological gas accretion, *Mon. Not. R. Astron. Soc.* . **429**, 3353–3370 (Mar., 2013). doi: 10.1093/mnras/sts595.
12. M. Hirschmann, K. Dolag, A. Saro et al., Cosmological simulations of black hole growth: AGN luminosities and downsizing, *Mon. Not. R. Astron. Soc.* . **442**(3), 2304–2324 (Aug, 2014). doi: 10.1093/mnras/stu1023.
13. L. K. Steinborn, K. Dolag, M. Hirschmann et al., A refined sub-grid model for black hole accretion and AGN feedback in large cosmological simulations, *Mon. Not. R. Astron. Soc.* . **448**, 1504–1525 (Apr., 2015). doi: 10.1093/mnras/stv072.
14. Y. Dubois, C. Pichon, C. Welker et al., Dancing in the dark: galactic properties trace spin swings along the cosmic web, *Mon. Not. R. Astron. Soc.* . **444**, 1453–1468 (Oct., 2014). doi: 10.1093/mnras/stu1227.

15. M. Volonteri, Y. Dubois, C. Pichon *et al.*, The cosmic evolution of massive black holes in the Horizon-AGN simulation, *Mon. Not. R. Astron. Soc.* . **460**(3), 2979–2996 (Aug, 2016). doi: 10.1093/mnras/stw1123.
16. J. Schaye, R. A. Crain, R. G. Bower *et al.*, The EAGLE project: simulating the evolution and assembly of galaxies and their environments, *Mon. Not. R. Astron. Soc.* . **446**, 521–554 (Jan., 2015). doi: 10.1093/mnras/stu2058.
17. Y. M. Rosas-Guevara, R. G. Bower, J. Schaye *et al.*, The impact of angular momentum on black hole accretion rates in simulations of galaxy formation, *Mon. Not. R. Astron. Soc.* . **454**, 1038–1057 (Nov., 2015). doi: 10.1093/mnras/stv2056.
18. Y. Rosas-Guevara, R. G. Bower, J. Schaye *et al.*, Supermassive black holes in the EAGLE Universe. Revealing the observables of their growth, *Mon. Not. R. Astron. Soc.* . **462**(1), 190–205 (Oct, 2016). doi: 10.1093/mnras/stw1679.
19. S. Genel, M. Vogelsberger, V. Springel *et al.*, Introducing the Illustris project: the evolution of galaxy populations across cosmic time, *Mon. Not. R. Astron. Soc.* . **445** (1), 175–200 (Nov, 2014). doi: 10.1093/mnras/stu1654.
20. M. Vogelsberger, S. Genel, V. Springel *et al.*, Introducing the Illustris Project: simulating the coevolution of dark and visible matter in the Universe, *Mon. Not. R. Astron. Soc.* . **444**, 1518–1547 (Oct., 2014). doi: 10.1093/mnras/stu1536.
21. D. Sijacki, M. Vogelsberger, S. Genel *et al.*, The Illustris simulation: the evolving population of black holes across cosmic time, *Mon. Not. R. Astron. Soc.* . **452**, 575–596 (Sept., 2015). doi: 10.1093/mnras/stv1340.
22. N. Khandai, T. Di Matteo, R. Croft *et al.*, The MassiveBlack-II simulation: the evolution of haloes and galaxies to  $z \sim 0$ , *Mon. Not. R. Astron. Soc.* . **450**(2), 1349–1374 (June, 2015). doi: 10.1093/mnras/stv627.
23. C. DeGraf, T. Di Matteo, T. Treu *et al.*, Scaling relations between black holes and their host galaxies: comparing theoretical and observational measurements, and the impact of selection effects, *Mon. Not. R. Astron. Soc.* . **454**, 913–932 (Nov., 2015). doi: 10.1093/mnras/stv2002.
24. Y. Feng, T. Di-Matteo, R. A. Croft *et al.*, The BlueTides simulation: first galaxies and reionization, *Mon. Not. R. Astron. Soc.* . **455**, 2778–2791 (Jan., 2016). doi: 10.1093/mnras/stv2484.
25. T. Di Matteo, R. A. C. Croft, Y. Feng *et al.*, The origin of the most massive black holes at high- $z$ : BlueTides and the next quasar frontier, *Mon. Not. R. Astron. Soc.* . **467**(4), 4243–4251 (June, 2017). doi: 10.1093/mnras/stx319.
26. K.-W. Huang, T. Di Matteo, A. K. Bhowmick *et al.*, BLUETIDES simulation: establishing black hole-galaxy relations at high redshift, *Mon. Not. R. Astron. Soc.* . **478**, 5063–5073 (Aug., 2018). doi: 10.1093/mnras/sty1329.
27. Y. Ni, T. Di Matteo, R. Gilli *et al.*, QSO obscuration at high redshift ( $z \gtrsim 7$ ): predictions from the BLUETIDES simulation, *Mon. Not. R. Astron. Soc.* . **495**(2), 2135–2151 (June, 2020). doi: 10.1093/mnras/staa1313.
28. M. Tremmel, M. Karcher, F. Governato *et al.*, The Romulus cosmological simulations: a physical approach to the formation, dynamics and accretion models of SMBHs, *Mon. Not. R. Astron. Soc.* . **470**, 1121–1139 (Sept., 2017). doi: 10.1093/mnras/stx1160.
29. A. Ricarte, M. Tremmel, P. Natarajan *et al.*, Tracing black hole and galaxy co-evolution in the ROMULUS simulations, *Mon. Not. R. Astron. Soc.* . **489**(1), 802–819 (Oct, 2019). doi: 10.1093/mnras/stz2161.
30. R. S. Sharma, A. M. Brooks, R. S. Somerville *et al.*, Black Hole Growth and Feedback in Isolated ROMULUS25 Dwarf Galaxies, *Astrophys. J.* . 897(1):103 (July, 2020). doi: 10.3847/1538-4357/ab960e.

31. R. Weinberger, V. Springel, L. Hernquist *et al.*, Simulating galaxy formation with black hole driven thermal and kinetic feedback, *Mon. Not. R. Astron. Soc.* . **465**, 3291–3308 (Mar., 2017). doi: 10.1093/mnras/stw2944.
32. A. Pillepich, V. Springel, D. Nelson *et al.*, Simulating galaxy formation with the IllustrisTNG model, *Mon. Not. R. Astron. Soc.* . **473**(3), 4077–4106 (Jan, 2018). doi: 10.1093/mnras/stx2656.
33. M. Habouzit, S. Genel, R. S. Somerville *et al.*, Linking galaxy structural properties and star formation activity to black hole activity with IllustrisTNG, *Mon. Not. R. Astron. Soc.* . **484**(4), 4413–4443 (Apr, 2019). doi: 10.1093/mnras/stz102.
34. B. A. Terrazas, E. F. Bell, A. Pillepich *et al.*, The relationship between black hole mass and galaxy properties: examining the black hole feedback model in IllustrisTNG, *Mon. Not. R. Astron. Soc.* . **493**(2), 1888–1906 (Apr., 2020). doi: 10.1093/mnras/staa374.
35. R. Davé, D. Anglés-Alcázar, D. Narayanan *et al.*, SIMBA: Cosmological simulations with black hole growth and feedback, *Mon. Not. R. Astron. Soc.* . **486**(2), 2827–2849 (Jun, 2019). doi: 10.1093/mnras/stz937.
36. N. Thomas, R. Davé, D. Anglés-Alcázar *et al.*, Black hole - Galaxy correlations in SIMBA, *Mon. Not. R. Astron. Soc.* . **487**(4), 5764–5780 (Aug, 2019). doi: 10.1093/mnras/stz1703.
37. N. Thomas, R. Davé, M. J. Jarvis *et al.*, The Radio Galaxy Population in the SIMBA Simulations, *Mon. Not. R. Astron. Soc.* (Mar., 2021). doi: 10.1093/mnras/stab654.
38. J. Borrow, D. Anglés-Alcázar and R. Davé, Cosmological baryon transfer in the SIMBA simulations, *Mon. Not. R. Astron. Soc.* . **491**(4), 6102–6119 (Feb., 2020). doi: 10.1093/mnras/stz3428.
39. N. Chen, Y. Ni, A. M. Holgado *et al.*, Massive Black Hole Mergers with Orbital Information: Predictions from the ASTRID Simulation, *arXiv e-prints*. art. arXiv:2112.08555 (Dec., 2021).
40. Y. Ni, T. Di Matteo, S. Bird *et al.*, The ASTRID simulation: the evolution of Supermassive Black Holes, *arXiv e-prints*. art. arXiv:2110.14154 (Oct., 2021).
41. S. Bird, Y. Ni, T. D. Matteo *et al.*, The ASTRID Simulation: Galaxy Formation and Reionization, *Mon. Not. R. Astron. Soc.* (Mar., 2022). doi: 10.1093/mnras/stac648.
42. F. Villaescusa-Navarro, D. Anglés-Alcázar, S. Genel *et al.*, The CAMELS Project: Cosmology and Astrophysics with Machine-learning Simulations, *Astrophys. J.* . 915 (1):71 (July, 2021). doi: 10.3847/1538-4357/abf7ba.
43. F. Villaescusa-Navarro, S. Genel, D. Anglés-Alcázar *et al.*, The CAMELS project: public data release, *arXiv e-prints*. art. arXiv:2201.01300 (Jan., 2022).
44. T. Sawala, C. S. Frenk, A. Fattahi *et al.*, The APOSTLE simulations: solutions to the Local Group’s cosmic puzzles, *Mon. Not. R. Astron. Soc.* . **457**(2), 1931–1943 (Apr., 2016). doi: 10.1093/mnras/stw145.
45. R. J. J. Grand, F. A. Gómez, F. Marinacci *et al.*, The Auriga Project: the properties and formation mechanisms of disc galaxies across cosmic time, *Mon. Not. R. Astron. Soc.* . **467**(1), 179–207 (May, 2017). doi: 10.1093/mnras/stx071.
46. L. Wang, A. A. Dutton, G. S. Stinson *et al.*, NIHAO project - I. Reproducing the inefficiency of galaxy formation across cosmic time with a large sample of cosmological hydrodynamical simulations, *Mon. Not. R. Astron. Soc.* . **454**(1), 83–94 (Nov., 2015). doi: 10.1093/mnras/stv1937.
47. M. Blank, A. V. Macciò, A. A. Dutton *et al.*, NIHAO - XXII. Introducing black hole formation, accretion, and feedback into the NIHAO simulation suite, *Mon. Not. R. Astron. Soc.* . **487**(4), 5476–5489 (Aug, 2019). doi: 10.1093/mnras/stz1688.
48. Y. M. Bahé, D. J. Barnes, C. Dalla Vecchia *et al.*, The Hydrangea simulations:

- galaxy formation in and around massive clusters, *Mon. Not. R. Astron. Soc.* . **470** (4), 4186–4208 (Oct., 2017). doi: 10.1093/mnras/stx1403.
49. D. J. Barnes, S. T. Kay, Y. M. Bahé *et al.*, The Cluster-EAGLE project: global properties of simulated clusters with resolved galaxies, *Mon. Not. R. Astron. Soc.* . **471**(1), 1088–1106 (Oct., 2017). doi: 10.1093/mnras/stx1647.
  50. W. Cui, A. Knebe, G. Yepes *et al.*, The Three Hundred project: a large catalogue of theoretically modelled galaxy clusters for cosmological and astrophysical applications, *Mon. Not. R. Astron. Soc.* . **480**(3), 2898–2915 (Nov., 2018). doi: 10.1093/mnras/sty2111.
  51. W. Cui, R. Dave, A. Knebe *et al.*, The Three Hundred project: The Gizmo-Simba runs, *arXiv e-prints*. art. arXiv:2202.14038 (Feb., 2022).
  52. E. Choi, J. P. Ostriker, T. Naab *et al.*, The impact of mechanical AGN feedback on the formation of massive early-type galaxies, *Mon. Not. R. Astron. Soc.* . **449**, 4105–4116 (June, 2015). doi: 10.1093/mnras/stv575.
  53. E. Choi, R. S. Somerville, J. P. Ostriker *et al.*, The Role of Black Hole Feedback on Size and Structural Evolution in Massive Galaxies, *Astrophys. J.* . 866(2):91 (Oct, 2018). doi: 10.3847/1538-4357/aae076.
  54. E. Choi, R. Brennan, R. S. Somerville *et al.*, The Impact of Outflows Driven by Active Galactic Nuclei on Metals in and around Galaxies, *Astrophys. J.* . 904(1):8 (Nov., 2020). doi: 10.3847/1538-4357/abba7d.
  55. T. Costa, D. Sijacki, M. Trenti *et al.*, The environment of bright QSOs at  $z \sim 6$ : star-forming galaxies and X-ray emission, *Mon. Not. R. Astron. Soc.* . **439**(2), 2146–2174 (Apr., 2014). doi: 10.1093/mnras/stu101.
  56. T. Costa, D. Sijacki and M. G. Haehnelt, Fast cold gas in hot AGN outflows., *Mon. Not. R. Astron. Soc.* . **448**, L30–L34 (Mar., 2015). doi: 10.1093/mnrasl/slu193.
  57. T. Costa, J. Rosdahl, D. Sijacki *et al.*, Quenching star formation with quasar outflows launched by trapped IR radiation, *Mon. Not. R. Astron. Soc.* . **479**(2), 2079–2111 (Sept., 2018). doi: 10.1093/mnras/sty1514.
  58. J. M. Bellovary, C. E. Cleary, F. Munshi *et al.*, Multimessenger signatures of massive black holes in dwarf galaxies, *Mon. Not. R. Astron. Soc.* . **482**(3), 2913–2923 (Jan., 2019). doi: 10.1093/mnras/sty2842.
  59. J. M. Bellovary, S. Hayoune, K. Chafra *et al.*, The origins of off-centre massive black holes in dwarf galaxies, *Mon. Not. R. Astron. Soc.* . **505**(4), 5129–5141 (Aug., 2021). doi: 10.1093/mnras/stab1665.
  60. E. Applebaum, A. M. Brooks, C. R. Christensen *et al.*, Ultrafaint Dwarfs in a Milky Way Context: Introducing the Mint Condition DC Justice League Simulations, *Astrophys. J.* . 906(2):96 (Jan., 2021). doi: 10.3847/1538-4357/abcafa.
  61. M. Volonteri, H. Pfister, R. S. Beckmann *et al.*, Black hole mergers from dwarf to massive galaxies with the NewHorizon and Horizon-AGN simulations, *Mon. Not. R. Astron. Soc.* . **498**(2), 2219–2238 (Oct., 2020). doi: 10.1093/mnras/staa2384.
  62. Y. Dubois, R. Beckmann, F. Bournaud *et al.*, Introducing the NEWHORIZON simulation: Galaxy properties with resolved internal dynamics across cosmic time, *Astron. Astrophys.* . 651:A109 (July, 2021). doi: 10.1051/0004-6361/202039429.
  63. D. Anglés-Alcázar, C.-A. Faucher-Giguère, E. Quataert *et al.*, Black holes on FIRE: stellar feedback limits early feeding of galactic nuclei, *Mon. Not. R. Astron. Soc.* . **472**, L109–L114 (Nov., 2017). doi: 10.1093/mnrasl/slx161.
  64. P. F. Hopkins, A. Wetzel, D. Kereš *et al.*, FIRE-2 simulations: physics versus numerics in galaxy formation, *Mon. Not. R. Astron. Soc.* . **480**, 800–863 (Oct., 2018). doi: 10.1093/mnras/sty1690.
  65. D. Anglés-Alcázar, E. Quataert, P. F. Hopkins *et al.*, Cosmological Simulations of

- Quasar Fueling to Subparsec Scales Using Lagrangian Hyper-refinement, *Astrophys. J.* . 917(2):53 (Aug., 2021). doi: 10.3847/1538-4357/ac09e8.
66. O. Çatmabacak, R. Feldmann, D. Anglés-Alcázar *et al.*, Black hole-galaxy scaling relations in FIRE: the importance of black hole location and mergers, *Mon. Not. R. Astron. Soc.* . **511**(1), 506–535 (Mar., 2022). doi: 10.1093/mnras/stac040.
  67. P. F. Hopkins, A. Wetzel, C. Wheeler *et al.*, FIRE-3: Updated Stellar Evolution Models, Yields, & Microphysics and Fitting Functions for Applications in Galaxy Simulations, *arXiv e-prints*. art. arXiv:2203.00040 (Feb., 2022).
  68. S. Wellons, C.-A. Faucher-Giguère, P. F. Hopkins *et al.*, Exploring supermassive black hole physics and galaxy quenching across halo mass in FIRE cosmological zoom simulations, *arXiv e-prints*. art. arXiv:2203.06201 (Mar., 2022).
  69. M. Volonteri, Formation of supermassive black holes, *Astronomy and Astrophysics Reviews*. **18**, 279–315 (July, 2010). doi: 10.1007/s00159-010-0029-x.
  70. K. Inayoshi, E. Visbal and Z. Haiman, The Assembly of the First Massive Black Holes, *Annu. Rev. Astron. Astrophys.* . **58**, 27–97 (Aug., 2020). doi: 10.1146/annurev-astro-120419-014455.
  71. P. Madau and M. J. Rees, Massive Black Holes as Population III Remnants, *Astrophys. J.* . **551**, L27–L30 (Apr., 2001). doi: 10.1086/319848.
  72. M. Volonteri, F. Haardt and P. Madau, The Assembly and Merging History of Supermassive Black Holes in Hierarchical Models of Galaxy Formation, *Astrophys. J.* . **582**(2), 559–573 (Jan., 2003). doi: 10.1086/344675.
  73. M. C. Begelman, M. Volonteri and M. J. Rees, Formation of supermassive black holes by direct collapse in pre-galactic haloes, *Mon. Not. R. Astron. Soc.* . **370**, 289–298 (July, 2006). doi: 10.1111/j.1365-2966.2006.10467.x.
  74. G. Lodato and P. Natarajan, Supermassive black hole formation during the assembly of pre-galactic discs, *Mon. Not. R. Astron. Soc.* . **371**(4), 1813–1823 (Oct., 2006). doi: 10.1111/j.1365-2966.2006.10801.x.
  75. G. Lodato and P. Natarajan, The mass function of high-redshift seed black holes, *Mon. Not. R. Astron. Soc.* . **377**(1), L64–L68 (May, 2007). doi: 10.1111/j.1745-3933.2007.00304.x.
  76. T. Di Matteo, J. Colberg, V. Springel *et al.*, Direct Cosmological Simulations of the Growth of Black Holes and Galaxies, *Astrophys. J.* . **676**, 33–53 (Mar., 2008). doi: 10.1086/524921.
  77. C. M. Booth and J. Schaye, Cosmological simulations of the growth of supermassive black holes and feedback from active galactic nuclei: method and tests, *Mon. Not. R. Astron. Soc.* . **398**, 53–74 (Sept., 2009). doi: 10.1111/j.1365-2966.2009.15043.x.
  78. D. Anglés-Alcázar, R. Davé, C.-A. Faucher-Giguère *et al.*, Gravitational torque-driven black hole growth and feedback in cosmological simulations, *Mon. Not. R. Astron. Soc.* . **464**, 2840–2853 (Jan., 2017). doi: 10.1093/mnras/stw2565.
  79. J. M. Bellovary, F. Governato, T. R. Quinn *et al.*, Wandering Black Holes in Bright Disk Galaxy Halos, *Astrophys. J.* . **721**, L148–L152 (Oct., 2010). doi: 10.1088/2041-8205/721/2/L148.
  80. J. Bellovary, M. Volonteri, F. Governato *et al.*, The First Massive Black Hole Seeds and Their Hosts, *Astrophys. J.* . 742(1):13 (Nov., 2011). doi: 10.1088/0004-637X/742/1/13.
  81. P. Taylor and C. Kobayashi, Seeding black holes in cosmological simulations, *Mon. Not. R. Astron. Soc.* . **442**(3), 2751–2767 (Aug., 2014). doi: 10.1093/mnras/stu983.
  82. M. Habouzit, M. Volonteri and Y. Dubois, Blossoms from black hole seeds: properties and early growth regulated by supernova feedback, *Mon. Not. R. Astron. Soc.* . **468**,

- 3935–3948 (July, 2017). doi: 10.1093/mnras/stx666.
83. L. Ma, P. F. Hopkins, X. Ma *et al.*, Seeds Don't Sink: Even Massive Black Hole "Seeds" Cannot Migrate to Galaxy Centers Efficiently, *arXiv e-prints*. art. arXiv:2101.02727 (Jan., 2021).
  84. V. Springel, T. Di Matteo and L. Hernquist, Modelling feedback from stars and black holes in galaxy mergers, *Mon. Not. R. Astron. Soc.* . **361**, 776–794 (Aug., 2005). doi: 10.1111/j.1365-2966.2005.09238.x.
  85. S. E. Woosley, A. Heger and T. A. Weaver, The evolution and explosion of massive stars, *Reviews of Modern Physics*. **74**(4), 1015–1071 (Nov., 2002). doi: 10.1103/RevModPhys.74.1015.
  86. S. Hirano, T. Hosokawa, N. Yoshida *et al.*, One Hundred First Stars: Protostellar Evolution and the Final Masses, *Astrophys. J.* . 781(2):60 (Feb., 2014). doi: 10.1088/0004-637X/781/2/60.
  87. M. Volonteri and P. Natarajan, Journey to the  $M_{BH}-\sigma$  relation: the fate of low-mass black holes in the Universe, *Mon. Not. R. Astron. Soc.* . **400**(4), 1911–1918 (Dec., 2009). doi: 10.1111/j.1365-2966.2009.15577.x.
  88. S. van Wassenhove, M. Volonteri, M. G. Walker *et al.*, Massive black holes lurking in Milky Way satellites, *Mon. Not. R. Astron. Soc.* . **408**(2), 1139–1146 (Oct., 2010). doi: 10.1111/j.1365-2966.2010.17189.x.
  89. S. Bonoli, L. Mayer, S. Kazantzidis *et al.*, Black hole starvation and bulge evolution in a Milky Way-like galaxy, *Mon. Not. R. Astron. Soc.* . **459**, 2603–2617 (July, 2016). doi: 10.1093/mnras/stw694.
  90. D. Anglés-Alcázar, F. Özel and R. Davé, Black Hole-Galaxy Correlations without Self-regulation, *Astrophys. J.* . 770:5 (June, 2013). doi: 10.1088/0004-637X/770/1/5.
  91. D. Anglés-Alcázar, F. Özel, R. Davé *et al.*, Torque-limited Growth of Massive Black Holes in Galaxies across Cosmic Time, *Astrophys. J.* . 800:127 (Feb., 2015). doi: 10.1088/0004-637X/800/2/127.
  92. M. Habouzit, M. Volonteri, M. Latif *et al.*, On the number density of 'direct collapse' black hole seeds, *Mon. Not. R. Astron. Soc.* . **463**(1), 529–540 (Nov., 2016). doi: 10.1093/mnras/stw1924.
  93. C. DeGraf and D. Sijacki, Cosmological simulations of massive black hole seeds: predictions for next-generation electromagnetic and gravitational wave observations, *Mon. Not. R. Astron. Soc.* . **491**(4), 4973–4992 (Feb., 2020). doi: 10.1093/mnras/stz3309.
  94. S. Chandrasekhar, Dynamical Friction. I. General Considerations: the Coefficient of Dynamical Friction., *Astrophys. J.* . **97**, 255 (Mar., 1943). doi: 10.1086/144517.
  95. E. C. Ostriker, Dynamical Friction in a Gaseous Medium, *Astrophys. J.* . **513**(1), 252–258 (Mar., 1999). doi: 10.1086/306858.
  96. R. S. Beckmann, A. Slyz and J. Devriendt, Bondi or not Bondi: the impact of resolution on accretion and drag force modelling for supermassive black holes, *Mon. Not. R. Astron. Soc.* . **478**(1), 995–1016 (Jul, 2018). doi: 10.1093/mnras/sty931.
  97. K. Park and T. Bogdanović, Gaseous Dynamical Friction in Presence of Black Hole Radiative Feedback, *Astrophys. J.* . 838(2):103 (Apr., 2017). doi: 10.3847/1538-4357/aa65ce.
  98. L. del Valle and M. Volonteri, The effect of AGN feedback on the migration time-scale of supermassive black holes binaries, *Mon. Not. R. Astron. Soc.* . **480**(1), 439–450 (Oct., 2018). doi: 10.1093/mnras/sty1815.
  99. A. Gruzinov, Y. Levin and C. D. Matzner, Negative dynamical friction on compact objects moving through dense gas, *Mon. Not. R. Astron. Soc.* . **492**(2), 2755–2761 (Feb., 2020). doi: 10.1093/mnras/staa013.

100. D. Toyouchi, T. Hosokawa, K. Sugimura et al., Gaseous dynamical friction under radiative feedback: do intermediate-mass black holes speed up or down?, *Mon. Not. R. Astron. Soc.* . **496**(2), 1909–1921 (Aug., 2020). doi: 10.1093/mnras/staa1338.
101. T. Bogdanović, M. C. Miller and L. Blecha, Electromagnetic counterparts to massive black-hole mergers, *Living Reviews in Relativity*. 25(1):3 (Dec., 2022). doi: 10.1007/s41114-022-00037-8.
102. H. Pfister, A. Lupi, P. R. Capelo et al., The birth of a supermassive black hole binary, *Mon. Not. R. Astron. Soc.* . **471**(3), 3646–3656 (Nov., 2017). doi: 10.1093/mnras/stx1853.
103. T. Okamoto, R. S. Nemmen and R. G. Bower, The impact of radio feedback from active galactic nuclei in cosmological simulations: formation of disc galaxies, *Mon. Not. R. Astron. Soc.* . **385**(1), 161–180 (Mar., 2008). doi: 10.1111/j.1365-2966.2008.12883.x.
104. J. Wurster and R. J. Thacker, A comparative study of AGN feedback algorithms, *Mon. Not. R. Astron. Soc.* . **431**, 2513–2534 (May, 2013). doi: 10.1093/mnras/stt346.
105. Y. M. Bahé, J. Schaye, M. Schaller et al., The importance of black hole repositioning for galaxy formation simulations, *arXiv e-prints*. art. arXiv:2109.01489 (Sept., 2021).
106. N. Chen, Y. Ni, M. Tremmel et al., Dynamical friction modelling of massive black holes in cosmological simulations and effects on merger rate predictions, *Mon. Not. R. Astron. Soc.* . **510**(1), 531–550 (Feb., 2022). doi: 10.1093/mnras/stab3411.
107. P. Biernacki, R. Teyssier and A. Bleuler, On the dynamics of supermassive black holes in gas-rich, star-forming galaxies: the case for nuclear star cluster co-evolution, *Mon. Not. R. Astron. Soc.* . **469**, 295–313 (July, 2017). doi: 10.1093/mnras/stx845.
108. M. Tremmel, F. Governato, M. Volonteri et al., Off the beaten path: a new approach to realistically model the orbital decay of supermassive black holes in galaxy formation simulations, *Mon. Not. R. Astron. Soc.* . **451**, 1868–1874 (Aug., 2015). doi: 10.1093/mnras/stv1060.
109. H. Pfister, M. Volonteri, Y. Dubois et al., The erratic dynamical life of black hole seeds in high-redshift galaxies, *Mon. Not. R. Astron. Soc.* . **486**(1), 101–111 (June, 2019). doi: 10.1093/mnras/stz822.
110. Y. Dubois, M. Volonteri, J. Silk et al., Black hole evolution - I. Supernova-regulated black hole growth, *Mon. Not. R. Astron. Soc.* . **452**, 1502–1518 (Sept., 2015). doi: 10.1093/mnras/stv1416.
111. M. Trebitsch, M. Volonteri and Y. Dubois, Modelling a bright  $z = 6$  galaxy at the faint end of the AGN luminosity function, *Mon. Not. R. Astron. Soc.* . **494**(3), 3453–3463 (May, 2020). doi: 10.1093/mnras/staa1012.
112. D. Fiacconi, L. Mayer, R. Roškar et al., Massive Black Hole Pairs in Clumpy, Self-gravitating Circumnuclear Disks: Stochastic Orbital Decay, *Astrophys. J.* . 777:L14 (Nov., 2013). doi: 10.1088/2041-8205/777/1/L14.
113. R. Roškar, D. Fiacconi, L. Mayer et al., Orbital decay of supermassive black hole binaries in clumpy multiphase merger remnants, *Mon. Not. R. Astron. Soc.* . **449**(1), 494–505 (May, 2015). doi: 10.1093/mnras/stv312.
114. V. Tamburello, P. R. Capelo, L. Mayer et al., Supermassive black hole pairs in clumpy galaxies at high redshift: delayed binary formation and concurrent mass growth, *Mon. Not. R. Astron. Soc.* . **464**(3), 2952–2962 (Jan., 2017). doi: 10.1093/mnras/stw2561.
115. T. Tamfal, P. R. Capelo, S. Kazantzidis et al., Formation of LISA Black Hole Binaries in Merging Dwarf Galaxies: The Imprint of Dark Matter, *Astrophys. J.* . 864(1):L19 (Sept., 2018). doi: 10.3847/2041-8213/aada4b.
116. M. Tremmel, F. Governato, M. Volonteri et al., Dancing to CHANGA: a self-

- consistent prediction for close SMBH pair formation time-scales following galaxy mergers, *Mon. Not. R. Astron. Soc.* . **475**(4), 4967–4977 (Apr., 2018). doi: 10.1093/mnras/sty139.
117. A. E. Reines, J. J. Condon, J. Darling *et al.*, A New Sample of (Wandering) Massive Black Holes in Dwarf Galaxies from High-resolution Radio Observations, *Astrophys. J.* . **888**(1):36 (Jan., 2020). doi: 10.3847/1538-4357/ab4999.
  118. M. Mezcua and H. Domínguez Sánchez, Hidden AGNs in Dwarf Galaxies Revealed by MaNGA: Light Echoes, Off-nuclear Wanderers, and a New Broad-line AGN, *Astrophys. J.* . **898**(2):L30 (Aug., 2020). doi: 10.3847/2041-8213/aba199.
  119. A. Ricarte, M. Tremmel, P. Natarajan *et al.*, Origins and demographics of wandering black holes, *Mon. Not. R. Astron. Soc.* . **503**(4), 6098–6111 (June, 2021). doi: 10.1093/mnras/stab866.
  120. R. S. Sharma, A. M. Brooks, M. Tremmel *et al.*, A hidden population of massive black holes in simulated dwarf galaxies, *arXiv e-prints*. art. arXiv:2203.05580 (Mar., 2022).
  121. L. Blecha, T. J. Cox, A. Loeb *et al.*, Recoiling black holes in merging galaxies: relationship to active galactic nucleus lifetimes, starbursts and the  $M_{BH}-\sigma$  relation, *Mon. Not. R. Astron. Soc.* . **412**, 2154–2182 (Apr., 2011). doi: 10.1111/j.1365-2966.2010.18042.x.
  122. D. Sijacki, V. Springel and M. G. Haehnelt, Gravitational recoils of supermassive black holes in hydrodynamical simulations of gas-rich galaxies, *Mon. Not. R. Astron. Soc.* . **414**, 3656–3670 (July, 2011). doi: 10.1111/j.1365-2966.2011.18666.x.
  123. L. Blecha, D. Sijacki, L. Z. Kelley *et al.*, Recoiling black holes: prospects for detection and implications of spin alignment, *Mon. Not. R. Astron. Soc.* . **456**, 961–989 (Feb., 2016). doi: 10.1093/mnras/stv2646.
  124. H. Bondi and F. Hoyle, On the mechanism of accretion by stars, *Mon. Not. R. Astron. Soc.* . **104**, 273 (1944).
  125. H. Bondi, On spherically symmetrical accretion, *Mon. Not. R. Astron. Soc.* . **112**, 195 (1952).
  126. T. Di Matteo, V. Springel and L. Hernquist, Energy input from quasars regulates the growth and activity of black holes and their host galaxies, *Nature* . **433**, 604–607 (Feb., 2005). doi: 10.1038/nature03335.
  127. F. I. Pelupessy, T. Di Matteo and B. Ciardi, How Rapidly Do Supermassive Black Hole “Seeds” Grow at Early Times?, *Astrophys. J.* . **665**(1), 107–119 (Aug., 2007). doi: 10.1086/519235.
  128. Y.-F. Jiang, J. M. Stone and S. W. Davis, A Global Three-dimensional Radiation Magneto-hydrodynamic Simulation of Super-Eddington Accretion Disks, *Astrophys. J.* . **796**:106 (Dec., 2014). doi: 10.1088/0004-637X/796/2/106.
  129. Y.-F. Jiang, J. M. Stone and S. W. Davis, Super-Eddington Accretion Disks around Supermassive Black Holes, *Astrophys. J.* . **880**(2):67 (Aug., 2019). doi: 10.3847/1538-4357/ab29ff.
  130. A. Lupi, F. Haardt, M. Dotti *et al.*, Growing massive black holes through supercritical accretion of stellar-mass seeds, *Mon. Not. R. Astron. Soc.* . **456**(3), 2993–3003 (Mar., 2016). doi: 10.1093/mnras/stv2877.
  131. Q. Yu and S. Tremaine, Observational constraints on growth of massive black holes, *Mon. Not. R. Astron. Soc.* . **335**, 965–976 (Oct., 2002). doi: 10.1046/j.1365-8711.2002.05532.x.
  132. J. Kormendy and L. C. Ho, Coevolution (Or Not) of Supermassive Black Holes and Host Galaxies, *Annu. Rev. Astron. Astrophys.* . **51**(1), 511–653 (Aug., 2013). doi: 10.1146/annurev-astro-082708-101811.

133. A. W. Graham, Galaxy Bulges and Their Massive Black Holes: A Review, Galactic Bulges, **418**, 263 (2016). doi: 10.1007/978-3-319-19378-6\_11.
134. P. F. Hopkins and E. Quataert, How do massive black holes get their gas?, Mon. Not. R. Astron. Soc. . **407**, 1529–1564 (Sept., 2010). doi: 10.1111/j.1365-2966.2010.17064.x.
135. P. F. Hopkins and E. Quataert, An analytic model of angular momentum transport by gravitational torques: from galaxies to massive black holes, Mon. Not. R. Astron. Soc. . **415**, 1027–1050 (Aug., 2011). doi: 10.1111/j.1365-2966.2011.18542.x.
136. A. Hobbs, C. Power, S. Nayakshin et al., Modelling supermassive black hole growth: towards an improved sub-grid prescription, Mon. Not. R. Astron. Soc. . **421**(4), 3443–3449 (Apr, 2012). doi: 10.1111/j.1365-2966.2012.20563.x.
137. M. Gaspari, M. Ruszkowski and S. P. Oh, Chaotic cold accretion on to black holes, Mon. Not. R. Astron. Soc. . **432**(4), 3401–3422 (July, 2013). doi: 10.1093/mnras/stt692.
138. P. F. Hopkins, P. Torrey, C.-A. Faucher-Giguère et al., Stellar and quasar feedback in concert: effects on AGN accretion, obscuration, and outflows, Mon. Not. R. Astron. Soc. . **458**, 816–831 (May, 2016). doi: 10.1093/mnras/stw289.
139. A. Negri and M. Volonteri, Black hole feeding and feedback: the physics inside the ‘sub-grid’, Mon. Not. R. Astron. Soc. . **467**, 3475–3492 (May, 2017). doi: 10.1093/mnras/stx362.
140. M. Habouzit, Y. Li, R. S. Somerville et al., Supermassive black holes in cosmological simulations I:  $M_{BH} - M_*$  relation and black hole mass function, Mon. Not. R. Astron. Soc. . **503**(2), 1940–1975 (May, 2021). doi: 10.1093/mnras/stab496.
141. R. S. Beckmann, J. Devriendt and A. Slyz, Zooming in on supermassive black holes: how resolving their gas cloud host renders their accretion episodic, Mon. Not. R. Astron. Soc. . **483**(3), 3488–3509 (Mar, 2019). doi: 10.1093/mnras/sty2890.
142. O. Çatmabacak, R. Feldmann, D. Anglés-Alcázar et al., Black hole – galaxy co-evolution in FIRE: the importance of black hole location and mergers, arXiv e-prints. art. arXiv:2007.12185 (July, 2020).
143. F. Bournaud, A. Dekel, R. Teyssier et al., Black Hole Growth and Active Galactic Nuclei Obscuration by Instability-driven Inflows in High-redshift Disk Galaxies Fed by Cold Streams, Astrophys. J. . 741:L33 (Nov., 2011). doi: 10.1088/2041-8205/741/2/L33.
144. A. Hobbs, S. Nayakshin, C. Power et al., Feeding supermassive black holes through supersonic turbulence and ballistic accretion, Mon. Not. R. Astron. Soc. . **413**(4), 2633–2650 (June, 2011). doi: 10.1111/j.1365-2966.2011.18333.x.
145. J. M. Gabor and F. Bournaud, Simulations of supermassive black hole growth in high-redshift disc galaxies, Mon. Not. R. Astron. Soc. . **434**(1), 606–620 (Sep, 2013). doi: 10.1093/mnras/stt1046.
146. C. Power, S. Nayakshin and A. King, The accretion disc particle method for simulations of black hole feeding and feedback, Mon. Not. R. Astron. Soc. . **412**(1), 269–276 (Mar, 2011). doi: 10.1111/j.1365-2966.2010.17901.x.
147. D. Fiacconi, D. Sijacki and J. E. Pringle, Galactic nuclei evolution with spinning black holes: method and implementation, Mon. Not. R. Astron. Soc. . **477**(3), 3807–3835 (Jul, 2018). doi: 10.1093/mnras/sty893.
148. R. Y. Talbot, M. A. Bourne and D. Sijacki, Blandford-Znajek jets in galaxy formation simulations: method and implementation, Mon. Not. R. Astron. Soc. . **504**(3), 3619–3650 (July, 2021). doi: 10.1093/mnras/stab804.
149. Y. Dubois, M. Volonteri and J. Silk, Black hole evolution - III. Statistical properties of mass growth and spin evolution using large-scale hydrodynamical cosmological

- simulations, *Mon. Not. R. Astron. Soc.* . **440**(2), 1590–1606 (May, 2014). doi: 10.1093/mnras/stu373.
150. S. Bustamante and V. Springel, Spin evolution and feedback of supermassive black holes in cosmological simulations, *Mon. Not. R. Astron. Soc.* . **490**(3), 4133–4153 (Dec., 2019). doi: 10.1093/mnras/stz2836.
151. J. M. Bardeen, W. H. Press and S. A. Teukolsky, Rotating Black Holes: Locally Non-rotating Frames, Energy Extraction, and Scalar Synchrotron Radiation, *Astrophys. J.* . **178**, 347–370 (Dec., 1972). doi: 10.1086/151796.
152. A. C. Fabian, Observational Evidence of Active Galactic Nuclei Feedback, *Annu. Rev. Astron. Astrophys.* . **50**, 455–489 (Sept., 2012). doi: 10.1146/annurev-astro-081811-125521.
153. J. Silk and M. J. Rees, Quasars and galaxy formation, *Astron. Astrophys.* . **331**, L1–L4 (Mar., 1998).
154. N. Murray, E. Quataert and T. A. Thompson, On the Maximum Luminosity of Galaxies and Their Central Black Holes: Feedback from Momentum-driven Winds, *Astrophys. J.* . **618**, 569–585 (Jan., 2005). doi: 10.1086/426067.
155. F. Tombesi, M. Cappi, J. N. Reeves *et al.*, Unification of X-ray winds in Seyfert galaxies: from ultra-fast outflows to warm absorbers, *Mon. Not. R. Astron. Soc.* . **430**, 1102–1117 (Apr., 2013). doi: 10.1093/mnras/sts692.
156. E. Nardini, J. N. Reeves, J. Gofford *et al.*, Black hole feedback in the luminous quasar PDS 456, *Science*. **347**, 860–863 (Feb., 2015). doi: 10.1126/science.1259202.
157. J. E. Greene, N. L. Zakamska and P. S. Smith, A Spectacular Outflow in an Obscured Quasar, *Astrophys. J.* . 746:86 (Feb., 2012). doi: 10.1088/0004-637X/746/1/86.
158. C. Cicone, R. Maiolino, E. Sturm *et al.*, Massive molecular outflows and evidence for AGN feedback from CO observations, *Astron. Astrophys.* . 562:A21 (Feb., 2014). doi: 10.1051/0004-6361/201322464.
159. N. L. Zakamska and J. E. Greene, Quasar feedback and the origin of radio emission in radio-quiet quasars, *Mon. Not. R. Astron. Soc.* . **442**, 784–804 (July, 2014). doi: 10.1093/mnras/stu842.
160. D. Wylezalek, A. M. Flores, N. L. Zakamska *et al.*, Ionized gas outflow signatures in SDSS-IV MaNGA active galactic nuclei, *Mon. Not. R. Astron. Soc.* . **492**(4), 4680–4696 (Mar., 2020). doi: 10.1093/mnras/staa062.
161. J. Hlavacek-Larrondo, A. C. Fabian, A. C. Edge *et al.*, Extreme AGN feedback in the MAssive Cluster Survey: a detailed study of X-ray cavities at  $z > 0.3$ , *Mon. Not. R. Astron. Soc.* . **421**(2), 1360–1384 (Apr., 2012). doi: 10.1111/j.1365-2966.2011.20405.x.
162. R. Trainor and C. C. Steidel, Constraints on Hyperluminous QSO Lifetimes via Fluorescent Ly $\alpha$  Emitters at  $Z \sim 2.7$ , *Astrophys. J.* . 775(1):L3 (Sept., 2013). doi: 10.1088/2041-8205/775/1/L3.
163. A.-C. Eilers, F. B. Davies, J. F. Hennawi *et al.*, Implications of  $z \sim 6$  Quasar Proximity Zones for the Epoch of Reionization and Quasar Lifetimes, *Astrophys. J.* . 840(1):24 (May, 2017). doi: 10.3847/1538-4357/aa6c60.
164. I. K. Baldry, S. P. Driver, J. Loveday *et al.*, Galaxy And Mass Assembly (GAMA): the galaxy stellar mass function at  $z < 0.06$ , *Mon. Not. R. Astron. Soc.* . **421**(1), 621–634 (Mar., 2012). doi: 10.1111/j.1365-2966.2012.20340.x.
165. M. Bernardi, A. Meert, R. K. Sheth *et al.*, The high mass end of the stellar mass function: Dependence on stellar population models and agreement between fits to the light profile, *Mon. Not. R. Astron. Soc.* . **467**(2), 2217–2233 (May, 2017). doi: 10.1093/mnras/stx176.
166. I. K. Baldry, M. L. Balogh, R. G. Bower *et al.*, Galaxy bimodality versus stellar

- mass and environment, *Mon. Not. R. Astron. Soc.* . **373**(2), 469–483 (Dec., 2006). doi: 10.1111/j.1365-2966.2006.11081.x.
167. G. B. Brammer, K. E. Whitaker, P. G. van Dokkum *et al.*, The Dead Sequence: A Clear Bimodality in Galaxy Colors from  $z = 0$  to  $z = 2.5$ , *Astrophys. J.* . **706**(1), L173–L177 (Nov., 2009). doi: 10.1088/0004-637X/706/1/L173.
  168. J. Debuhr, E. Quataert, C.-P. Ma *et al.*, Self-regulated black hole growth via momentum deposition in galaxy merger simulations, *Mon. Not. R. Astron. Soc.* . **406**(1), L55–L59 (July, 2010). doi: 10.1111/j.1745-3933.2010.00881.x.
  169. J. Debuhr, E. Quataert and C.-P. Ma, Galaxy-scale outflows driven by active galactic nuclei, *Mon. Not. R. Astron. Soc.* . **420**, 2221–2231 (Mar., 2012). doi: 10.1111/j.1365-2966.2011.20187.x.
  170. T. Costa, J. Rosdahl, D. Sijacki *et al.*, Driving gas shells with radiation pressure on dust in radiation-hydrodynamic simulations, *Mon. Not. R. Astron. Soc.* . **473**(3), 4197–4219 (Jan., 2018). doi: 10.1093/mnras/stx2598.
  171. E. Choi, J. P. Ostriker, T. Naab *et al.*, Radiative and Momentum-based Mechanical Active Galactic Nucleus Feedback in a Three-dimensional Galaxy Evolution Code, *Astrophys. J.* . 754:125 (Aug., 2012). doi: 10.1088/0004-637X/754/2/125.
  172. A. J. Richings and C.-A. Faucher-Giguère, The origin of fast molecular outflows in quasars: molecule formation in AGN-driven galactic winds, *Mon. Not. R. Astron. Soc.* . **474**(3), 3673–3699 (Mar, 2018). doi: 10.1093/mnras/stx3014.
  173. P. Torrey, P. F. Hopkins, C.-A. Faucher-Giguère *et al.*, The impact of AGN wind feedback in simulations of isolated galaxies with a multiphase ISM, *Mon. Not. R. Astron. Soc.* . **497**(4), 5292–5308 (Oct., 2020). doi: 10.1093/mnras/staa2222.
  174. A. J. Richings, C.-A. Faucher-Giguère and J. Stern, Unravelling the physics of multiphase AGN winds through emission line tracers, *Mon. Not. R. Astron. Soc.* . **503**(2), 1568–1585 (May, 2021). doi: 10.1093/mnras/stab556.
  175. J.-h. Kim, J. H. Wise, M. A. Alvarez *et al.*, Galaxy Formation with Self-consistently Modeled Stars and Massive Black Holes. I. Feedback-regulated Star Formation and Black Hole Growth, *Astrophys. J.* . 738(1):54 (Sept., 2011). doi: 10.1088/0004-637X/738/1/54.
  176. R. R. Gibson, L. Jiang, W. N. Brandt *et al.*, A Catalog of Broad Absorption Line Quasars in Sloan Digital Sky Survey Data Release 5, *Astrophys. J.* . **692**(1), 758–777 (Feb., 2009). doi: 10.1088/0004-637X/692/1/758.
  177. J. Gofford, J. N. Reeves, D. E. McLaughlin *et al.*, The Suzaku view of highly ionized outflows in AGN - II. Location, energetics and scalings with bolometric luminosity, *Mon. Not. R. Astron. Soc.* . **451**(4), 4169–4182 (Aug., 2015). doi: 10.1093/mnras/stv1207.
  178. T. Costa, R. Pakmor and V. Springel, Powering galactic superwinds with small-scale AGN winds, *Mon. Not. R. Astron. Soc.* . **497**(4), 5229–5255 (Oct., 2020). doi: 10.1093/mnras/staa2321.
  179. C.-A. Faucher-Giguère and E. Quataert, The physics of galactic winds driven by active galactic nuclei, *Mon. Not. R. Astron. Soc.* . **425**, 605–622 (Sept., 2012). doi: 10.1111/j.1365-2966.2012.21512.x.
  180. K. Zubovas and A. King, Clearing Out a Galaxy, *Astrophys. J.* . 745(2):L34 (Feb., 2012). doi: 10.1088/2041-8205/745/2/L34.
  181. T. M. Heckman and P. N. Best, The Coevolution of Galaxies and Supermassive Black Holes: Insights from Surveys of the Contemporary Universe, *Annu. Rev. Astron. Astrophys.* . **52**, 589–660 (Aug., 2014). doi: 10.1146/annurev-astro-081913-035722.
  182. D. Sijacki, V. Springel, T. Di Matteo *et al.*, A unified model for AGN feedback in

- cosmological simulations of structure formation, *Mon. Not. R. Astron. Soc.* . **380**, 877–900 (Sept., 2007). doi: 10.1111/j.1365-2966.2007.12153.x.
183. M. A. Bourne and D. Sijacki, AGN jet feedback on a moving mesh: cocoon inflation, gas flows and turbulence, *Mon. Not. R. Astron. Soc.* . **472**(4), 4707–4735 (Dec, 2017). doi: 10.1093/mnras/stx2269.
184. R. Weinberger, K. Ehlert, C. Pfrommer et al., Simulating the interaction of jets with the intracluster medium, *Mon. Not. R. Astron. Soc.* . **470**(4), 4530–4546 (Oct., 2017). doi: 10.1093/mnras/stx1409.
185. K.-Y. Su, P. F. Hopkins, G. L. Bryan et al., Which AGN jets quench star formation in massive galaxies?, *Mon. Not. R. Astron. Soc.* . **507**(1), 175–204 (Oct., 2021). doi: 10.1093/mnras/stab2021.
186. S. Cole, C. G. Lacey, C. M. Baugh et al., Hierarchical galaxy formation, *Mon. Not. R. Astron. Soc.* . **319**(1), 168–204 (Nov., 2000). doi: 10.1046/j.1365-8711.2000.03879.x.
187. A. J. Benson, R. G. Bower, C. S. Frenk et al., What Shapes the Luminosity Function of Galaxies?, *Astrophys. J.* . **599**(1), 38–49 (Dec., 2003). doi: 10.1086/379160.
188. G. L. Granato, G. De Zotti, L. Silva et al., A Physical Model for the Coevolution of QSOs and Their Spheroidal Hosts, *Astrophys. J.* . **600**, 580–594 (Jan., 2004).
189. C. M. Baugh, A primer on hierarchical galaxy formation: the semi-analytical approach, *Reports on Progress in Physics.* **69**(12), 3101–3156 (Dec., 2006). doi: 10.1088/0034-4885/69/12/R02.
190. R. G. Bower, A. J. Benson, R. Malbon et al., Breaking the hierarchy of galaxy formation, *Mon. Not. R. Astron. Soc.* . **370**(2), 645–655 (Aug., 2006). doi: 10.1111/j.1365-2966.2006.10519.x.
191. A. Cattaneo, A. Dekel, J. Devriendt et al., Modelling the galaxy bimodality: shut-down above a critical halo mass, *Mon. Not. R. Astron. Soc.* . **370**(4), 1651–1665 (Aug., 2006). doi: 10.1111/j.1365-2966.2006.10608.x.
192. D. J. Croton, V. Springel, S. D. M. White et al., The many lives of active galactic nuclei: cooling flows, black holes and the luminosities and colours of galaxies, *Mon. Not. R. Astron. Soc.* . **365**, 11–28 (Jan., 2006). doi: 10.1111/j.1365-2966.2005.09675.x.
193. G. De Lucia, V. Springel, S. D. M. White et al., The formation history of elliptical galaxies, *Mon. Not. R. Astron. Soc.* . **366**, 499–509 (Feb., 2006). doi: 10.1111/j.1365-2966.2005.09879.x.
194. N. Menci, A. Fontana, E. Giallongo et al., The Abundance of Distant and Extremely Red Galaxies: The Role of AGN Feedback in Hierarchical Models, *Astrophys. J.* . **647**(2), 753–762 (Aug., 2006). doi: 10.1086/505528.
195. P. Monaco, F. Fontanot and G. Taffoni, The MORGANA model for the rise of galaxies and active nuclei, *Mon. Not. R. Astron. Soc.* . **375**(4), 1189–1219 (Mar., 2007). doi: 10.1111/j.1365-2966.2006.11253.x.
196. R. S. Somerville and J. R. Primack, Semi-analytic modelling of galaxy formation: the local Universe, *Mon. Not. R. Astron. Soc.* . **310**(4), 1087–1110 (Dec., 1999). doi: 10.1046/j.1365-8711.1999.03032.x.
197. R. S. Somerville, P. F. Hopkins, T. J. Cox et al., A semi-analytic model for the co-evolution of galaxies, black holes and active galactic nuclei, *Mon. Not. R. Astron. Soc.* . **391**(2), 481–506 (Dec., 2008). doi: 10.1111/j.1365-2966.2008.13805.x.
198. Q. Guo, S. White, M. Boylan-Kolchin et al., From dwarf spheroidals to cD galaxies: simulating the galaxy population in a  $\Lambda$ CDM cosmology, *Mon. Not. R. Astron. Soc.* . **413**(1), 101–131 (May, 2011). doi: 10.1111/j.1365-2966.2010.18114.x.
199. A. J. Benson, G ALACTICUS: A semi-analytic model of galaxy formation, *Nature* . **17**(2), 175–197 (Feb., 2012). doi: 10.1016/j.newast.2011.07.004.

200. M. Hirschmann, R. S. Somerville, T. Naab *et al.*, Origin of the antihierarchical growth of black holes, *Mon. Not. R. Astron. Soc.* . **426**(1), 237–257 (Oct., 2012). doi: 10.1111/j.1365-2966.2012.21626.x.
201. B. M. B. Henriques, S. D. M. White, P. A. Thomas *et al.*, Simulations of the galaxy population constrained by observations from  $z = 3$  to the present day: implications for galactic winds and the fate of their ejecta, *Mon. Not. R. Astron. Soc.* . **431**(4), 3373–3395 (June, 2013). doi: 10.1093/mnras/stt415.
202. D. J. Croton, A. R. H. Stevens, C. Tonini *et al.*, Semi-Analytic Galaxy Evolution (SAGE): Model Calibration and Basic Results, *Astrophys. J. Suppl.* . 222(2):22 (Feb., 2016). doi: 10.3847/0067-0049/222/2/22.
203. C. G. Lacey, C. M. Baugh, C. S. Frenk *et al.*, A unified multiwavelength model of galaxy formation, *Mon. Not. R. Astron. Soc.* . **462**(4), 3854–3911 (Nov., 2016). doi: 10.1093/mnras/stw1888.
204. C. d. P. Lagos, R. J. Tobar, A. S. G. Robotham *et al.*, Shark: introducing an open source, free, and flexible semi-analytic model of galaxy formation, *Mon. Not. R. Astron. Soc.* . **481**(3), 3573–3603 (Dec., 2018). doi: 10.1093/mnras/sty2440.
205. A. Cattaneo, I. Koutsouridou, E. Tollet *et al.*, GalICS 2.1: a new semianalytic model for cold accretion, cooling, feedback, and their roles in galaxy formation, *Mon. Not. R. Astron. Soc.* . **497**(1), 279–301 (Sept., 2020). doi: 10.1093/mnras/staa1832.
206. F. Fontanot, G. De Lucia, M. Hirschmann *et al.*, The rise of active galactic nuclei in the galaxy evolution and assembly semi-analytic model, *Mon. Not. R. Astron. Soc.* . **496**(3), 3943–3960 (Aug., 2020). doi: 10.1093/mnras/staa1716.
207. F. Marulli, S. Bonoli, E. Branchini *et al.*, Modelling the cosmological co-evolution of supermassive black holes and galaxies - I. BH scaling relations and the AGN luminosity function, *Mon. Not. R. Astron. Soc.* . **385**, 1846–1858 (Apr., 2008). doi: 10.1111/j.1365-2966.2008.12988.x.
208. N. Menci, F. Fiore, S. Puccetti *et al.*, The Blast Wave Model for AGN Feedback: Effects on AGN Obscuration, *Astrophys. J.* . **686**(1), 219–229 (Oct., 2008). doi: 10.1086/591438.
209. S. Bonoli, F. Marulli, V. Springel *et al.*, Modelling the cosmological co-evolution of supermassive black holes and galaxies - II. The clustering of quasars and their dark environment, *Mon. Not. R. Astron. Soc.* . p. 606 (May, 2009). doi: 10.1111/j.1365-2966.2009.14701.x.
210. N. Fanidakis, C. M. Baugh, A. J. Benson *et al.*, The evolution of active galactic nuclei across cosmic time: what is downsizing?, *Mon. Not. R. Astron. Soc.* . **419**(4), 2797–2820 (Feb., 2012). doi: 10.1111/j.1365-2966.2011.19931.x.
211. G. Kauffmann and M. Haehnelt, A unified model for the evolution of galaxies and quasars, *Mon. Not. R. Astron. Soc.* . **311**(3), 576–588 (Jan., 2000). doi: 10.1046/j.1365-8711.2000.03077.x.
212. M. Umemura, A. Loeb and E. L. Turner, Early Cosmic Formation of Massive Black Holes, *Astrophys. J.* . **419**, 459–+ (Dec., 1993). doi: 10.1086/173499.
213. A. Lapi, F. Shankar, J. Mao *et al.*, Quasar Luminosity Functions from Joint Evolution of Black Holes and Host Galaxies, *Astrophys. J.* . **650**(1), 42–56 (Oct., 2006). doi: 10.1086/507122.
214. P. F. Hopkins, L. Hernquist, T. J. Cox *et al.*, The Evolution in the Faint-End Slope of the Quasar Luminosity Function, *Astrophys. J.* . **639**(2), 700–709 (Mar., 2006). doi: 10.1086/499351.
215. R. K. Malbon, C. M. Baugh, C. S. Frenk *et al.*, Black hole growth in hierarchical galaxy formation, *Mon. Not. R. Astron. Soc.* . **382**(4), 1394–1414 (Dec., 2007). doi: 10.1111/j.1365-2966.2007.12317.x.

216. A. Lidz, P. F. Hopkins, T. J. Cox *et al.*, The Luminosity Dependence of Quasar Clustering, *Astrophys. J.* . **641**(1), 41–49 (Apr., 2006). doi: 10.1086/500444.
217. J. Silk and M. J. Rees, Quasars and galaxy formation, *Astron. Astrophys.* . **331**, L1–L4 (Mar., 1998).
218. A. Soltan, Masses of quasars., *Mon. Not. R. Astron. Soc.* . **200**, 115–122 (July, 1982). doi: 10.1093/mnras/200.1.115.
219. N. Häring and H.-W. Rix, On the Black Hole Mass-Bulge Mass Relation, *Astrophys. J.* . **604**(2), L89–L92 (Apr., 2004). doi: 10.1086/383567.
220. A. W. Graham, C. A. Onken, E. Athanassoula *et al.*, An expanded  $M_{bh}$ - $\sigma$  diagram, and a new calibration of active galactic nuclei masses, *Mon. Not. R. Astron. Soc.* . **412**(4), 2211–2228 (Apr., 2011). doi: 10.1111/j.1365-2966.2010.18045.x.
221. A. W. Graham, P. Erwin, N. Caon *et al.*, A Correlation between Galaxy Light Concentration and Supermassive Black Hole Mass, *Astrophys. J.* . **563**(1), L11–L14 (Dec., 2001). doi: 10.1086/338500.
222. Á. Bogdán and A. D. Goulding, Connecting Dark Matter Halos with the Galaxy Center and the Supermassive Black Hole, *Astrophys. J.* . 800(2):124 (Feb., 2015). doi: 10.1088/0004-637X/800/2/124.
223. A. Marconi, G. Risaliti, R. Gilli *et al.*, Local supermassive black holes, relics of active galactic nuclei and the X-ray background, *Mon. Not. R. Astron. Soc.* . **351**(1), 169–185 (June, 2004). doi: 10.1111/j.1365-2966.2004.07765.x.
224. F. Shankar, D. H. Weinberg and J. Miralda-Escudé, Accretion-driven evolution of black holes: Eddington ratios, duty cycles and active galaxy fractions, *Mon. Not. R. Astron. Soc.* . **428**(1), 421–446 (Jan., 2013). doi: 10.1093/mnras/sts026.
225. Y. Ueda, M. Akiyama, G. Hasinger *et al.*, Toward the Standard Population Synthesis Model of the X-Ray Background: Evolution of X-Ray Luminosity and Absorption Functions of Active Galactic Nuclei Including Compton-thick Populations, *Astrophys. J.* . 786(2):104 (May, 2014). doi: 10.1088/0004-637X/786/2/104.
226. F. Shankar, D. H. Weinberg, C. Marsden *et al.*, Probing black hole accretion tracks, scaling relations, and radiative efficiencies from stacked X-ray active galactic nuclei, *Mon. Not. R. Astron. Soc.* . **493**(1), 1500–1511 (Mar., 2020). doi: 10.1093/mnras/stz3522.
227. T. T. Ananna, C. M. Urry, E. Treister *et al.*, Accretion History of AGNs. III. Radiative Efficiency and AGN Contribution to Reionization, *Astrophys. J.* . 903(2):85 (Nov., 2020). doi: 10.3847/1538-4357/abb815.
228. F. Duras, A. Bongiorno, F. Ricci *et al.*, Universal bolometric corrections for active galactic nuclei over seven luminosity decades, *Astron. Astrophys.* . 636:A73 (Apr., 2020). doi: 10.1051/0004-6361/201936817.
229. F. Shankar, M. Bernardi, R. K. Sheth *et al.*, Selection bias in dynamically measured supermassive black hole samples: its consequences and the quest for the most fundamental relation, *Mon. Not. R. Astron. Soc.* . **460**(3), 3119–3142 (Aug., 2016). doi: 10.1093/mnras/stw678.
230. T. A. Small and R. D. Blandford, Quasar evolution and the growth of black holes., *Mon. Not. R. Astron. Soc.* . **259**, 725–737 (Dec., 1992). doi: 10.1093/mnras/259.4.725.
231. F. Shankar, D. H. Weinberg and J. Miralda-Escudé, Self-Consistent Models of the AGN and Black Hole Populations: Duty Cycles, Accretion Rates, and the Mean Radiative Efficiency, *Astrophys. J.* . **690**(1), 20–41 (Jan., 2009). doi: 10.1088/0004-637X/690/1/20.
232. R. Aversa, A. Lapi, G. de Zotti *et al.*, Black Hole and Galaxy Coevolution from Continuity Equation and Abundance Matching, *Astrophys. J.* . 810(1):74 (Sept.,

- 2015). doi: 10.1088/0004-637X/810/1/74.
233. M. Tucci and M. Volonteri, Constraining supermassive black hole evolution through the continuity equation, *Astron. Astrophys.* . 600:A64 (Apr., 2017). doi: 10.1051/0004-6361/201628419.
234. F. Shankar, V. Allevato, M. Bernardi et al., Constraining black hole-galaxy scaling relations and radiative efficiency from galaxy clustering, *Nature Astronomy*. **4**, 282–291 (Jan., 2020). doi: 10.1038/s41550-019-0949-y.
235. S. W. Davis and A. Laor, The Radiative Efficiency of Accretion Flows in Individual Active Galactic Nuclei, *Astrophys. J.* . 728(2):98 (Feb., 2011). doi: 10.1088/0004-637X/728/2/98.
236. X. Cao, Cosmological Evolution of Massive Black Holes: Effects of Eddington Ratio Distribution and Quasar Lifetime, *Astrophys. J.* . **725**(1), 388–393 (Dec., 2010). doi: 10.1088/0004-637X/725/1/388.
237. F. Shankar, M. Crocce, J. Miralda-Escudé et al., On the Radiative Efficiencies, Eddington Ratios, and Duty Cycles of Luminous High-redshift Quasars, *Astrophys. J.* . **718**(1), 231–250 (July, 2010). doi: 10.1088/0004-637X/718/1/231.
238. P. F. Hopkins, J. D. Younger, C. C. Hayward et al., Mergers, active galactic nuclei and ‘normal’ galaxies: contributions to the distribution of star formation rates and infrared luminosity functions, *Mon. Not. R. Astron. Soc.* . **402**(3), 1693–1713 (Mar., 2010). doi: 10.1111/j.1365-2966.2009.15990.x.
239. G. Yang, C. T. J. Chen, F. Vito et al., Black Hole Growth Is Mainly Linked to Host-galaxy Stellar Mass Rather Than Star Formation Rate, *Astrophys. J.* . 842(2): 72 (June, 2017). doi: 10.3847/1538-4357/aa7564.
240. H. Zhang, P. Behroozi, M. Volonteri et al., Trinity I: Self-Consistently Modeling the Dark Matter Halo-Galaxy-Supermassive Black Hole Connection from  $z = 0 - 10$ , *arXiv e-prints*. art. arXiv:2105.10474 (May, 2021).
241. A. Georgakakis, J. Comparat, A. Merloni et al., Exploring the halo occupation of AGN using dark-matter cosmological simulations, *Mon. Not. R. Astron. Soc.* . **487**(1), 275–295 (July, 2019). doi: 10.1093/mnras/sty3454.
242. J. Aird and A. L. Coil, The AGN-galaxy-halo connection: the distribution of AGN host halo masses to  $z = 2.5$ , *Mon. Not. R. Astron. Soc.* . **502**(4), 5962–5980 (Apr., 2021). doi: 10.1093/mnras/stab312.
243. V. Allevato, F. Shankar, C. Marsden et al., Building Robust Active Galactic Nuclei Mock Catalogs to Unveil Black Hole Evolution and for Survey Planning, *Astrophys. J.* . 916(1):34 (July, 2021). doi: 10.3847/1538-4357/abfe59.
244. A. Viitanen, V. Allevato, A. Finoguenov et al., The role of scatter and satellites in shaping the large-scale clustering of X-ray AGN as a function of host galaxy stellar mass, *Mon. Not. R. Astron. Soc.* . **507**(4), 6148–6160 (Nov., 2021). doi: 10.1093/mnras/stab2538.
245. R. Carraro, F. Shankar, V. Allevato et al., An Eddington ratio-driven origin for the  $L_X - M_*$  relation in quiescent and star forming active galaxies, *Mon. Not. R. Astron. Soc.* (Feb., 2022). doi: 10.1093/mnras/stac441.
246. C. Conroy and M. White, A Simple Model for Quasar Demographics, *Astrophys. J.* . 762(2):70 (Jan., 2013). doi: 10.1088/0004-637X/762/2/70.
247. R. Laureijs, J. Amiaux, S. Arduini et al., Euclid Definition Study Report, *arXiv e-prints*. art. arXiv:1110.3193 (Oct., 2011).
248. J. Yao, M. Ishak, M. A. Troxel et al. Effect of Self-Calibration of Intrinsic Alignment on the Cosmological Parameter Constraints for LSST. In *American Astronomical Society Meeting Abstracts #229*, vol. 229, *American Astronomical Society Meeting Abstracts*, p. 125.07 (Jan, 2017).

249. A. V. Kravtsov, A. A. Berlind, R. H. Wechsler *et al.*, The Dark Side of the Halo Occupation Distribution, *Astrophys. J.* . **609**(1), 35–49 (July, 2004). doi: 10.1086/420959.
250. A. Vale and J. P. Ostriker, Linking halo mass to galaxy luminosity, *Mon. Not. R. Astron. Soc.* . **353**(1), 189–200 (Sept., 2004). doi: 10.1111/j.1365-2966.2004.08059.x.
251. F. Shankar, A. Lapi, P. Salucci *et al.*, New Relationships between Galaxy Properties and Host Halo Mass, and the Role of Feedbacks in Galaxy Formation, *Astrophys. J.* . **643**(1), 14–25 (May, 2006). doi: 10.1086/502794.
252. B. P. Moster, R. S. Somerville, C. Maulbetsch *et al.*, Constraints on the Relationship between Stellar Mass and Halo Mass at Low and High Redshift, *Astrophys. J.* . **710**(2), 903–923 (Feb., 2010). doi: 10.1088/0004-637X/710/2/903.
253. B. P. Moster, T. Naab and S. D. M. White, Galactic star formation and accretion histories from matching galaxies to dark matter haloes, *Mon. Not. R. Astron. Soc.* . **428**(4), 3121–3138 (Feb., 2013). doi: 10.1093/mnras/sts261.
254. P. S. Behroozi, R. H. Wechsler and C. Conroy, The Average Star Formation Histories of Galaxies in Dark Matter Halos from  $z = 0-8$ , *Astrophys. J.* . **770**(1):57 (June, 2013). doi: 10.1088/0004-637X/770/1/57.
255. A. V. Kravtsov, A. A. Vikhlinin and A. V. Meshcheryakov, Stellar Mass—Halo Mass Relation and Star Formation Efficiency in High-Mass Halos, *Astronomy Letters*. **44**(1), 8–34 (Jan., 2018). doi: 10.1134/S1063773717120015.
256. M. Vika, S. P. Driver, A. W. Graham *et al.*, The Millennium Galaxy Catalogue: the  $M_{bh}$ - $L_{spheroid}$  derived supermassive black hole mass function, *Mon. Not. R. Astron. Soc.* . **400**(3), 1451–1460 (Dec., 2009). doi: 10.1111/j.1365-2966.2009.15544.x.
257. P. F. Hopkins, L. Hernquist, T. J. Cox *et al.*, Dissipation and Extra Light in Galactic Nuclei. IV. Evolution in the Scaling Relations of Spheroids, *Astrophys. J.* . **691**(2), 1424–1458 (Feb., 2009). doi: 10.1088/0004-637X/691/2/1424.
258. J. Zavala, V. Avila-Reese, C. Firmani *et al.*, The growth of galactic bulges through mergers in  $\Lambda$  CDM haloes revisited - I. Present-day properties, *Mon. Not. R. Astron. Soc.* . **427**(2), 1503–1516 (Dec., 2012). doi: 10.1111/j.1365-2966.2012.22100.x.
259. F. Shankar, S. Mei, M. Huertas-Company *et al.*, Environmental dependence of bulge-dominated galaxy sizes in hierarchical models of galaxy formation. Comparison with the local Universe, *Mon. Not. R. Astron. Soc.* . **439**(4), 3189–3212 (Apr., 2014). doi: 10.1093/mnras/stt2470.
260. A. Cattaneo, G. A. Mamon, K. Warnick *et al.*, How do galaxies acquire their mass?, *Astron. Astrophys.* . **533**:A5 (Sept., 2011). doi: 10.1051/0004-6361/201015780.
261. S. Buchan and F. Shankar, Setting firmer constraints on the evolution of the most massive, central galaxies from their local abundances and ages, *Mon. Not. R. Astron. Soc.* . **462**(2), 2001–2010 (Oct., 2016). doi: 10.1093/mnras/stw1771.
262. P. J. Grylls, F. Shankar, L. Zanisi *et al.*, A statistical semi-empirical model: satellite galaxies in groups and clusters, *Mon. Not. R. Astron. Soc.* . **483**(2), 2506–2523 (Feb., 2019). doi: 10.1093/mnras/sty3281.
263. P. J. Grylls, F. Shankar, J. Leja *et al.*, Predicting fully self-consistent satellite richness, galaxy growth, and star formation rates from the Statistical sEmi-Empirical modeL STEEL, *Mon. Not. R. Astron. Soc.* . **491**(1), 634–654 (Jan., 2020). doi: 10.1093/mnras/stz2956.
264. P. J. Grylls, F. Shankar and C. J. Conselice, The significant effects of stellar mass estimation on galaxy pair fractions., *Mon. Not. R. Astron. Soc.* . **499**(2), 2265–2275 (Dec., 2020). doi: 10.1093/mnras/staa2966.
265. J. A. O’Leary, B. P. Moster and E. Krämer, EMERGE: constraining merging probabilities and time-scales of close galaxy pairs, *Mon. Not. R. Astron. Soc.* . **503**(4),

- 5646–5657 (June, 2021). doi: 10.1093/mnras/stab889.
266. B. P. Moster, T. Naab and S. D. M. White, EMERGE - an empirical model for the formation of galaxies since  $z \sim 10$ , *Mon. Not. R. Astron. Soc.* . **477**(2), 1822–1852 (June, 2018). doi: 10.1093/mnras/sty655.
  267. P. Behroozi, R. H. Wechsler, A. P. Hearin et al., UNIVERSEMACHINE: The correlation between galaxy growth and dark matter halo assembly from  $z = 0-10$ , *Mon. Not. R. Astron. Soc.* . **488**(3), 3143–3194 (Sept., 2019). doi: 10.1093/mnras/stz1182.
  268. J. S. B. Wyithe and A. Loeb, Self-regulated Growth of Supermassive Black Holes in Galaxies as the Origin of the Optical and X-Ray Luminosity Functions of Quasars, *Astrophys. J.* . **595**(2), 614–623 (Oct., 2003). doi: 10.1086/377475.
  269. P. F. Hopkins, L. Hernquist, T. J. Cox et al., Luminosity-dependent Quasar Lifetimes: A New Interpretation of the Quasar Luminosity Function, *Astrophys. J.* . **630**(2), 716–720 (Sept., 2005). doi: 10.1086/432463.
  270. Y. Shen, Supermassive Black Holes in the Hierarchical Universe: A General Framework and Observational Tests, *Astrophys. J.* . **704**(1), 89–108 (Oct., 2009). doi: 10.1088/0004-637X/704/1/89.
  271. F. Shankar. Merger-Induced Quasars, Their Light Curves, and Their Host Halos. In eds. B. M. Peterson, R. S. Somerville and T. Storchi-Bergmann, *Co-Evolution of Central Black Holes and Galaxies*, vol. 267, pp. 248–253 (May, 2010). doi: 10.1017/S1743921310006356.
  272. Z. Haiman and L. Hui, Constraining the Lifetime of Quasars from Their Spatial Clustering, *Astrophys. J.* . **547**(1), 27–38 (Jan., 2001). doi: 10.1086/318330.
  273. P. Martini and D. H. Weinberg, Quasar Clustering and the Lifetime of Quasars, *Astrophys. J.* . **547**(1), 12–26 (Jan., 2001). doi: 10.1086/318331.
  274. A. Sesana, F. Shankar, M. Bernardi et al., Selection bias in dynamically measured supermassive black hole samples: consequences for pulsar timing arrays, *Mon. Not. R. Astron. Soc.* . **463**(1), L6–L11 (Nov., 2016). doi: 10.1093/mnrasl/slw139.
  275. P. F. Hopkins, L. Hernquist, T. J. Cox et al., A Unified, Merger-driven Model of the Origin of Starbursts, Quasars, the Cosmic X-Ray Background, Supermassive Black Holes, and Galaxy Spheroids, *Astrophys. J. Suppl.* . **163**(1), 1–49 (Mar., 2006). doi: 10.1086/499298.
  276. T. Di Matteo, R. A. C. Croft, Y. Feng et al., The origin of the most massive black holes at high- $z$ : BlueTides and the next quasar frontier, *Mon. Not. R. Astron. Soc.* . **467**, 4243–4251 (June, 2017). doi: 10.1093/mnras/stx319.
  277. A. Tenneti, S. M. Wilkins, T. Di Matteo et al., A tiny host galaxy for the first giant black hole:  $z = 7.5$  quasar in BlueTides, *Mon. Not. R. Astron. Soc.* . **483**(1), 1388–1399 (Feb., 2019). doi: 10.1093/mnras/sty3161.
  278. Y. Ni, T. Di Matteo and Y. Feng, Not all peaks are created equal: the early growth of supermassive black holes, *Mon. Not. R. Astron. Soc.* . **509**(2), 3043–3064 (Jan., 2022). doi: 10.1093/mnras/stab3162.
  279. K.-W. Huang, Y. Ni, Y. Feng et al., The early growth of supermassive black holes in cosmological hydrodynamic simulations with constrained Gaussian realizations, *Mon. Not. R. Astron. Soc.* . **496**(1), 1–12 (June, 2020). doi: 10.1093/mnras/staa1515.
  280. E. Bertschinger, Path Integral Methods for Primordial Density Perturbations: Sampling of Constrained Gaussian Random Fields, *Astrophys. J.* . **323**, L103 (Dec., 1987). doi: 10.1086/185066.
  281. J. Binney and T. Quinn, Gaussian random fields in spherical coordinates, *Mon. Not. R. Astron. Soc.* . **249**, 678–683 (Apr., 1991). doi: 10.1093/mnras/249.4.678.
  282. R. van de Weygaert and E. Bertschinger, Peak and gravity constraints in Gaussian primordial density fields: An application of the Hoffman-Ribak method, *Mon. Not.*

- R. Astron. Soc. . **281**, 84 (July, 1996). doi: 10.1093/mnras/281.1.84.
283. M. A. Latif and A. Ferrara, Formation of Supermassive Black Hole Seeds, Publ. Astron. Soc. Australia. 33:e051 (Oct., 2016). doi: 10.1017/pasa.2016.41.
284. P. Madau, F. Haardt and M. Dotti, Super-critical Growth of Massive Black Holes from Stellar-mass Seeds, Astrophys. J. . 784(2):L38 (Apr., 2014). doi: 10.1088/2041-8205/784/2/L38.
285. M. Volonteri, J. Silk and G. Dubus, The Case for Supercritical Accretion onto Massive Black Holes at High Redshift, Astrophys. J. . 804(2):148 (May, 2015). doi: 10.1088/0004-637X/804/2/148.
286. A. Lupi, F. Haardt, M. Dotti et al., Growing massive black holes through supercritical accretion of stellar-mass seeds, Mon. Not. R. Astron. Soc. . **456**(3), 2993–3003 (Mar., 2016). doi: 10.1093/mnras/stv2877.
287. J. A. Regan, T. P. Downes, M. Volonteri et al., Super-Eddington accretion and feedback from the first massive seed black holes, Mon. Not. R. Astron. Soc. . **486**(3), 3892–3906 (July, 2019). doi: 10.1093/mnras/stz1045.
288. T. Di Matteo, N. Khandai, C. DeGraf et al., Cold Flows and the First Quasars, Astrophys. J. . 745:L29 (Feb., 2012). doi: 10.1088/2041-8205/745/2/L29.
289. L. Mayer and S. Bonoli, The route to massive black hole formation via merger-driven direct collapse: a review, Reports on Progress in Physics. 82(1):016901 (Jan., 2019). doi: 10.1088/1361-6633/aad6a5.
290. L. Boco, A. Lapi and L. Danese, Growth of Supermassive Black Hole Seeds in ETG Star-forming Progenitors: Multiple Merging of Stellar Compact Remnants via Gaseous Dynamical Friction and Gravitational-wave Emission, Astrophys. J. . 891(1):94 (Mar., 2020). doi: 10.3847/1538-4357/ab7446.
291. H. Tagawa, Z. Haiman and B. Kocsis, Making a Supermassive Star by Stellar Bombardment, Astrophys. J. . 892(1):36 (Mar., 2020). doi: 10.3847/1538-4357/ab7922.
292. A. Trinca, R. Schneider, R. Valiante et al., The low-end of the black hole mass function at cosmic dawn, Mon. Not. R. Astron. Soc. . **511**(1), 616–640 (Mar., 2022). doi: 10.1093/mnras/stac062.
293. N. J. McConnell and C.-P. Ma, Revisiting the Scaling Relations of Black Hole Masses and Host Galaxy Properties, Astrophys. J. . 764:184 (Feb., 2013). doi: 10.1088/0004-637X/764/2/184.
294. A. E. Reines and M. Volonteri, Relations between Central Black Hole Mass and Total Galaxy Stellar Mass in the Local Universe, Astrophys. J. . 813:82 (Nov., 2015). doi: 10.1088/0004-637X/813/2/82.
295. B. Trakhtenbrot and H. Netzer, The evolution of  $M_*/M_{BH}$  between  $z = 2$  and  $z = 0$ , Mon. Not. R. Astron. Soc. . **406**, L35–L39 (July, 2010). doi: 10.1111/j.1745-3933.2010.00876.x.
296. A. Bongiorno, R. Maiolino, M. Brusa et al., The  $M_{BH}$ - $M_*$  relation for X-ray-obscured, red QSOs at  $1.2 < z < 2.6$ , Mon. Not. R. Astron. Soc. . **443**, 2077–2091 (Sept., 2014). doi: 10.1093/mnras/stu1248.
297. A. Schulze and L. Wisotzki, Accounting for selection effects in the BH-bulge relations: no evidence for cosmological evolution, Mon. Not. R. Astron. Soc. . **438**, 3422–3433 (Mar., 2014). doi: 10.1093/mnras/stt2457.
298. Y. Shen, J. E. Greene, L. C. Ho et al., The Sloan Digital Sky Survey Reverberation Mapping Project: No Evidence for Evolution in the  $M_\sigma$  Relation to  $z = 1$ , Astrophys. J. . 805:96 (June, 2015). doi: 10.1088/0004-637X/805/2/96.
299. M. Sun, J. R. Trump, W. N. Brandt et al., Evolution in the Black Hole Galaxy Scaling Relations and the Duty Cycle of Nuclear Activity in Star-forming Galaxies, Astrophys. J. . 802:14 (Mar., 2015). doi: 10.1088/0004-637X/802/1/14.

300. C. J. Willott, J. Bergeron and A. Omont, Star Formation Rate and Dynamical Mass of  $10^8$  Solar Mass Black Hole Host Galaxies At Redshift 6, *Astrophys. J.* . 801:123 (Mar., 2015). doi: 10.1088/0004-637X/801/2/123.
301. A. King, Black Holes, Galaxy Formation, and the  $M_{BH}-\sigma$  Relation, *Astrophys. J.* . **596**, L27–L29 (Oct., 2003). doi: 10.1086/379143.
302. P. F. Hopkins, L. Hernquist, T. J. Cox et al., A Theoretical Interpretation of the Black Hole Fundamental Plane, *Astrophys. J.* . **669**, 45–66 (Nov., 2007). doi: 10.1086/521590.
303. C. Y. Peng, How Mergers May Affect the Mass Scaling Relation between Gravitationally Bound Systems, *Astrophys. J.* . **671**, 1098–1107 (Dec., 2007). doi: 10.1086/522774.
304. M. Hirschmann, S. Khochfar, A. Burkert et al., On the evolution of the intrinsic scatter in black hole versus galaxy mass relations, *Mon. Not. R. Astron. Soc.* . **407**, 1016–1032 (Sept., 2010). doi: 10.1111/j.1365-2966.2010.17006.x.
305. K. Jahnke and A. V. Macciò, The Non-causal Origin of the Black-hole-galaxy Scaling Relations, *Astrophys. J.* . 734:92 (June, 2011). doi: 10.1088/0004-637X/734/2/92.
306. G. Kauffmann and T. M. Heckman, Feast and Famine: regulation of black hole growth in low-redshift galaxies, *Mon. Not. R. Astron. Soc.* . **397**, 135–147 (July, 2009). doi: 10.1111/j.1365-2966.2009.14960.x.
307. C.-T. J. Chen, R. C. Hickox, S. Alberts et al., A Correlation between Star Formation Rate and Average Black Hole Accretion in Star-forming Galaxies, *Astrophys. J.* . 773: 3 (Aug., 2013). doi: 10.1088/0004-637X/773/1/3.
308. Y. Li, M. Habouzit, S. Genel et al., Correlations between Black Holes and Host Galaxies in the Illustris and IllustrisTNG Simulations, *Astrophys. J.* . 895(2):102 (June, 2020). doi: 10.3847/1538-4357/ab8f8d.
309. R. A. Crain, J. Schaye, R. G. Bower et al., The EAGLE simulations of galaxy formation: calibration of subgrid physics and model variations, *Mon. Not. R. Astron. Soc.* . **450**, 1937–1961 (June, 2015). doi: 10.1093/mnras/stv725.
310. B. A. Terrazas, E. F. Bell, J. Woo et al., Supermassive Black Holes as the Regulators of Star Formation in Central Galaxies, *Astrophys. J.* . 844(2):170 (Aug., 2017). doi: 10.3847/1538-4357/aa7d07.
311. R. G. Bower, J. Schaye, C. S. Frenk et al., The dark nemesis of galaxy formation: why hot haloes trigger black hole growth and bring star formation to an end, *Mon. Not. R. Astron. Soc.* . **465**, 32–44 (Feb., 2017). doi: 10.1093/mnras/stw2735.
312. J. Prieto, A. Escala, M. Volonteri et al., How AGN and SN Feedback Affect Mass Transport and Black Hole Growth in High-redshift Galaxies, *Astrophys. J.* . 836:216 (Feb., 2017). doi: 10.3847/1538-4357/aa5be5.
313. S. McAlpine, R. G. Bower, D. J. Rosario et al., The rapid growth phase of supermassive black holes, *Mon. Not. R. Astron. Soc.* . **481**, 3118–3128 (Dec., 2018). doi: 10.1093/mnras/sty2489.
314. M. Trebitsch, M. Volonteri, Y. Dubois et al., Escape of ionizing radiation from high-redshift dwarf galaxies: role of AGN feedback, *Mon. Not. R. Astron. Soc.* . **478**(4), 5607–5625 (Aug, 2018). doi: 10.1093/mnras/sty1406.
315. A. Lupi, M. Volonteri, R. Decarli et al., High-redshift quasars and their host galaxies - I. Kinematical and dynamical properties and their tracers, *Mon. Not. R. Astron. Soc.* . **488**(3), 4004–4022 (Sep, 2019). doi: 10.1093/mnras/stz1959.
316. S. Lapiner, A. Dekel and Y. Dubois, Compaction-driven black hole growth, *Mon. Not. R. Astron. Soc.* . **505**(1), 172–190 (July, 2021). doi: 10.1093/mnras/stab1205.
317. M. T. Tillman, S. Wellons, C.-A. Faucher-Giguère et al., Running late: testing delayed supermassive black hole growth models against the quasar luminos-

- ity function, *Mon. Not. R. Astron. Soc.* . **511**(4), 5756–5767 (Apr., 2022). doi: 10.1093/mnras/stac398.
318. A. W. Graham and N. Scott, The  $M_{BH}$ - $L_{spheroid}$  Relation at High and Low Masses, the Quadratic Growth of Black Holes, and Intermediate-mass Black Hole Candidates, *Astrophys. J.* . 764:151 (Feb., 2013). doi: 10.1088/0004-637X/764/2/151.
319. G. A. D. Savorgnan, A. W. Graham, A. Marconi et al., Supermassive Black Holes and Their Host Spheroids. II. The Red and Blue Sequence in the  $M_{BH}$ - $M_{*,sph}$  Diagram, *Astrophys. J.* . 817:21 (Jan., 2016). doi: 10.3847/0004-637X/817/1/21.
320. C. DeGraf, T. Di Matteo, N. Khandai et al., Early black holes in cosmological simulations: luminosity functions and clustering behaviour, *Mon. Not. R. Astron. Soc.* . **424**, 1892–1898 (Aug., 2012). doi: 10.1111/j.1365-2966.2012.21294.x.
321. N. Häring and H.-W. Rix, On the Black Hole Mass-Bulge Mass Relation, *Astrophys. J.* . **604**, L89–L92 (Apr., 2004). doi: 10.1086/383567.
322. M. Hirschmann, S. Khochfar, A. Burkert et al., On the evolution of the intrinsic scatter in black hole versus galaxy mass relations, *Mon. Not. R. Astron. Soc.* . **407** (2), 1016–1032 (Sept., 2010). doi: 10.1111/j.1365-2966.2010.17006.x.
323. R. Carraro, G. Rodighiero, P. Cassata et al., Coevolution of black hole accretion and star formation in galaxies up to  $z = 3.5$ , *Astron. Astrophys.* . 642:A65 (Oct., 2020). doi: 10.1051/0004-6361/201936649.
324. Y. Shen, J. E. Greene, L. C. Ho et al., The Sloan Digital Sky Survey Reverberation Mapping Project: No Evidence for Evolution in the  $M_{\bullet}$ - $\sigma_{*}$  Relation to  $z \sim 1$ , *Astrophys. J.* . 805(2):96 (June, 2015). doi: 10.1088/0004-637X/805/2/96.
325. H. Suh, F. Civano, B. Trakhtenbrot et al., No Significant Evolution of Relations between Black Hole Mass and Galaxy Total Stellar Mass Up to  $z \sim 2.5$ , *Astrophys. J.* . 889(1):32 (Jan., 2020). doi: 10.3847/1538-4357/ab5f5f.
326. Y. Li, Y. Ni, R. A. C. Croft et al., AI-assisted superresolution cosmological simulations, *Proceedings of the National Academy of Science*. 118(19):2022038118 (May, 2021). doi: 10.1073/pnas.2022038118.
327. F. Shankar, M. Bernardi, K. Richardson et al., Black hole scaling relations of active and quiescent galaxies: Addressing selection effects and constraining virial factors, *Mon. Not. R. Astron. Soc.* . **485**(1), 1278–1292 (May, 2019). doi: 10.1093/mnras/stz376.
328. C. Marsden, F. Shankar, M. Bernardi et al., The weak dependence of velocity dispersion on disc fractions, mass-to-light ratio, and redshift: implications for galaxy and black hole evolution, *Mon. Not. R. Astron. Soc.* . **510**(4), 5639–5660 (Mar., 2022). doi: 10.1093/mnras/stab3705.
329. N. Sahu, A. W. Graham and B. L. Davis, Black Hole Mass Scaling Relations for Early-type Galaxies. I.  $M_{BH}$ - $M_{*,sph}$  and  $M_{BH}$ - $M_{*,gal}$ , *Astrophys. J.* . 876(2):155 (May, 2019). doi: 10.3847/1538-4357/ab0f32.
330. A. E. Reines and M. Volonteri, Relations between Central Black Hole Mass and Total Galaxy Stellar Mass in the Local Universe, *Astrophys. J.* . 813(2):82 (Nov., 2015). doi: 10.1088/0004-637X/813/2/82.
331. E. Giallongo, A. Grazian, F. Fiore et al., Faint AGNs at  $z > 4$  in the CANDELS GOODS-S field: looking for contributors to the reionization of the Universe, *Astron. Astrophys.* . 578:A83 (June, 2015). doi: 10.1051/0004-6361/201425334.
332. X. Fan, A. Barth, E. Banados et al., The First Luminous Quasars and Their Host Galaxies, *Bull. Am. Astron. Soc.* . 51(3):121 (May, 2019).
333. M. Habouzit, R. S. Somerville, Y. Li et al., Supermassive black holes in cosmological simulations - II: the AGN population and predictions for upcoming X-ray missions, *Mon. Not. R. Astron. Soc.* . **509**(2), 3015–3042 (Jan., 2022). doi: 10.1093/mnras/

stab3147.

334. J. A. Kollmeier, C. A. Onken, C. S. Kochanek et al., Black Hole Masses and Eddington Ratios at  $0.3 < z < 4$ , *Astrophys. J.* . **648**(1), 128–139 (Sept., 2006). doi: 10.1086/505646.
335. F. Shankar, D. H. Weinberg and J. Miralda-Escudé, Accretion-driven evolution of black holes: Eddington ratios, duty cycles and active galaxy fractions, *Mon. Not. R. Astron. Soc.* . **428**(1), 421–446 (Jan., 2013). doi: 10.1093/mnras/sts026.
336. P. Madau and M. Dickinson, Cosmic Star-Formation History, *Annu. Rev. Astron. Astrophys.* . **52**, 415–486 (Aug., 2014). doi: 10.1146/annurev-astro-081811-125615.
337. J. Aird, A. L. Coil and A. Georgakakis, X-rays across the galaxy population - II. The distribution of AGN accretion rates as a function of stellar mass and redshift., *Mon. Not. R. Astron. Soc.* . **474**, 1225–1249 (Jan., 2018). doi: 10.1093/mnras/stx2700.
338. Y. Ueda, M. Akiyama, G. Hasinger et al., Toward the Standard Population Synthesis Model of the X-Ray Background: Evolution of X-Ray Luminosity and Absorption Functions of Active Galactic Nuclei Including Compton-thick Populations, *Astrophys. J.* . 786(2):104 (May, 2014). doi: 10.1088/0004-637X/786/2/104.
339. J. Aird, A. L. Coil, A. Georgakakis et al., The evolution of the X-ray luminosity functions of unabsorbed and absorbed AGNs out to  $z \sim 5$ , *Mon. Not. R. Astron. Soc.* . **451**(2), 1892–1927 (Aug., 2015). doi: 10.1093/mnras/stv1062.
340. A. Merloni and S. Heinz, A synthesis model for AGN evolution: supermassive black holes growth and feedback modes, *Mon. Not. R. Astron. Soc.* . **388**(3), 1011–1030 (Aug., 2008). doi: 10.1111/j.1365-2966.2008.13472.x.
341. Y. Shen and B. C. Kelly, The Demographics of Broad-line Quasars in the Mass-Luminosity Plane. I. Testing FWHM-based Virial Black Hole Masses, *Astrophys. J.* . 746(2):169 (Feb., 2012). doi: 10.1088/0004-637X/746/2/169.
342. J. Buchner, A. Georgakakis, K. Nandra et al., Obscuration-dependent Evolution of Active Galactic Nuclei, *Astrophys. J.* . 802(2):89 (Apr., 2015). doi: 10.1088/0004-637X/802/2/89.
343. R. J. McLure and J. S. Dunlop, The cosmological evolution of quasar black hole masses, *Mon. Not. R. Astron. Soc.* . **352**(4), 1390–1404 (Aug., 2004). doi: 10.1111/j.1365-2966.2004.08034.x.
344. A. Merloni, The anti-hierarchical growth of supermassive black holes, *Mon. Not. R. Astron. Soc.* . **353**(4), 1035–1047 (Oct., 2004). doi: 10.1111/j.1365-2966.2004.08147.x.
345. F. Shankar, P. Salucci, G. L. Granato et al., Supermassive black hole demography: the match between the local and accreted mass functions, *Mon. Not. R. Astron. Soc.* . **354**(4), 1020–1030 (Nov., 2004). doi: 10.1111/j.1365-2966.2004.08261.x.
346. J. A. Kollmeier, C. A. Onken, C. S. Kochanek et al., Black Hole Masses and Eddington Ratios at  $0.3 < z < 4$ , *Astrophys. J.* . **648**(1), 128–139 (Sept., 2006). doi: 10.1086/505646.
347. X. Cao and F. Li, Rapidly spinning massive black holes in active galactic nuclei: evidence from the black hole mass function, *Mon. Not. R. Astron. Soc.* . **390**(2), 561–566 (Oct., 2008). doi: 10.1111/j.1365-2966.2008.13800.x.
348. J. D. Silverman, P. J. Green, W. A. Barkhouse et al., The Luminosity Function of X-Ray-selected Active Galactic Nuclei: Evolution of Supermassive Black Holes at High Redshift, *Astrophys. J.* . **679**(1), 118–139 (May, 2008). doi: 10.1086/529572.
349. C. Degraf, T. Di Matteo and V. Springel, Black hole clustering in cosmological hydrodynamic simulations: evidence for mergers, *Mon. Not. R. Astron. Soc.* . **413**, 1383–1394 (May, 2011). doi: 10.1111/j.1365-2966.2011.18221.x.

350. T. Oogi, M. Enoki, T. Ishiyama *et al.*, Quasar clustering in a galaxy and quasar formation model based on ultra high-resolution N-body simulations, *Mon. Not. R. Astron. Soc.* . **456**(1), L30–L34 (Feb., 2016). doi: 10.1093/mnras/slv169.
351. A. K. Bhowmick, T. Di Matteo, Y. Feng *et al.*, The clustering of  $z > 7$  galaxies: predictions from the BLUETIDES simulation, *Mon. Not. R. Astron. Soc.* . **474**, 5393–5405 (Mar., 2018). doi: 10.1093/mnras/stx3149.
352. Z. Haiman and L. Hui, Constraining the Lifetime of Quasars from Their Spatial Clustering, *Astrophys. J.* . **547**, 27–38 (Jan., 2001). doi: 10.1086/318330.
353. P. Martini and D. H. Weinberg, Quasar Clustering and the Lifetime of Quasars, *Astrophys. J.* . **547**, 12–26 (Jan., 2001). doi: 10.1086/318331.
354. A. K. Bhowmick, T. Di Matteo, Y. Feng *et al.*, The clustering of  $z > 7$  galaxies: predictions from the BLUETIDES simulation, *Mon. Not. R. Astron. Soc.* . **474**, 5393–5405 (Mar., 2018). doi: 10.1093/mnras/stx3149.
355. E. P. Farina, C. Montuori, R. Decarli *et al.*, Caught in the act: discovery of a physical quasar triplet, *Mon. Not. R. Astron. Soc.* . **431**(2), 1019–1025 (May, 2013). doi: 10.1093/mnras/stt209.
356. S. G. Djorgovski, F. Courbin, G. Meylan *et al.*, Discovery of a Probable Physical Triple Quasar, *Astrophys. J.* . **662**(1), L1–L5 (June, 2007). doi: 10.1086/519162.
357. R. S. Somerville and R. Davé, Physical Models of Galaxy Formation in a Cosmological Framework, *Annu. Rev. Astron. Astrophys.* . **53**, 51–113 (Aug., 2015). doi: 10.1146/annurev-astro-082812-140951.
358. DESI Collaboration, A. Aghamousa, J. Aguilar *et al.*, The DESI Experiment Part I: Science, Targeting, and Survey Design, *arXiv e-prints*. art. arXiv:1611.00036 (Oct., 2016).
359. T. M. C. Abbott, F. B. Abdalla, A. Alarcon *et al.*, Dark Energy Survey year 1 results: Cosmological constraints from galaxy clustering and weak lensing, *Phys. Rev. D* . **98**(4):043526 (Aug., 2018). doi: 10.1103/PhysRevD.98.043526.
360. Ž. Ivezić, S. M. Kahn, J. A. Tyson *et al.*, LSST: From Science Drivers to Reference Design and Anticipated Data Products, *Astrophys. J.* . **873**(2):111 (Mar., 2019). doi: 10.3847/1538-4357/ab042c.
361. D. Spergel, N. Gehrels, J. Breckinridge *et al.*, WFIRST-2.4: What Every Astronomer Should Know, *arXiv e-prints*. art. arXiv:1305.5425 (May, 2013).
362. R. Laureijs, J. Amiaux, S. Arduini *et al.*, Euclid Definition Study Report, *arXiv e-prints*. art. arXiv:1110.3193 (Oct., 2011).
363. N. E. Chisari, A. J. Mead, S. Joudaki *et al.*, Modelling baryonic feedback for survey cosmology, *The Open Journal of Astrophysics*. **2**(1):4 (June, 2019). doi: 10.21105/astro.1905.06082.
364. M. P. van Daalen, J. Schaye, C. M. Booth *et al.*, The effects of galaxy formation on the matter power spectrum: a challenge for precision cosmology, *Mon. Not. R. Astron. Soc.* . **415**(4), 3649–3665 (Aug., 2011). doi: 10.1111/j.1365-2966.2011.18981.x.
365. E. Semboloni, H. Hoekstra, J. Schaye *et al.*, Quantifying the effect of baryon physics on weak lensing tomography, *Mon. Not. R. Astron. Soc.* . **417**, 2020–2035 (Nov., 2011). doi: 10.1111/j.1365-2966.2011.19385.x.
366. A. Tenneti, R. Mandelbaum and T. Di Matteo, Intrinsic alignments of disk and elliptical galaxies in the MassiveBlack-II and Illustris simulations, *ArXiv e-prints* (Oct., 2015).
367. N. E. Chisari, M. L. A. Richardson, J. Devriendt *et al.*, The impact of baryons on the matter power spectrum from the Horizon-AGN cosmological hydrodynamical simulation, *Mon. Not. R. Astron. Soc.* . **480**(3), 3962–3977 (Nov., 2018). doi: 10.1093/mnras/sty2093.

368. V. Springel, R. Pakmor, A. Pillepich et al., First results from the IllustrisTNG simulations: matter and galaxy clustering, *Mon. Not. R. Astron. Soc.* . **475**, 676–698 (Mar., 2018). doi: 10.1093/mnras/stx3304.
369. M. P. van Daalen, I. G. McCarthy and J. Schaye, Exploring the effects of galaxy formation on matter clustering through a library of simulation power spectra, *Mon. Not. R. Astron. Soc.* . **491**(2), 2424–2446 (Jan., 2020). doi: 10.1093/mnras/stz3199.
370. Y. Dubois, C. Pichon, J. Devriendt et al., Blowing cold flows away: the impact of early AGN activity on the formation of a brightest cluster galaxy progenitor, *Mon. Not. R. Astron. Soc.* . **428**(4), 2885–2900 (Feb., 2013). doi: 10.1093/mnras/sts224.
371. N. Menci, F. Fiore, C. Feruglio et al., Outflows in the Disks of Active Galaxies, *Astrophys. J.* . 877(2):74 (June, 2019). doi: 10.3847/1538-4357/ab1a3a.
372. N. Menci, M. Gatti, F. Fiore et al., Triggering active galactic nuclei in hierarchical galaxy formation: disk instability vs. interactions, *Astron. Astrophys.* . 569:A37 (Sept., 2014). doi: 10.1051/0004-6361/201424217.
373. F. Fiore, C. Feruglio, F. Shankar et al., AGN wind scaling relations and the co-evolution of black holes and galaxies, *Astron. Astrophys.* . 601:A143 (May, 2017). doi: 10.1051/0004-6361/201629478.
374. P. Amaro-Seoane, H. Audley, S. Babak et al., Laser Interferometer Space Antenna, *arXiv e-prints*. art. arXiv:1702.00786 (Feb., 2017).
375. C. M. F. Mingarelli, T. J. W. Lazio, A. Sesana et al., The local nanohertz gravitational-wave landscape from supermassive black hole binaries, *Nature Astronomy*. **1**, 886–892 (Nov., 2017). doi: 10.1038/s41550-017-0299-6.
376. P. Amaro-Seoane, S. Aoudia, S. Babak et al., Low-frequency gravitational-wave science with eLISA/NGO, *Classical and Quantum Gravity*. 29(12):124016 (June, 2012). doi: 10.1088/0264-9381/29/12/124016.
377. P. Amaro-Seoane, S. Aoudia, S. Babak et al., Low-frequency gravitational-wave science with eLISA/NGO, *Classical and Quantum Gravity*. 29(12):124016 (June, 2012). doi: 10.1088/0264-9381/29/12/124016.
378. P. Amaro-Seoane, S. Aoudia, S. Babak et al., eLISA: Astrophysics and cosmology in the millihertz regime, *GW Notes*, Vol. 6, p. 4-110. **6**, 4–110 (May, 2013).
379. J. S. B. Wyithe and A. Loeb, Low-Frequency Gravitational Waves from Massive Black Hole Binaries: Predictions for LISA and Pulsar Timing Arrays, *Astrophys. J.* . **590**, 691–706 (June, 2003). doi: 10.1086/375187.
380. M. Enoki, K. T. Inoue, M. Nagashima et al., Gravitational Waves from Supermassive Black Hole Coalescence in a Hierarchical Galaxy Formation Model, *Astrophys. J.* . **615**, 19–28 (Nov., 2004). doi: 10.1086/424475.
381. S. M. Koushiappas and A. R. Zentner, Testing Models of Supermassive Black Hole Seed Formation through Gravity Waves, *Astrophys. J.* . **639**, 7–22 (Mar., 2006). doi: 10.1086/499325.
382. M. Micic, K. Holley-Bockelmann, S. Sigurdsson et al., Supermassive black hole growth and merger rates from cosmological N-body simulations, *Mon. Not. R. Astron. Soc.* . **380**, 1533–1540 (Oct., 2007). doi: 10.1111/j.1365-2966.2007.12162.x.
383. A. Sesana, J. Gair, I. Mandel et al., Observing Gravitational Waves from the First Generation of Black Holes, *Astrophys. J.* . **698**, L129–L132 (June, 2009). doi: 10.1088/0004-637X/698/2/L129.
384. A. Klein, E. Barausse, A. Sesana et al., Science with the space-based interferometer eLISA: Supermassive black hole binaries, *Phys. Rev. D* . 93(2):024003 (Jan., 2016). doi: 10.1103/PhysRevD.93.024003.
385. M. Colpi and M. Dotti, Massive Binary Black Holes in the Cosmic Landscape, *Advanced Science Letters*. **4**, 181–203 (Feb., 2011). doi: 10.1166/asl.2011.1205.

386. L. Mayer, Massive black hole binaries in gas-rich galaxy mergers; multiple regimes of orbital decay and interplay with gas inflows, *Classical and Quantum Gravity*. 30 (24):244008 (Dec., 2013). doi: 10.1088/0264-9381/30/24/244008.
387. M. Colpi, Massive Binary Black Holes in Galactic Nuclei and Their Path to Coalescence, *Space Science Reviews*. **183**, 189–221 (Sept., 2014). doi: 10.1007/s11214-014-0067-1.
388. G. D. Quinlan, The dynamical evolution of massive black hole binaries I. Hardening in a fixed stellar background, *Nature*. **1**(1), 35–56 (July, 1996). doi: 10.1016/S1384-1076(96)00003-6.
389. P. Berczik, D. Merritt, R. Spurzem *et al.*, Efficient Merger of Binary Supermassive Black Holes in Nonaxisymmetric Galaxies, *Astrophys. J.* . **642**(1), L21–L24 (May, 2006). doi: 10.1086/504426.
390. A. Sesana, F. Haardt and P. Madau, Interaction of Massive Black Hole Binaries with Their Stellar Environment. II. Loss Cone Depletion and Binary Orbital Decay, *Astrophys. J.* . **660**(1), 546–555 (May, 2007). doi: 10.1086/513016.
391. I. Berentzen, M. Preto, P. Berczik *et al.*, Binary Black Hole Merger in Galactic Nuclei: Post-Newtonian Simulations, *Astrophys. J.* . **695**(1), 455–468 (Apr., 2009). doi: 10.1088/0004-637X/695/1/455.
392. F. M. Khan, A. Just and D. Merritt, Efficient Merger of Binary Supermassive Black Holes in Merging Galaxies, *Astrophys. J.* . 732(2):89 (May, 2011). doi: 10.1088/0004-637X/732/2/89.
393. F. M. Khan, K. Holley-Bockelmann, P. Berczik *et al.*, Supermassive Black Hole Binary Evolution in Axisymmetric Galaxies: The Final Parsec Problem is Not a Problem, *Astrophys. J.* . 773(2):100 (Aug., 2013). doi: 10.1088/0004-637X/773/2/100.
394. E. Vasiliev, F. Antonini and D. Merritt, The Final-parsec Problem in the Collisionless Limit, *Astrophys. J.* . 810(1):49 (Sept., 2015). doi: 10.1088/0004-637X/810/1/49.
395. Z. Haiman, B. Kocsis and K. Menou, The Population of Viscosity- and Gravitational Wave-driven Supermassive Black Hole Binaries Among Luminous Active Galactic Nuclei, *Astrophys. J.* . **700**(2), 1952–1969 (Aug., 2009). doi: 10.1088/0004-637X/700/2/1952.
396. M. Bonetti, F. Haardt, A. Sesana *et al.*, Post-Newtonian evolution of massive black hole triplets in galactic nuclei - II. Survey of the parameter space, *Mon. Not. R. Astron. Soc.* . **477**(3), 3910–3926 (July, 2018). doi: 10.1093/mnras/sty896.
397. M. Tremmel, M. Karcher, F. Governato *et al.*, The Romulus cosmological simulations: a physical approach to the formation, dynamics and accretion models of SMBHs, *Mon. Not. R. Astron. Soc.* . **470**(1), 1121–1139 (Sept., 2017). doi: 10.1093/mnras/stx1160.
398. M. Mannerkoski, P. H. Johansson, A. Rantala *et al.*, Signatures of the Many Supermassive Black Hole Mergers in a Cosmologically Forming Massive Early-Type Galaxy, *arXiv e-prints*. art. arXiv:2112.03576 (Dec., 2021).
399. N. Chen, Y. Ni, A. M. Holgado *et al.*, Massive Black Hole Mergers with Orbital Information: Predictions from the ASTRID Simulation, *arXiv e-prints*. art. arXiv:2112.08555 (Dec., 2021).
400. M. Tremmel, F. Governato, M. Volonteri *et al.*, Off the beaten path: a new approach to realistically model the orbital decay of supermassive black holes in galaxy formation simulations, *Mon. Not. R. Astron. Soc.* . **451**(2), 1868–1874 (Aug., 2015). doi: 10.1093/mnras/stv1060.
401. G. F. Snyder, P. Torrey, J. M. Lotz *et al.*, Galaxy morphology and star formation in the Illustris Simulation at  $z = 0$ , *Mon. Not. R. Astron. Soc.* . **454**(2), 1886–1908 (oct,

- 2015). ISSN 0035-8711. doi: 10.1093/mnras/stv2078. URL <http://adsabs.harvard.edu/abs/2015MNRAS.454.1886S>.
402. G. F. Snyder, J. Lotz, C. Moody *et al.*, Diverse structural evolution at  $z \lesssim 1$  in cosmologically simulated gal axes, *Mon. Not. R. Astron. Soc.* . **451**(4), 4290–4310 (jun, 2015). ISSN 0035-8711. doi: 10.1093/mnras/stv1231. URL <http://adsabs.harvard.edu/abs/2015MNRAS.451.4290S>.
403. S. Banks, K. Lee, N. Azimi *et al.*, On the detectability of massive black hole merger events by LISA, *arXiv e-prints*, art. arXiv:2107.09084 (July, 2021).
404. D. B. Bowen, V. Mewes, M. Campanelli *et al.*, Quasi-periodic Behavior of Mini-disks in Binary Black Holes Approaching Merger, *Astrophys. J.* . 853:L17 (Jan., 2018). doi: 10.3847/2041-8213/aaa756.
405. C. O. Lousto, Y. Zlochower and M. Campanelli, Modeling the Black Hole Merger of QSO 3C 186, *Astrophys. J.* . 841:L28 (June, 2017). doi: 10.3847/2041-8213/aa733c.
406. B. D. Farris, P. Duffell, A. I. MacFadyen *et al.*, Characteristic signatures in the thermal emission from accreting binary black holes, *Mon. Not. R. Astron. Soc.* . **446**, L36–L40 (Jan., 2015). doi: 10.1093/mnras/slu160.
407. E. Barausse, I. Dvorkin, M. Tremmel *et al.*, Massive Black Hole Merger Rates: The Effect of Kiloparsec Separation Wandering and Supernova Feedback, *Astrophys. J.* . 904(1):16 (Nov., 2020). doi: 10.3847/1538-4357/abba7f.
408. D. Izquierdo-Villalba, A. Sesana, S. Bonoli *et al.*, Massive black hole evolution models confronting the n-Hz amplitude of the stochastic gravitational wave background, *Mon. Not. R. Astron. Soc.* . **509**(3), 3488–3503 (Jan., 2022). doi: 10.1093/mnras/stab3239.
409. A. Sicilia, A. Lapi, L. Boco *et al.*, The Black Hole Mass Function across Cosmic Time. II. Heavy Seeds and (Super)Massive Black Holes, *Astrophys. J.* . 934(1):66 (July, 2022). doi: 10.3847/1538-4357/ac7873.
410. S. Peirani and J. A. de Freitas Pacheco, Dark matter accretion into supermassive black holes, *Phys. Rev. D* . 77(6):064023 (Mar., 2008). doi: 10.1103/PhysRevD.77.064023.
411. K. S. Croker, M. Zevin, D. Farrah *et al.*, Cosmologically Coupled Compact Objects: A Single-parameter Model for LIGO-Virgo Mass and Redshift Distributions, *Astrophys. J.* . 921(2):L22 (Nov., 2021). doi: 10.3847/2041-8213/ac2fad.